STRUCTURAL INVESTIGATIONS IN OXIDE CERAMICS

A THESIS
SUBMITTED TO THE
UNIVERSITY OF POONA
FOR THE DEGREE OF
DOCTOR OF PHILOSOPHY
(IN CHEMISTRY)

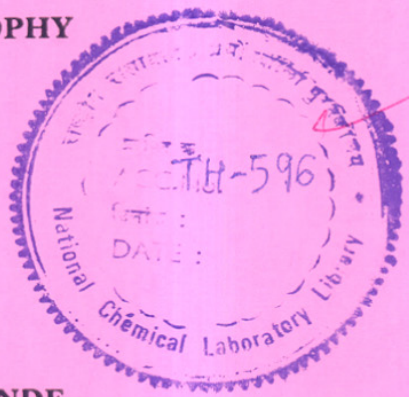

BY

RAMESH FAKIRA SHINDE
M. Sc.

PHYSICAL CHEMISTRY DIVISION
NATIONAL CHEMICAL LABORATORY
PUNE- 411 008

DECEMBER 1989

CERTIFICATE

This is to certify that the thesis entitled 'Structural Investigations in Oxide Ceramics' describes the research work done by Mr. Ramesh Fakira Shinde under my supervision for the Degree of Doctor of Philosophy in Chemistry of the University of Poona. Such material as has been obtained from other sources has been duly acknowledged in the thesis.

S.K. Date

N.C.L.
Pune-8

[S.K. DATE]
Research Guide

CONTENTS

Page No.

CHAPTER-1

Review of the Various Properties of Cadmium Oxide

1.1 Structure of Cadmium Oxide

Structural properties of cadmium oxide have been reported by several investigators[1-7]. According to these studies, CdO exhibits NaCl-type of cubic (F_{m3m}) crystal structure[1,2] (Figure 1.1). The lattice parameter value at room temperature[3,4] was determined to be a=4.6951 ±0.0002 A. The lattice parameter values at elevated temperatures were determined by several researchers[3-5] and are summarized in Table 1.1. The cubic crystal structure of CdO was observed to be stable upto 1300K at atmospheric pressure[3,4].

1.2 Thermal Properties of Cadmium Oxide

Thermal properties of CdO have been investigated using different experimental techniques[8-13]. The experimental studies have also been carried out in various temperature range. These studies[8,9] revealed that CdO is stable upto 773K and starts vaporizing above 773K. The vaporization was attributed to the partial dissociation of CdO. The thermodynamic constants like standard enthalpy of formation, entropy, heat of formation and heat of sublimation were also reported in the literature[10-13]. The thermodynamic properties of CdO were reported to be independent of nonstoichiometry of CdO.

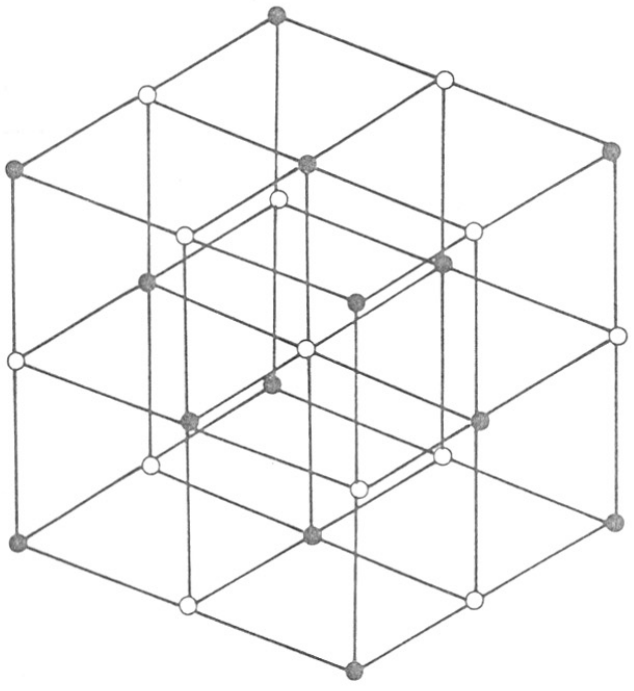

FIG.1.1. SODIUM CHLORIDE TYPE CUBIC CRYSTAL STRUCTURE OF CADMIUM OXIDE. SOLID SPHERES: Cd^{2+} AND HOLLOW SPHERES: O^{2-}

Table 1.1

Lattice parameter values of cubic cadmium oxide

Sr. No.	Temperature °C	Lattice parameter, a Å	References
1	Room temp.	4.692	6
2	Room temp.	4.6946	7
3	Room temp.	4.6951	3,4
4	32	4.6957	5
5	103	4.7002	"
6	167	4.7042	"
7	256	4.7100	"
8	352	4.7164	"
9	445	4.7226	"
10	541	4.7293	"
11	638	4.7361	"
12	732	4.7429	"

1.3 Electrical Properties of Powder Compacts of Cadmium Oxide

Several studies of the electrical properties of CdO, in their powder compact forms, have been reported in the literature [14-21]. The various properties like electrical conductivity, Hall constant and thermoelectric power were studied. The important results of these studies are summarized below:

i) The resistivity of unheated powder compacts of CdO was 10^{8} ohm-cm[14]. After prolong heating above 550K, the resistivity dropped to about 10^{-1} ohm-cm.

ii) The variation of the resistivity in the temperature range from room temperature to 823K, was observed to be linear[15]. The linear variation yielded the activation energy, ΔE_g =0.4 eV, as defined by the equation

$$\sigma = \exp\left(-\frac{\Delta E}{kT}\right).$$

iii) The resistivity measurements in the temperature range 1 to 300K, showed the absence of superconductivity, even though the temperature variation of CdO resembled that of metals[16].

iv) A series of resistivity measurements over the temperature range 300-800-300K were carried out. In the first cycle, linear increase of resistance with temperature, due to the degenerated nature of the CdO,

was observed. While the last cycle showed normal behaviour of non-degenerated semiconductor, that is an exponential decrease of resistance with the variation of the temperature. The effects of the intermediate cycles were attributed to the reaction of oxygen with the electron donors like Cd interstitial[19].

v) CdO was considered as impure metal with all impurities ionized in the lattice[17].

vi) Hall constant was found to have a constant value[18] of about 4.5×10^9 in the temperature range 273 to 773K.

vii) Hall constant was also approximately independent of resistance[14]. The change of resistance by a factor of 10^4 does not affect the value of Hall constant.

viii) At temperature above 900K, the temperature dependence of electron concentration was in agreement with the mass action theory of point defects[21]. The activation energy of the point defect was found to be 0.75 eV.

ix) The comparison of experimental data with the theory of polar crystal[20] gave the effective mass as 0.07 m.

To explain the experimental results, the theory of degenerate semiconductor was developed[18]. The materials whose conductivity was due to nonstoichiometry (point defects in the crystal lattice) or impurity

(present in crystal lattice) were found to show the semiconducting behaviour. These materials were classified into two groups. (a) Classical semiconductors: The semiconductors which had so few electrons that the classical distribution of the energy amongst the electrons were used with sufficient accuracy.
(b) Degenerate semiconductors: The semiconducting materials which had so many free electrons that the Fermi-Dirac statistics were applied to the electrons. The Fermi-Dirac statistical distribution was used to derive expressions for number of electrons, conductivity, thermoelectric power and Hall constant[18]. The derived equations were then used to explain the observed electrical properties[16-18,20].

1.4 Electrical Properties of Single Crystals of Cadmium Oxide

Apart from these studies on powder compacts of CdO, the electrical properties of single crystals ($\approx$ 1 mm^3) of CdO were also reported by Koffyberg[22-24]. The measurements of Hall coefficient and electrical conductivity of these crystals were carried out. The results were explained on the basis of model in which the conduction band was deviated from the simple parabolic shape by the addition of donor energy levels.

The model also incorporated qualitatively the main features of the theory of heavily doped semiconductors. The measured donor concentration was in agreement with the defect concentration determined earlier by chemical[25], electrical[26] and diffusion[27] measurements. The donors were stated to be doubly-ionized oxygen vacancy or a cadmium interstitial[23].

1.5 Magnetic Properties of Cadmium Oxide

Abd. El-Hody and coworkers[2] have studied the magnetic susceptibilities of different CdO samples. The susceptibility was found to increase with the temperature of preparation. The mean magnetic susceptibilities were - 0.287 x 10^{-6} to 0.318 x 10^{-6} emu/gm.

Mookherjee[28] have reported the origin of diamagnetism in CdO. He observed the experimental susceptibility of - 48.74 x 10^{-6} emu/gm. The susceptibility was then calculated assuming that both inner and outer electrons obey the Langvein equation. The two values of the susceptibility were not in agreement. The method of covalent bonding with partial ionic character was used. With this the susceptibility was calculated to be - 49.23 x 10^{-6} emu/gm. This value was in good agreement with the experimental value, which confirmed the

applicability of the covalent bond model with partial ionic character for CdO.

The electron paramagnetic resonance studies of CdO have also been reported in the literature [29-31]. The g values of the observed lines were 1.796, 1.977 and 2.17. The lines were attributed to the conduction electron [29,30], paramagnetic centers [30] of Cd^+ and F-centers [31] respectively. The second line at g=1.977 showed sharp splitting due to hyperfine and superhyperfine interactions [30]. The superhyperfine interaction was attributed to the interaction of unpaired electron with twelve nearest neighbours at a distance of $\sqrt{2}$ x 2.34 A.

1.6 Electronic structure of Cadmium Oxide

The electronic structure of CdO have been determined by using four different theoretical methods [32-35]. The values determined for the indirect band gaps of CdO are summarized in Table 1.2. The energy bands were calculated for two values of ionicity, namely, zero and one [33]. The simplified band structure of CdO for ionic and neutral configuration is shown in Figure 1.2. For ionic configuration, the Fermi level was found to lie just above the valence band. This explained the

Table 1.2

Indirect band gaps of cadmium oxide

Sr. No.	Indirect band gap eV	Remark	References
1	0.8 1.2	-	32
2	0.95 1.11	For ionic configuration	33
3	1.12 1.18	-	34
4	0.8 0.5	-	35

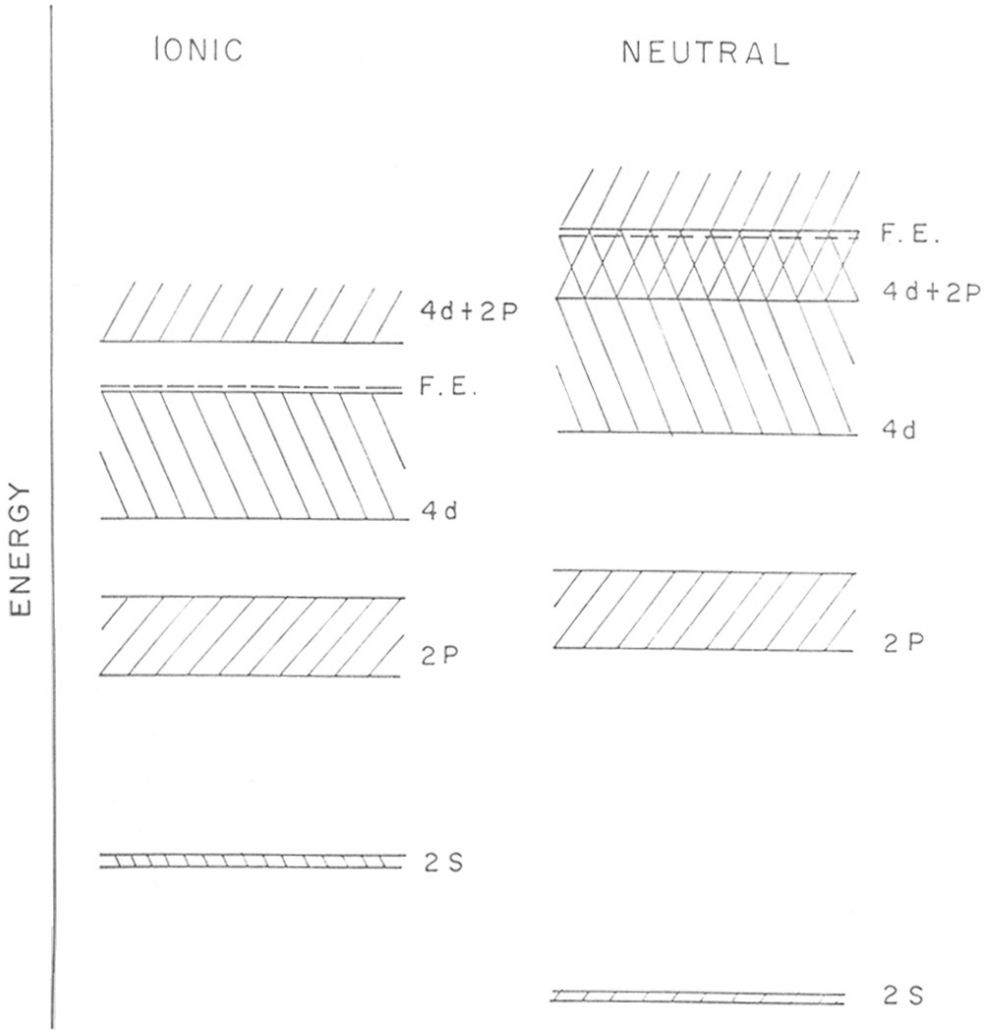

FIG.I.2 SCHEMATIC BAND STRUCTURE OF CdO FOR IONIC AND NEUTRAL CONFIGURATION.[27]

metallic behaviour of CdO. Thus, the pure metallic behaviour was found for neutral CdO, which was observed to change to semiconducting behaviour, when the ionicity was increased from zero to one[33].

1.7 Thin and Thick Films of Cadmium Oxide

The layer structure of the material on suitable support can be called as the film. The thickness of the film can vary from few tens of micron to few tens of Angstrom. The films in the lower range of thickness (Angstrom) are called as thin films, while those in higher range of thickness (microns) are called as thick films. However, general definition of thick films has been given as the films obtained by screen printing and subsequent firing of specially formulated paste onto suitable substrate[36]. On the contrary, thin films can be obtained by various techniques like sputtering, evaporation, vapour deposition, electrodeposition, chemical and laser deposition techniques[37-39]. The films have numerous applications in the electronic industry. The properties of thin and thick films of CdO are summarized below.

The electrical conductivity and absorption in visible region for thin films of CdO have been reported[40].

The films were obtained by sputtering technique. The concentration of the carriers was found to vary with the sputtering parameters. The variation of conductivity with temperature was extrapolated to obtain activation energy of 1.2 eV. The same value was obtained for indirect band gap from the absorption data.

Tanaka and coworkers[41] have reported electrical and optical properties of sputtered CdO films. They have explained their results on the basis of energy band model of degenerated semiconductors. Their schematic energy band diagram of degenerated CdO film is shown in Figure 1.3. The variation in the absorption edge was attributed to the shift of Fermi level caused by the change in carrier concentrations as follows. It was observed that the heat treatment of the films gave rise to the different values of the absorption edge and the carrier concentration. The variation of absorption edge as a function of carrier concentration was plotted. A theoretical curve, based on the band model was obtained. Both the curves were in good agreement. However, for the non-annealed films, the absorption edge was found to decrease with increasing carrier concentration. This variation was not in agreement with the theoretical curve because the band

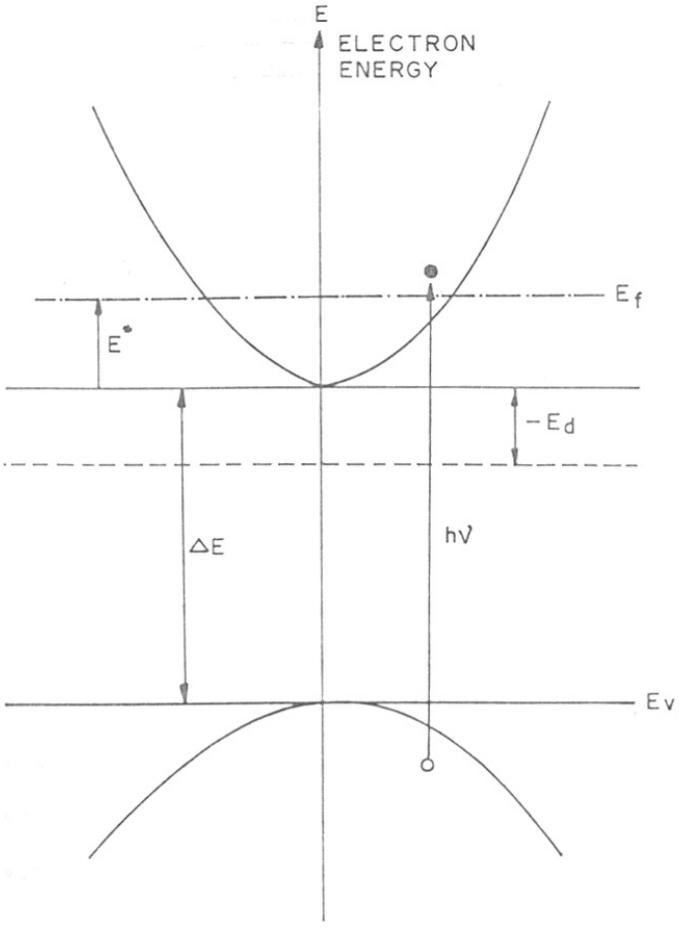

FIG. I.3 SCHEMATIC ENERGY BAND DIAGRAM OF DEGENERATED CdO FILMS[38]

gap (Δ E) and the effective mass (m*) were taken as constant. These quantities were not constant, since the different degree of crystallization led to different energy gap and effective mass. The different degree of crystallization was in turn due to the different sputtering voltages.

Wu and coworkers [42] have studied the electrical properties of thick films of CdO. The sheet resistivity showed linear variation with the valence of dopant for three different types of glass frit binders. The resistivity was lower for the dopants CuO and Cu_2O. This was explained on the basis of deficit type of semiconductor. Further, it was observed that the stability of the films was improved by coating the films with glass or epoxy resin.

Shen-Li Fu and Gi-Chang Lin [43] have also reported the effect of dopant on the electrical properties of thick films of CdO. The sheet resistivity values of undoped film was found to decrease with decreasing amount of the binder. The decrease in sheet resistivity observed for small amount of the dopant Cu_2O was explained on the basis of valency compensation effects.

There is good amount of patent literature [44-46] covering the various aspects of thick films of CdO. The patent literature can be classified into three categories: (1) Compositions containing CdO and glass frit binders [44-48], (2) Compositions where glass contained different additives [49-61] and (3) Compositions where solid solutions of CdO with other oxides were used to prepare thick films of CdO [62-66]. Tables 1.3, 1.4 and 1.5 respectively summarize these compositions.

Table 1.3

Compositions containing CdO and glass frit powders

Composition of paste Wt.% of			Composition of glass Wt.% of							Ref.
CdO	Glass	Organic vehicle	PbO	B_2O_3	SiO_2	SnO_2	CeO_2	ZrO_2	Sb_2O_3	
53.28	20.72	26	78	15	7	-	-	-	-	44
59.26	14.81	25.93	85	10	-	5	-	-	-	45
59.26	14.81	25.93	85	10	-	-	5	-	-	46
59.26	14.81	25.93	85	10	-	-	-	5	-	47
59.26	14.81	25.93	85	10	-	-	-	-	5	48

Table 1.4

Compositions where glass contained different additives

Composition of glass Wt.% of							
BaO	CaO	B_2O_3	Al_2O_3	Additive	Type of Additive	Sheet resistivity Ω/sq.	Ref.
65.984	9.998	13.997	9.998	0.023	ZrO_2	30	49
65.93	10.00	13.99	10.00	0.030	Fe_2O_3	30	50
29.99	10.00	54.99	5.00	0.02	MnO_2	$3x10^4$	51
65.977	9.996	13.996	9.996	0.035	In_2O_3	30	52
65.97	10.00	13.99	10.00	0.04	PbO	30	53
29.970	9.990	54.946	4.995	0.100	Bi_2O_3	$3x10^4$	54
29.996	9.999	54.992	4.999	0.015	SnO_2	$3x10^6$	55
29.996	9.999	54.992	4.998	0.014	CuO	$3x10^6$	56
65.97	10.00	13.99	AlF_3 10.00	0.04	Bi_2O_3	30	57
65.983	9.998	13.996	AlF_3 9.998	0.025	In_2O_3	30	58
65.977	9.997	13.995	AlF_3 9.997	0.034	SnO_2	30	59
65.97	10.00	13.99	AlF_3 10.00	0.04	CuO	30	60
44.78	9.95	29.85	AlF_3 14.93	0.49	ZrO_2	30	61

Table 1.5

Composition of solid solutions of CdO with other oxides used to prepare thick films

Composition of solid solution mole% of		Type of Dopant	Composition of glass Wt.% of			Sheet resistivity k Ω/sq.	Ref.
CdO	Dopant		PbO	B_2O_3	SiO_2		
99	1	Fe_2O_3	85	7.5	7.5	1.5	62
99	1	V_2O_5	85	7.5	7.5	1.5	63
99	1	Nb_2O_5	85	7.5	7.5	1.52	64
99	1	CoO	85	7.5	7.5	1.0	65
99	1	TiO_2	85	7.5	7.5	1.82	66

CHAPTER-2

Synthesis and Physicochemical Techniques of Characterization of Cadmium Oxide Ceramics

2.1 Introduction

Ceramics are the ancient materials[80]. Common and traditional examples of ceramic products are pottery, artware, structural clay products, glass and cement. Unlike such old ceramic, the high-tech ceramics are the high value added materials and are subjects of thrust area programmes of research and development in many laboratories all over the world[81,82]. The experimental research efforts on high-tech ceramics are focussed on what happens to these products at atomic, molecular or microcrystal level during their actual synthesis, characterization and extensive usage[81]. The variety of different experimental and theoretical investigations on these ceramics mainly deal with the synthesis technique and its consequently resulting in better performance parameters[67-69]. For example, many synthesis techniques like attrition milling[67], reaction sintering[68], decomposition of coprecipitated and sol-gel products[69-71], hydrothermal processes[72-75], spray ICP technique[76], arc melting[77], liquid mix technique[78] and solid state reaction[79] have been reported for the preparation of ceramics. Apart from these techniques, there are few other methods of obtaining the materials in the form of films for their numerous applications in the electronic industry. These methods[34-36] include sputtering, evaporation, vapour deposition, electrodeposition, laser

deposition and screen printing. These synthesised ceramics are characterised for their performance parameters by different characterization techniques like, XRD, SEM/EPMA, TEM, ESCA, NMR, IR, ESR, etc. The preparation and physicochemical characterization of cadmium oxide ceramics dealing with (1) synthesis, (2) electronic process and (3) thick film forms are carried out in our laboratory. In the present chapter II, the preparation procedure and the techniques used for the physicochemical characterization of the prepared materials are described.

2.2 Preparation of solid solutions of CdO and MnO ($Cd_{1-x}Mn_xO$)

Commercially available analytical reagent grade cadmium carbonate (Renal Co., Budapest, Hungary) was used to prepare cadmium oxide. The preparation was carried out by the usual decomposition reaction, monitored through the simultaneous DTA/TG/DTG plots. The cadmium carbonate was taken in an platinum dish and covered with platinum foil. The dish was heated at 500°C in an electric furnace for four hours and then allowed to cool down to room temperature outside the furnace. The cooled sample was examined by the X-ray diffractometer to identify the single cubic phase of

CdO. This CdO was used as functional material in the preparation of thick films of CdO.

Cadmium oxide (Danpha Chemicals, India) and manganese carbonate (Sarabhai Chemicals, India) were used for the preparation of solid solutions of CdO and MnO. The solid solutions were prepared by chemical (coprecipitation-decomposition) and ceramic (solid state reaction) techniques. The details of the preparation techniques are given below.

In the chemical procedure, weighed quantities of CdO and $MnCO_3$ were dissolved in about 5N solution of HCl to give clear solution of the ingredients. The 10% solution of $NaHCO_3$ was slowly added to the solution of the ingredients with constant stirring untill white precipitate was formed. The white precipitate was filtered and washed free from chloride ions (Cl^-). The washed precipitate was dried at 100°C for two hours. The precipitate was characterized by thermal analysis. The calcination of the precipitate was carried out at 600°C for 6 hours in an electric furnace. The heated mass was then air quenched to give polycrystalline material. This procedure was followed for the preparation of various compositions listed in Table 2.1.

Table 2.1

Compositions of solid solutions of CdO and MnO

Sr. No.	Mole percent of CdO	Mole percent of MnO	Method of preparation	Nomenclature
1	99.9955	0.0045	Chemical	A
2	99.9911	0.0089	"	B
3	99.9877	0.0123	"	C
4	99.9185	0.0815	"	D
5	100	0	Ceramic	E
6	99.8884	0.1116	"	F
7	99.9877	0.0123	"	G

To follow the standard ceramic technique, the weighed quantities of CdO and $MnCO_3$ were taken in an agate mortar and mixed thoroughly in distilled and dry acetone with an agate pestle untill the mixture was dried. The mixture was then transferred to a clean and dry silica crucible, covered with a silica lid and heated in an electric furnace at 600°C for 6 hours. The heated mass was then air quenched uniform polycrystalline material. The compositions prepared by this procedure are given in Table 2.1. However, the solid solution of CdO containing 0.1116 mole % of MnO composition (F) was allowed to cool in the furnace itself.

2.3 Preparation of glass frit binders

Three different glass frit binders were prepared. The major ingredient was either PbO or ZnO or Bi_2O_3. The other ingredients were B_2O_3, SiO_2 and Al_2O_3. To prepare the glasses, the ingredient materials were dried in an electric oven at 100°C for two hours and cooled in a desicator. Weighed quantities of these dried ingredient materials, needed to give required compositions were wetmilled for 12 hours in a porcelain jar using porcelain balls. The wetmilling was carried out in the medium of distilled and dry acetone. The milled

mixture was then dried and transferred to a clean and dry platinum crucible. The crucible was introduced in an electric muffle furnace at 900°C and heated at this temperature for 30 minutes. The mixture was completely melted. The molten mass was poured into distilled water for fritting the glass. The glass frit was taken in a stainless steel mortar and powdered in distilled water with a stainless steel pestle. The powder was then wetmilled for 24 hours in a porcelain jar using porcelain balls. The wetmilling was done under the medium of distilled water. The milled glass frit powder was examined under optical microscope. The particle size was found to be of the order of 1 to 2 m. The different glasses and their compositions are listed in Table 2.2. This glass frit powders were used as the binders in preparation of thick films of CdO.

2.4 Preparation of thick films of CdO

In general, thick films have been defined as the films obtained by screen printing and firing the specially formulated paste onto an alumina or any other suitable substrate. The paste consists of electrically active materials, a low softening glass, organic fillers and solvents. Each of the components has a definite role to play in achieving good quality thick films.

Table 2.2

Compositions of the glasses prepared

Sr. No.	Weight percent of the ingredients						Nomenclature
	PbO	Bi_2O_3	ZnO	B_2O_3	SiO_2	Al_2O_3	
1	62	-	-	24	12	2	GL-1
2	-	62	-	24	12	2	GL-2
3	-	-	62	24	12	2	GL-3

The components which we have used with their specific role are listed in Table 2.3.

The volatility of the solvent system is an important factor for ease of screening. Excessively volatile solvent tends to dry out during the use and a solvent of very low volatility does not provide good wetting of the particles. Hence, a mixture of three solvents having different volatility is used. β-Terpineol 40%, butyl cellosolve 30% and butyl carbitol acetate 30% are mixed to give a solvent of desired characteristics.

To prepare paste, a weighed quantity of CdO was taken in an agate mortar and the amount of glass frit powder needed to give required composition was added to it and mixed thoroughly in distilled and dry acetone with an agate pestle. This mixture was then dried at 100°C for one hour in an electric oven. Weighed quantity of ethyl cellulose was taken in another clean and dry agate mortar and the amount of organic solvent needed to give the required composition was added to it and mixed thoroughly with an agate pestle. The above mixture of CdO and glass was then added and mixed thoroughly with an agate pestle to give paste-like structure.

This procedure was repeated using different types

Table 2.3

Components used in the paste and their functions

Sr. No.	Components	Materials used	Function of the material	Remarks
1.	Electrically active material	CdO	Conduction	-
2.	Glass frit powders	GL-1 GL-2 GL-3	Binder	GL-1, GL-2 and GL-3 nomenclature is given in Table 2.2
3.	Organic filler	Ethyl cellulose	Filler	-
4.	Organic solvent	β-Terpineol + Butyl cello-solve + Butyl carbitol acetate	Solvent	-

of glass frit powder binders to give the pastes listed in Table 2.4. These pastes were used to obtain thick films of CdO by standard screen printing technique. The films of different geometry were prepared for different types of measurements. The printed films were dried at 150°C for 15 minutes. The solvent was removed during this drying. The prints were then fired at temperature 500, 600, 700, 800 and 900°C for 10 minutes in three zone thick film furnace. In the firing process, the organic binder was burnt off and the glass particle fused and formed a vitreous bond between the CdO particles and the substrate.

2.5 Thermal analysis

Thermal analysis, used to study the physicochemical changes influenced by heating the sample, includes different experimental techniques like, thermogravimetry (TG), differential thermogravimetry (DTG) and differential thermal analysis (DTA). Thermogravimetry is based on the gradual heating of the sample and recording its weight as a function of temperature. The differential thermogravimetry involves the recording of the difference in weight between the sample and the reference material. The differential thermal analysis involves the measurement of the temperature difference between the sample

Table 2.4

Composition of the pastes prepared

Sr. No.	Weight percent of					Nomenclature of paste
	CdO	GL-1	GL-2	GL-3	Org. vehicle	
1	80	-	-	-	20	P-1
2	70	10	-	-	20	P-2
3	70	-	10	-	20	P-3
4	70	-	-	10	20	P-4
5	60	20	-	-	20	P-5
6	60	-	20	-	20	P-6
7	60	-	-	20	20	P-7

and the reference material. The NETZSCH STA 409 model thermal analyser (Netzsch Geratebau GmbH) was used in the present studies. The analyser includes the three experimental techniques. The output of the analyser is in the form of TG, DTG and DTA curves as a function of temperature. In the present work, these curves were obtained for a commercial cadmium carbonate and the coprecipitated samples of cadmium and manganese carbonates.

2.6 Powder X-ray diffraction technique

The use of powder X-ray diffraction technique for the structure analysis of powder materials is based on the Bragg law $n\lambda = 2d \sin\theta$. This law relates the spacing between the (hkl) planes of the lattice, d, and the glancing angle of the X-ray beam, θ . The wavelength of X-ray beam is λ . The Philips X-ray diffractometer model PW 1730 was employed in the present studies. The output of the spectrometer is the intensity of the X-ray reflected as a function of the angular position of the detector. The plotter plots this output as I vs 2θ data. The anode of the X-ray tube can be Cu, Co, Mo etc. Usually the Cu targets are used for inorganic materials because the characteristic α -radiation of the Cu target are suitable for these materials. The

components due to K_β radiations are completely supressed by using Ni filters. In the present work, the powder X-ray diffraction technique is used to study the following aspects:

(i) Detection of phases.

(ii) Determination of cubic lattice parameter.

(iii) Determination of the crystallite size.

2.7 EPR Spectroscopy

The use of electron paramagnetic resonance technique for the macro- and micro-structural investigation of the paramagnetic substances is based on the equation $h\nu = g\beta H$. This law emphasizes the exact matching of the photon radiation energy and the energy separation between the two energy levels. Therefore, the term resonance is applied and the law is called as resonance condition. The BRUKER X-band EPR spectrometer, model ER 200D-SRC was used in the present studies. The spectrometer mainly consists of a magnet, a magnetic power supply unit, a microwave bridge and a console consisting of a time base unit, a signal channel and a field controller. In addition to these four free-standing assemblies, three sub-assemblies are provided. These are a chart recorder, a microwave cavity and a

safety box. The chart recorder is mounted in the console. The cavity is supported between the poles of the magnet by a wave-guide, which connects it to the microwave bridge. The safety box is mounted in the magnet power supply unit. It isolates all power to the system. The output of the spectrometer is in the form of spectrograph covering a selected portion of the microwave region of the electromagnetic spectrum. The spectrograph can be displayed on a cathod ray tube or can also be plotted on a paper. In the present work, the EPR spectroscopy is used to study the following aspects of $CdO:Mn^{2+}$ system:

(i) Detection of various paramagnetic centers in the system.

(ii) Studies of hyperfine and superhyperfine structures in $CdO:Mn^{2+}$ system.

(iii) Detection of impurity phase grown during the aging of the system.

2.8 Scanning electron microscopy

The use of scanning electron microscopy for the topographical analysis of the material is based on the fact that when the material is bombarded with an electron beam, the secondary and backscattered electrons are

emitted from the materials which contains the information of the topology of the specimen. The Cambridge Stereoscan 150 scanning electron microscope was used in the present work. A fine 'probe' of electrons is scanned across the surface of the specimen. The secondary electrons and/or backscattered electrons produce an image on the cathode ray tube. The SEM image is recorded by photographing the face of a cathode ray tube on the negative film of 35 mm, which is developed into the positive scanning electron micrographs. In the present work, scanning electron micrographs of thick films of CdO without containing any binder were recorded.

2.9 Resistivity measurements

Thick films of CdO, 20 mm in length and 5 mm in width were obtained by the procedure described in section 2.4. Air drying type of silver paste was applied at the ends so that 2.5 mm of length of the CdO-film was covered with the silver paste. The dimensions of silver paste applied were 1 cm x 5 mm. The alumina substrate with thick films of CdO and the silver electrode was fixed on a teflon block with the help of phosphor bronze strips so that the strips were placed on the electrodes. The phosphor bronze strips along

with eyelets were screwed on the teflon block. The eyelets were soldered with copper wire. The other ends of the copper wire were fixed to the terminals. The resistance across this terminal was measured using a Yamuna digital multimeter.

The resistance of thick films of CdO, CdO-PbO, CdO-ZnO, CdO-Bi_2O_3 system was measured and sheet resistivity was calculated using the following formula:

$$\sigma_s = R \frac{W}{L}$$

where, σ_s is sheet resistivity, ohm/sq.

R is resistance of the film, ohm.

W is width of the film, mm.

L is the length of the film, mm.

and $\frac{L}{W}$ is called the aspect ratio of thick films.

CHAPTER-3

Characterization of Solid Solutions of CdO and MnO

3.1 Introduction

This chapter describes the physicochemical characterization of solid solutions of CdO and MnO. The solid solutions of $Cd_{1-x}Mn_xO$ system have been characterized using various techniques for their thermal, structural and electrical properties. The techniques used were, simultaneous thermal analysis (DTA/TG/DTG), X-ray diffraction and EPR spectroscopy. The analysis of the resulting experimental data is also presented in this chapter.

3.2 Thermal analysis

Thermal analysis data (TG, DTG and DTA curves) of the dried white precipitate was obtained under the following conditions on Netzsch 409 STA analyser:

Sample size	: 30.4 mg
Reference compound	: α-Al_2O_3
Sample holder	: Platinum crucible
Temperature range	: 25-1000°C
Linear heating rate	: 10°C min^{-1}
Atmosphere	: Air

The data is shown in Fig.3.1. The TG curve shows a loss of 7.3 mg (24.01 weight percent) in the temperature range 282 to 368°C. In this temperature range DTA curve shows an endothermic peak. The probable endothermic reaction in

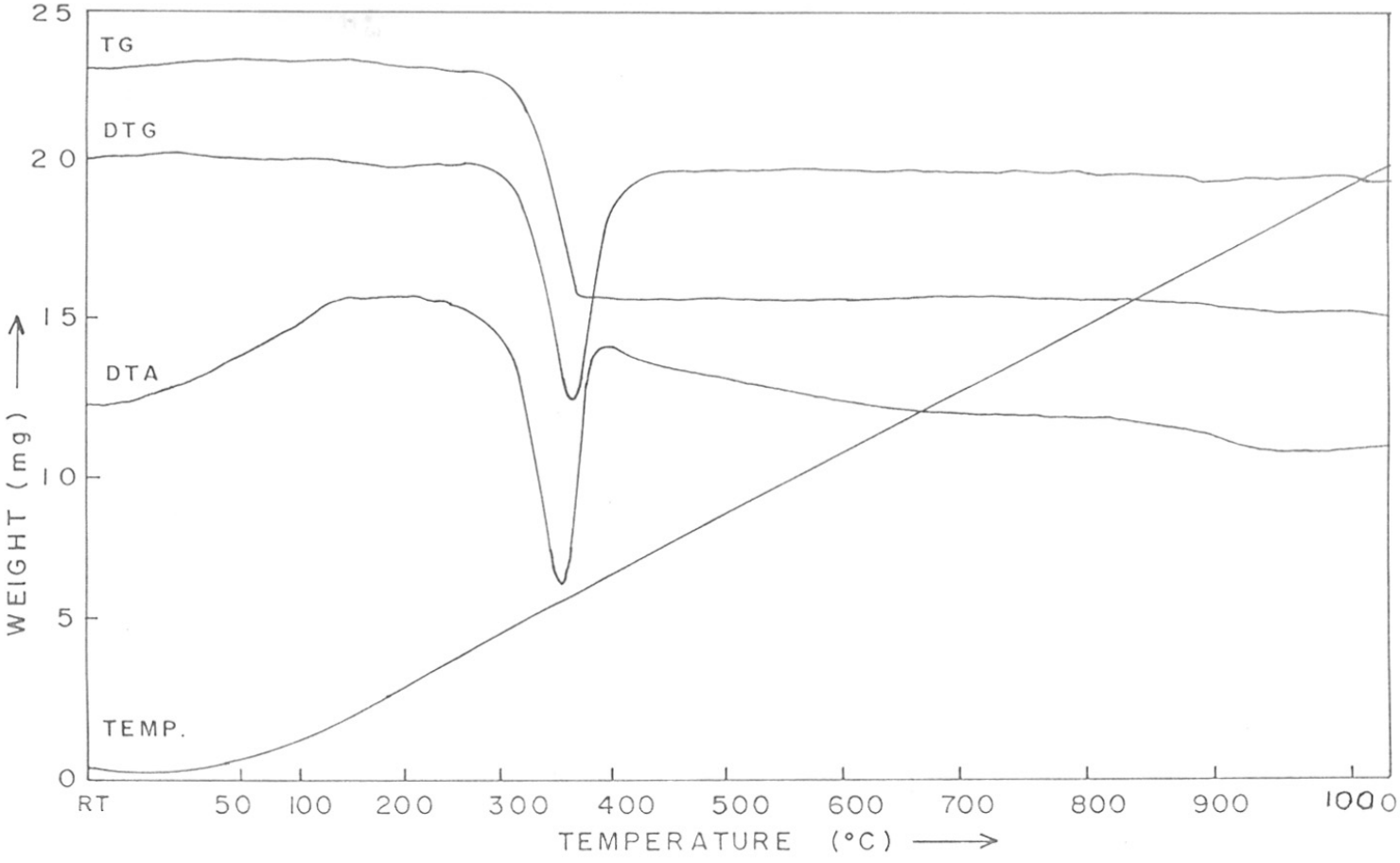

FIG. 3.1 : THERMOGRAM OF PRECIPITATE OF SAMPLE B.

the precipitate is the decomposition of $CdCO_3$ as follows:

$$CdCO_3 \longrightarrow CdO + CO_2 \uparrow$$

This reaction indicates that 30.4 mg of $CdCO_3$ sample shows a loss of 7.8 mg (25.66 weight percent) due to the loss of CO_2. This loss in weight is close to the loss observed from the TG curve. The TG curve further shows no loss in weight till 870°C. In the temperature range 870 to 1000°C, a gradual weight loss corresponding to 0.55 mg is showed by the TG curve. In this temperature range, the DTA curve showed a broad endothermic plateau. This gradual weight loss can be due to the slow vaporization of CdO[8,9]. These studies show that the decomposition of the precipitate can be carried out in temperature range of 368 to 870°C without any significant loss in weight due to the sublimation of CdO. We selected an intermediate temperature of 600°C for the decomposition of our precipitated samples.

3.3 X-ray diffraction studies

The X-ray diffraction patterns of samples A to D - prepared by chemical method, E to F - prepared by ceramic technique and sample F - aged for various time period, were recorded as shown in Figures 3.2, 3.3 and 3.4 respectively. From the patterns, the Bragg angle (2θ) and the normalized

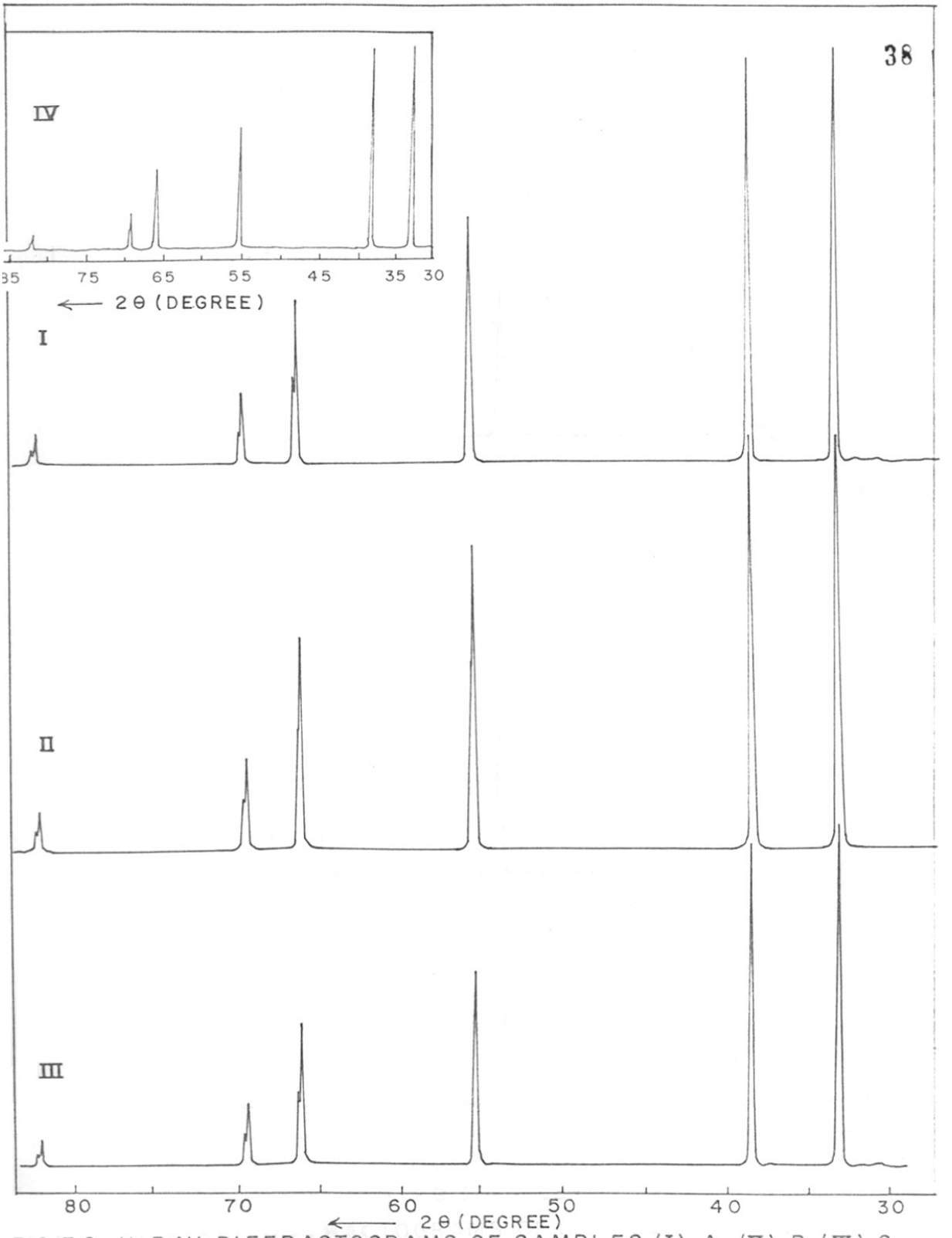

FIG.3.2. X-RAY DIFFRACTOGRAMS OF SAMPLES (I) A ,(II) B ,(III) C AND (IV) D.

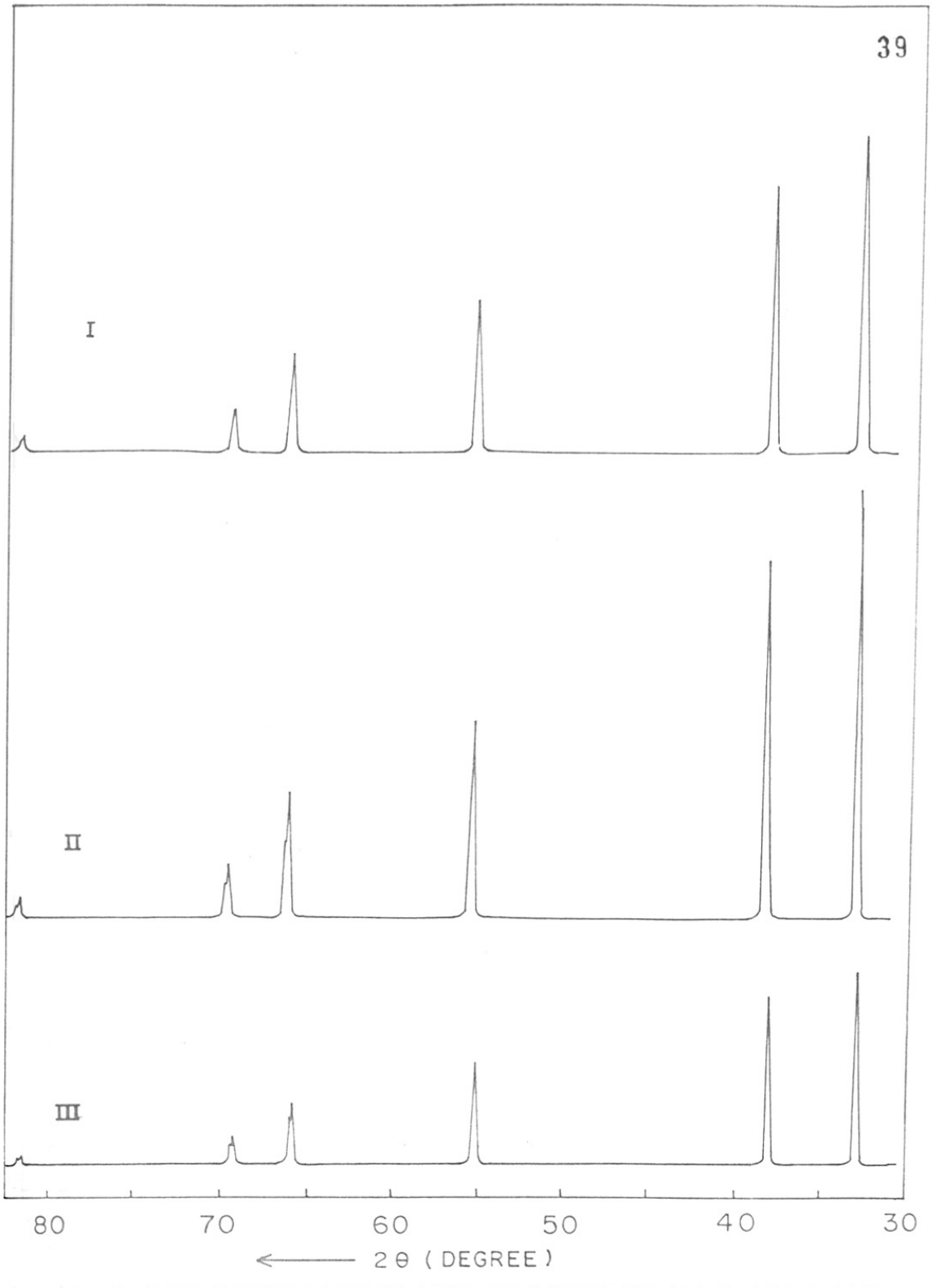

FIG. 3.3. X-RAY DIFFRACTOGRAMS OF SAMPLES (I) E, (II) F AND (III) G.

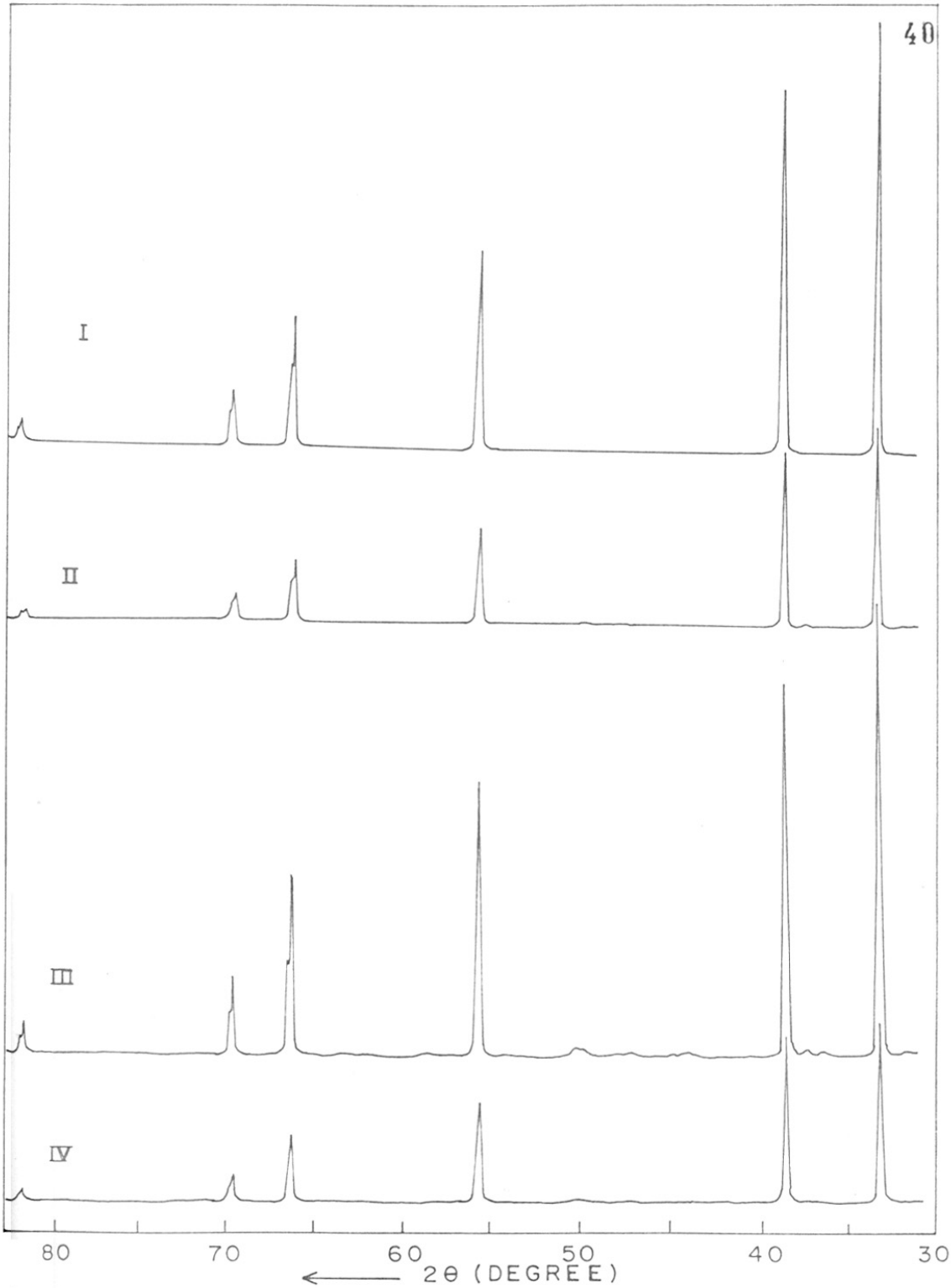

FIG.3.4. X-RAY DIFFRACTOGRAMS OF SAMPLES F FRESHLY PREPARED (I) AND AGED FOR 25 DAYS (II), 126 DAYS (III) AND 186 DAYS (IV)

intensity of the X-ray diffraction peaks were calculated. The d values corresponding to the Bragg angles were calculated from the X-ray conversion table. The d values were compared with the d values of the standard ASTM patterns[83-85] of CdO, $CdCO_3$ and $Cd(OH)_2$ as shown in Tables 3.1, 3.2 and 3.3. The comparison of the prepared sample indicated that they had rock salt structure. Hence, the lattice parameter was calculated using the relation

$$d_{hkl} = \left[\frac{h^2 + k^2 + l^2}{a^2}\right]^{-\frac{1}{2}}$$

The values of the lattice parameter for the samples are summarized in Table 3.4. The structural data of the aged sample (Table 3.3) showed the presence of impurity phases like $CdCO_3$ (hexagonal), $Cd(OH)_2$ (hexagonal) and a small amount of unidentified impurity (crystalline) phase. The impurity phases grow during the aging period. The aging effects are further discussed in section 3.7 of the present chapter.

3.4 Spin Hamiltonian formalism

The general approach of the interpretation of the EPR spectra is based on the spin Hamiltonian formalism[86-90]. The approach has been stated to have two advantages[86].

Table 3.1

Structural data for samples prepared by chemical method

Sr. No.	Sample-A			Sample-B			Sample-C			Sample-D			Reported data for cubic CdO		
	Int.	2θ Degree	d A	Int.	2θ Degree	d A	Int.	2θ Degree	d A	Int.	2θ Degree	d A	Int.	d A	hkl
1	100	33.10	2.7040	100	33.20	2.6961	100	33.08	2.7056	100	33.08	2.7056	100	2.712	111
2	88	38.36	2.3445	93	38.54	2.3339	75	38.32	2.3468	93	38.42	2.3410	88	2.349	200
3	43	55.40	1.6570	55	55.48	1.6548	45	55.34	1.6587	43	55.34	1.6587	43	1.661	220
4	29	66.02	1.4139	40	66.10	1.4123	30	65.98	1.4146	28	65.98	1.4146	28	1.416	311
5	13	69.34	1.3540	70	69.44	1.3523	14	69.32	1.3544	12	69.34	1.3540	13	1.355	222
6	6	82.18	1.1719	7	82.18	1.1719	6	82.08	1.1731	5	82.08	1.1731	5	1.1742	400

Table 3.2

Structural data for samples prepared by ceramic technique

Sr. No.	Sample-E			Sample-F			Sample-G			Reported data for CdO		
	Int.	2 θ Degree	d A	Int.	2 θ Degree	d A	Int.	2 θ Degree	d A	Int.	d A	hkl
1	100	33.08	2.7056	100	33.00	2.7120	100	32.50	2.8376	100	2.712	111
2	86	33.38	2.3435	84	38.34	2.3457	86	38.22	2.3527	88	2.349	100
3	48	55.34	1.6587	46	55.38	1.6576	49	55.20	1.6625	43	1.661	220
4	31	66.00	1.4142	30	66.00	1.4142	30	65.80	1.4180	28	1.416	311
5	13	69.30	1.3547	13	69.34	1.3540	12	69.16	1.3571	13	1.355	222
6	5	82.16	1.1722	5	82.16	1.1722	6	81.86	1.1757	5	1.1742	400

Table 3.3A

Structural data for sample-F aged for various time period

Sr. No.	Freshly prepared			Aged for 25 days			Aged for 126 days			Aged for 185 days			Reported data for CdO	
	Int.	2θ Degree	d Å	Int.	2θ Degree	d Å	Int.	2θ Degree	d Å	Int.	2θ Degree	d Å	Int.	d Å
1	100	33.00	2.7120	100	32.98	2.7136	100	33.02	2.7104	100	33.08	2.2056	100	2.710
2	84	38.34	2.3457	88	38.24	2.3516	86	33.38	2.3433	92	38.44	2.3398	88	2.349
3	46	55.38	1.6576	40	55.22	1.6625	48	55.40	1.6570	52	55.36	1.6581	43	1.661
4	30	66.00	1.4142	30	65.88	1.4165	32	66.00	1.4142	35	66.10	1.4123	28	1.410
5	13	69.34	1.3540	13	69.20	1.3564	14	69.48	1.3517	15	69.44	1.3523	13	1.355
6	5	82.16	1.1722	4	81.98	1.1743	5	82.24	1.1712	6	82.20	1.1717	5	1.1742

Table 3.3B

Additional X-ray diffraction peaks observed after various aging time period

Aging period days	Additional peaks Int.	2 θ Degree	d Å	Corresponding $CdCO_3$ Int.	d Å	Peaks for $Cd(OH)_2$ Int.	d Å
	1	31.50	2.8376	100	2.94		
25	2	37.18	2.4161	50	2.46		
	1	47.16	1.9255	80	1.83		
	0.5	49.60	1.8363	40	1.58		
	0.4	31.58	2.8306	100	2.94		
	0.8	36.44	2.4635	50	2.46		
	0.8	37.28	2.4099	-	-		
	0.6	43.98	2.0570	45	2.06		
	0.6	44.70	2.0256	-	-		
126	0.4	47.16	1.9255	33	1.88		
	0.8	49.60	1.8363	80	1.83		
	0.8	50.04	1.8212	-	-		
	0.4	58.36	1.5803	40	1.58		
	0.4	61.88	1.4981	17	1.50		
	0.4	63.16	1.4708	5	1.47		
	0.6	31.50	2.8376	100	2.94		
	0.6	35.50	2.5265	-	-	100	2.56
	0.6	36.60	2.4531	50	2.46		
	1.3	37.28	2.4099	-	-		
186	0.6	43.98	2.0570	45	2.06		
	0.6	44.66	2.0273	-	-		
	0.6	47.20	1.9239	33	1.88		
	1.9	49.90	1.8260	80	1.83		

Table 3.4

The lattice parameter value for the prepared samples

Sample	Mole percent of		Lattice parameter, a Å
	CdO	MnO	
A	99.9955	0.0045	4.688
B	99.9911	0.0089	4.684
C	99.9877	0.0123	4.692
D	99.9185	0.0815	4.691
E	100	0	4.691
F	99.8884	0.1116	4.689
G	99.9877	0.0123	4.702

(1) The choice of the spin multiplicity used for the interpretation of the EPR spectra is determined by the nature of the spectra. (2) Different interactions can easily be considered by adding the appropriate terms to the Hamiltonian. The general solution of the spin Hamiltonian has been reported by several investigators[91-105]. However, these solutions are cumbersome and have been replaced by simpler formulations that deals with particular cases of interest[86]. For example, the spin Hamiltonian for Mn^{2+} ions in orthorhombic symmetry is given as[106]

$$\mathcal{H} = g\beta\, H.S + \frac{a}{6}\left[S_x^4 + S_y^4 + S_z^4 - \frac{1}{5}S\,(S+1)(3S^2 + 3S-1)\right]$$

$$+ \frac{F}{180}\left[35S_z^4 - 30S\,(S+1)\,S_z^2 + 25S_z^2 - 6S\,(S+1) + 3S^2\,(S+1))\right]^2 + D\left[S_z^2 - \frac{1}{3}S\,(S+1)\right] + E\left[S_x^2 - S_y^2\right]$$

$$+ AS.I - g_I \beta_N\, H.I + P\left[I_z^2 - \frac{1}{3}I(I+1))\right] \ldots\ldots \quad (1)$$

where S and I are the electron and nuclear spin, g and g_I are the electron and nuclear gyromagnetic ratios, β and β_N are Bohr and nuclear magnetons, a is the cubic zerofield splitting parameter[106] and D, E and F are axial zerofield splitting parameters[86]. The parameters a and F essentially represent a cubic field plus a tetragonal

distortion. Generally, the values of the parameters associated with the quartic operators, a and F, are smaller than the parameters arising from the quadratic operators, D and E[106]. Hence, the terms with a and F are often neglected in the literature. The spin Hamiltonian, therefore, becomes

$$\mathcal{H} = g\beta H.S + D[S_z^2 - \tfrac{1}{3}S(S+1)] + E[S_x^2 - S_y^2]$$

$$+ A\,S.I + P[I_z^2 - \tfrac{1}{3}I(I+1)] - g_I\beta_N H.I \quad \ldots\ldots (2)$$

where g factor and hyperfine coupling constant A are isotropic within the experimental error. The Hamiltonian gives $(2S + 1)(2I + 1) = 36$ spin states. The five allowed transitions between the states $|M,m\rangle \leftrightarrow |M-1, m\rangle$ are defined by selection rule $\Delta M = \pm 1$ and $\Delta m = 0$ where M and m are respectively the magnetic quantum numbers for the electron spin (S) and the nuclear spin (I). The six allowed lines corresponding to $|\tfrac{1}{2}, m\rangle \leftrightarrow |-\tfrac{1}{2}, m\rangle$ transitions are readily seen in polycrystalline samples at magnetic field[88,106].

$$H = H_\circ + Am + (A^2/2H_\circ)(\tfrac{35}{4} - m) \quad \ldots\ldots (3)$$

Ten forbidden transitions (defined by selection rule $\Delta M = \pm 1$ and $\Delta m = \pm 1$) between the states $|\tfrac{1}{2}\,m\rangle \leftrightarrow |-\tfrac{1}{2}\,m-1\rangle$ and $|\tfrac{1}{2}\,m-1\rangle \leftrightarrow |-\tfrac{1}{2}\,m\rangle$ can also be seen in

polycrystalline samples at[106]

$$H = H_o + A(m-\frac{1}{2}) \pm (\frac{A^2}{2H_o})(\frac{17}{2}) + (\frac{A^2}{2H_o})$$

$$(\frac{33}{4} + m(m-1)) \pm g_I \beta_N H_o + P(2m-1) \qquad ...(4)$$

The ratio of the intensities of the forbidden to allowed lines is[106,107]

$$\frac{I_F}{I_A} = \frac{512}{15} (\frac{35}{4} - m^2 + m)(\frac{D^2}{H_o})^2 \qquad ..... (5)$$

Equation (4) gives the doublet splitting of the forbidden lines as

$$\delta_m = (\frac{A^2}{H_o})(\frac{17}{2}) + 2g_I \beta_N H_o + 2P(2m-1) \qquad .....(6)$$

The equation (6) for specific values of m reduces to

$$\delta_{5/2} - \delta_{-3/2} = 16P \qquad ..... (7)$$

The superhyperfine interaction of unpaired electrons of Mn^{2+} with Cd nuclei of nonzero spin can be accounted for, by adding the $A_{SHF}S.I$ term to the spin Hamiltonian of equation (1). This term gives rise to a (2n I+1) number of lines, where n is number of equivalent Cd nuclei with

nonzero nuclear spin I. These lines correspond to $|m, \bar{m}_I\rangle \longleftrightarrow |-m, -\bar{m}_I\rangle$ transitions. The position of the lines can be given as

$$H = H' + A_{SHF}\,\bar{m}_I \qquad \ldots\ldots (8)$$

where H' is the magnetic field at the centre of the super-hyperfine lines and $\bar{m}_I$ is the sum of the nuclear spins of the Cd nuclei.

These equations (1)-(8) will now be used to interpret the ESR spectra (of Mn^{2+} in CdO) at room temperature and are described in the next section 3.5.

3.5 EPR spectra of the prepared solid solutions of CdO and MnO

The wide range EPR spectra of the samples were obtained under the following experimental conditions:

Nature of sample : Polycrystalline solid
Temperature : Room temperature
Microwave frequency : 9.4 to 9.8 GHz
Microwave power : 20 dB, 2 mW
Modulation frequency: 100 KHz
Modulation intensity: 1.25 Gpp

Centre field : 3500 G

Scan range : 5000 G

Scan time : 200 S

The spectra of sample A to D are shown in Figure 3.5 A to D. While Figure 3.6 A to C presents the spectra of samples F and G. From the spectra, the g values for the observed EPR signals were calculated by using the resonance condition described in section 2.6. The main observations of the spectra are listed below:

(1) All samples showed hyperfine sextet centered at g = 1.999.

(2) The samples also showed a central signal at g = 1.985.

(3) Two EPR lines at g = 2.186 and 2.236 are observed for the samples synthesized by chemical method.

(4) For samples obtained by ceramic technique, a EPR line at g = 2.182 is observed.

The observations can be explained by using the reported literature of the related systems. Hyperfine sextet, centered at g values close to the free electron value g_e, have been observed for Mn^{2+} ions in different polycrystalline oxides systems [108-125]. Our observation (1) is thus characteristic of Mn^{2+} ions in polycrystalline CdO. The

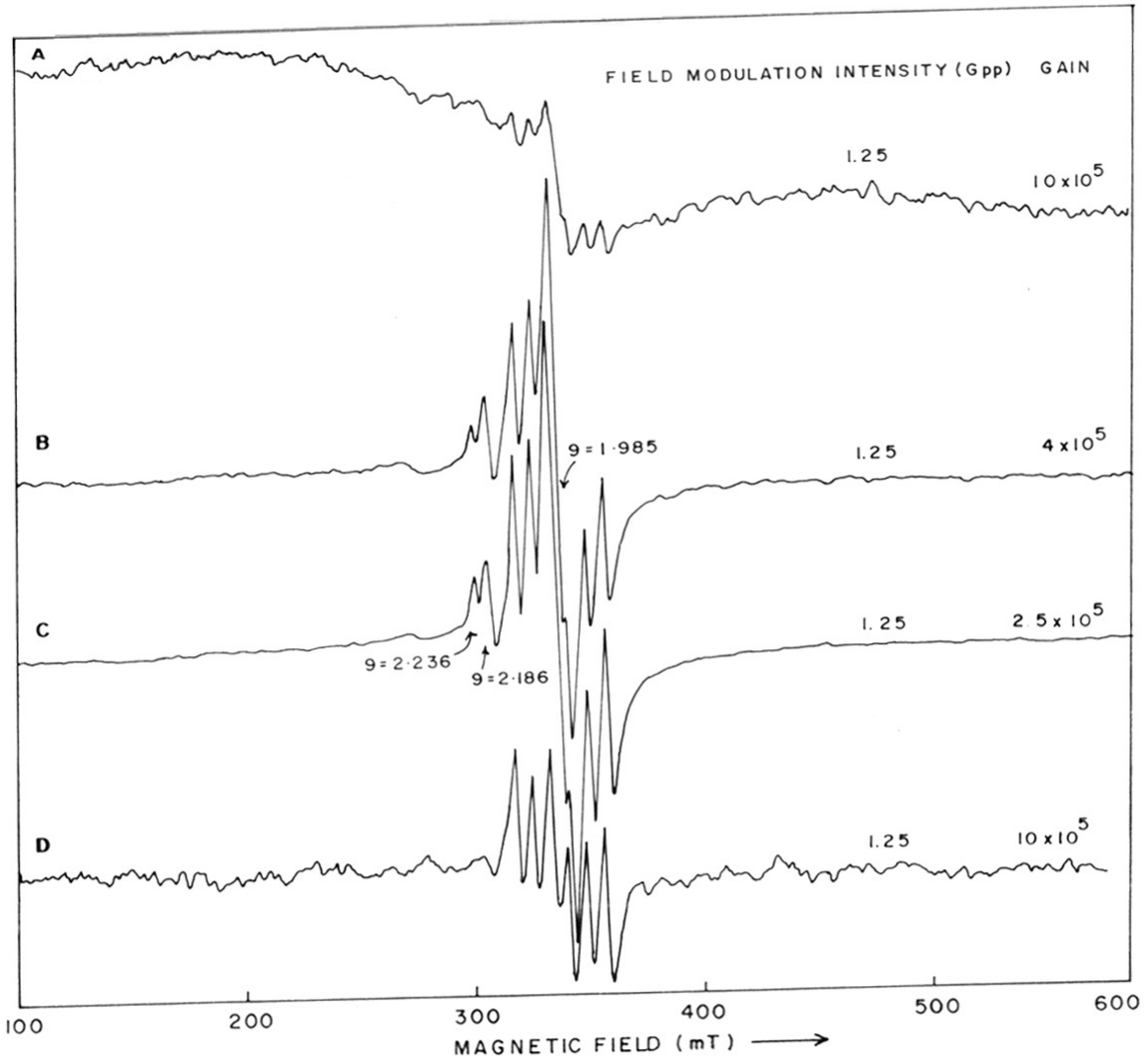

FIG. 3.5 EPR SPECTRA OF SAMPLES A, B, C AND D.

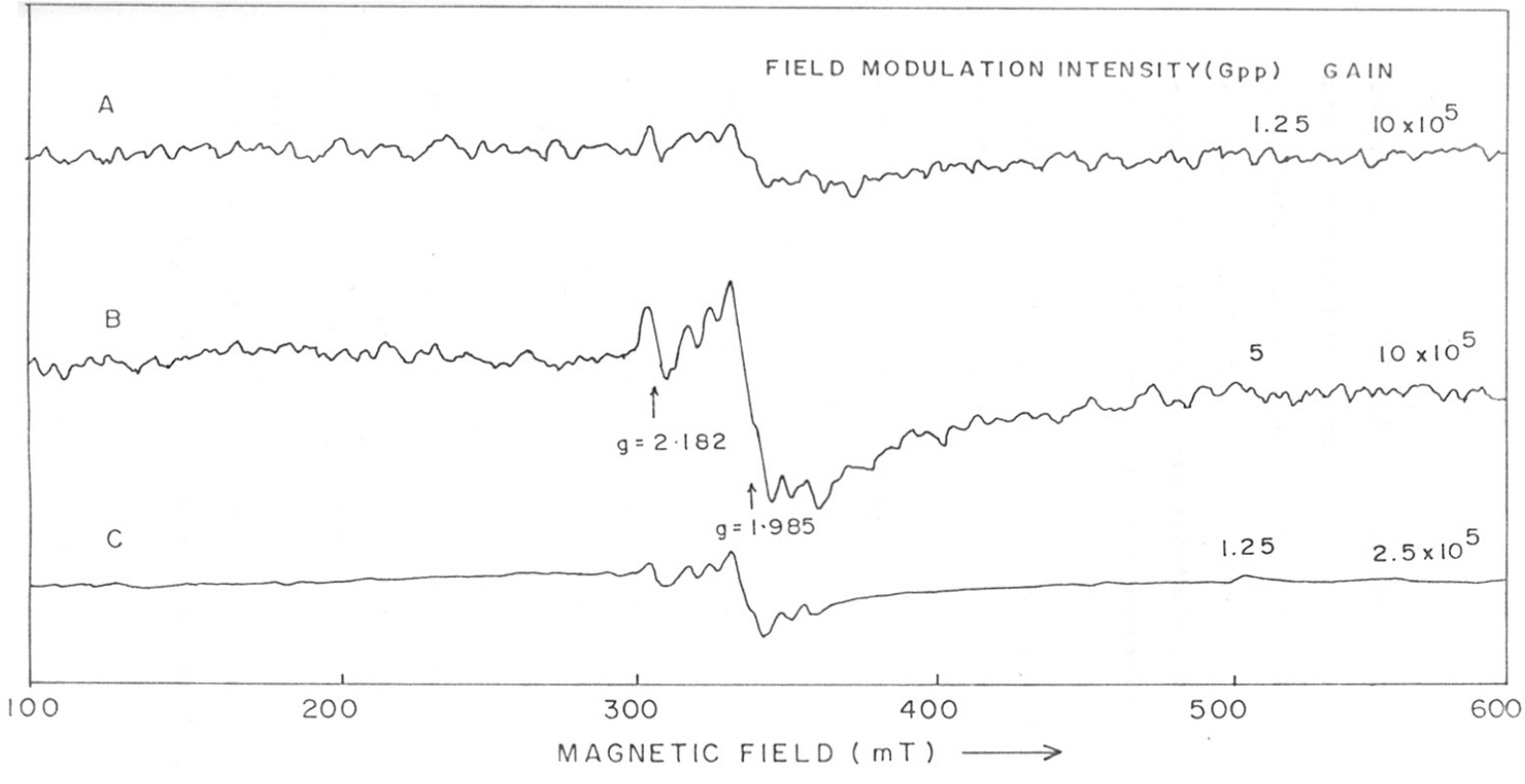

FIG. 3.6 EPR SPECTRA OF SAMPLES F (A AND B) AND G (C)

observation (2) and (4) are similar to the observations made by EPR studies of different specimens of CdO. Elshner and Schlaak[30] have reported EPR studies of single crystals of CdO. A signal at g = 1.977 was observed at room temperature. The signal was attributed to the Cd^{+} ion at the site of Cd^{++} ion. The same paramagnetic centers (Cd^{+} ions) were studied by Meinhold[31] in polycrystalline samples of CdO sintered at different temperatures. He observed the EPR signals at g = 1.97 and 1.98 respectively for CdO samples sintered at 750°C and 1000°C. Both the signals were assigned to the paramagnetic centers, Cd^{+} ions in place of Cd^{++} ions. The g value of 1.985 observed by us for the central signal (observation 2) is very close to the value 1.98 reported for Cd^{+} ion in CdO by Meinhold. Hence, the central signal can arise due to the Cd^{+} centers. Meinhold further observed an EPR signal at g = 2.17 due to the F-centres present in their samples. We have observed similar type of signal at g = 2.186 (observation 3) or 2.182 (observation 4) for our samples. These signals may arise due to F-centers. Lastly, the signal at g = 2.236 can be attributed to the R-centers formed upon the aggregation of the F-centers[126,127]. This signal is observed only in samples prepared by chemical method. This can be explained on the basis of different heating effects in the two preparation techniques. The heating of CdO has

been reported to cause a change in the EPR signal at g = 2.17 due to the loss of F-center on heating. Thus, in samples prepared by ceramic techniques, the F-centers are less in number to aggregate and produce R-centers.

3.6 Hyperfine lines

The high resolution technique is used to study the hyperfine lines. The EPR spectrum recorded at higher resolution scan for sample C is shown in Figure 3.7. A sextet of sharp lines and doublets of weak lines in between the adjacent pairs of the sharp lines are observed. The observations are characteristic of Mn^{2+} ions in different oxide systems[108-125]. The observed sextet of sharp lines are the allowed hyperfine lines corresponding to $|\frac{1}{2}, m\rangle \longleftrightarrow |-\frac{1}{2}, m\rangle$ transitions. Each line of the sextet can be designated by the values between $-\frac{5}{2}$ to $+\frac{5}{2}$ observed by m[87]. The weak doublets are the forbidden lines corresponding to $|\frac{1}{2}, m-1\rangle \longleftrightarrow |-\frac{1}{2}, m\rangle$ and $|\frac{1}{2}, m\rangle \longleftrightarrow |-\frac{1}{2}, m-1\rangle$ transitions. These allowed and forbidden lines were used to determine the spin Hamiltonian parameters.

The allowed six lines are centered at g = 1.999 with average hyperfine splitting |A| = 7.8 mT. The amplitude of the allowed lines were used in equation (5) to give the axial zero-field splitting parameter D = 3.5 mT. The

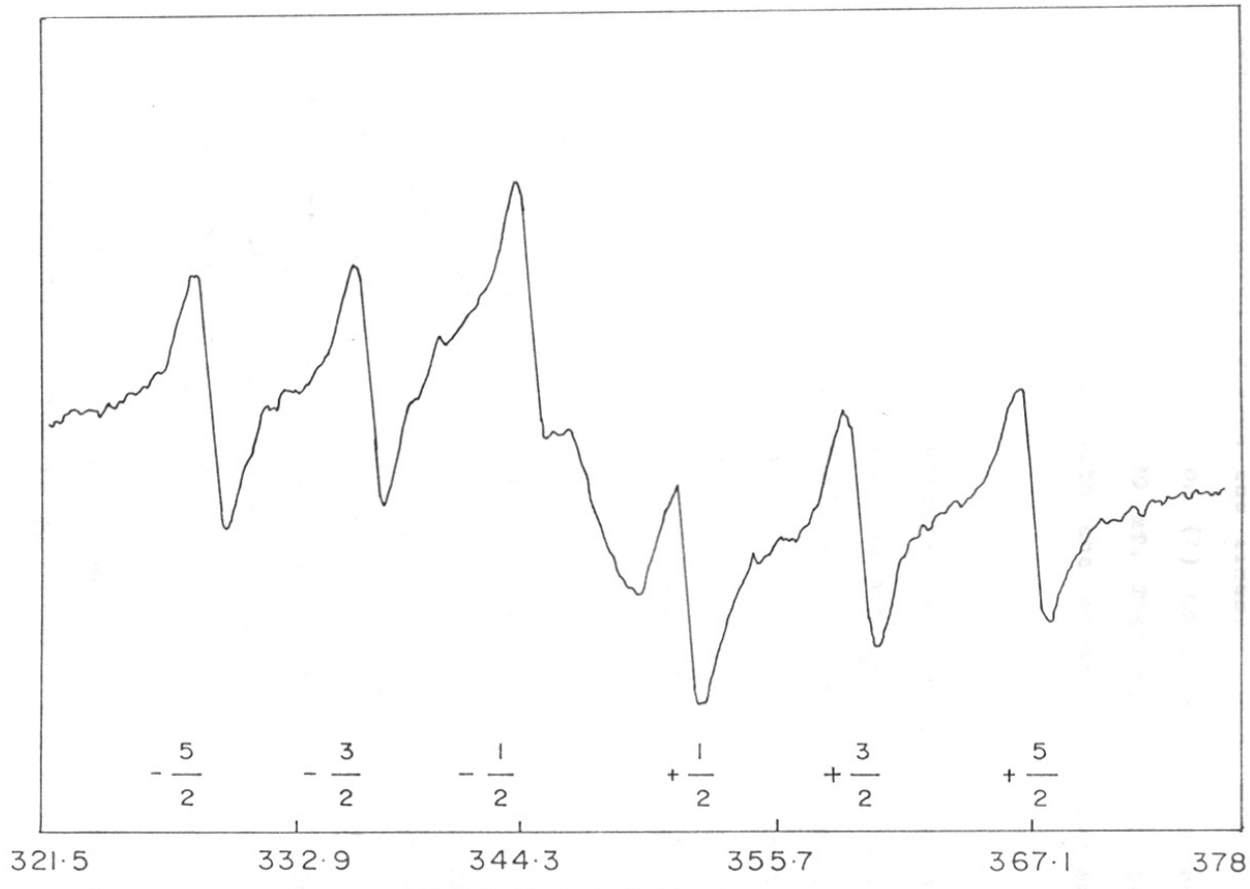

FIG.3.7 : EPR DERIVATIVE SILNAL OF Mn^{2+} IONS IN POLYCRYSTALLINE CdO (SAMPLE C).

doublet separation between the lines, $\delta_{+5/2}$ and $\delta_{-3/2}$, were substituted in equation (7) to give the nuclear quadrupole term |P| = 0.039 mT. The spin Hamiltonian parameters are compared with the other cubic system in Table 3.5.

The experimental parameters were substituted in equation (3) and (4) to predict the positions of the allowed and the forbidden lines. The predicted positions of these lines are compared with the observed positions in Table 3.6. It is really interesting to note the close agreement between the predicted and the observed line positions.

3.7 Superhyperfine lines

Six set of seven weak lines were superimposed on each of the six allowed hyperfine lines. The EPR spectrum of each of the allowed lines was recorded at higher resolution scan. One of the lines with lowest resonance field recorded at higher resolution scan is shown in Figure 3.8. Seven lines are clearly observed with experimental intensity ratio 0.8 : 12.3 : 68.8 : 128.1 : 68.0 : 12.0 : 0.8.

The six set of seven weak lines are the superhyperfine lines corresponding to the $|m\ \bar{m}_I\rangle \longleftrightarrow |-m-\bar{m}_I\rangle$ transitions. The superhyperfine lines have earlier been

Table 3.5

Spin Hamiltonian parameters for Mn^{2+} ions in different hosts

Host	g	A_{HF} mT	D mT	P mT	A_{SHF} mT	Ref.
CdO	1.999	7.8	3.5	0.039	0.36	Present work
MgO	2.0014	8.1	1.86	-	-	114
$MgAl_2O_4$	2.00	8.3	6.4	0.03	-	106

Table 3.6

Calculated and observed positions of allowed and forbidden lines for $CdO:Mn^{2+}$ system

m	Position of allowed lines in mT		Position of forbidden lines in mT		Doublet separation		
	Obs.	Cal.	Obs.	Cal.	Symbol	Obs.	Cal.
$\frac{5}{2}$	368.09	367.78	364.53 362.97	364.48 362.06	5/2	1.56	2.42
$\frac{3}{2}$	360.19	360.33	356.41 354.83	356.36 354.08	3/2	1.58	2.28
$\frac{1}{2}$	350.93	349.61	-	348.40 346.27	1/2	-	2.13
$-\frac{1}{2}$	344.37	341.02	340.17 338.67	340.62 338.63	-1/2	1.50	1.99
$-\frac{3}{2}$	336.68	336.95	332.90 331.97	333.02 331.17	-3/2	0.93	1.85
$-\frac{5}{2}$	329.27	328.81	-	-	-	-	-

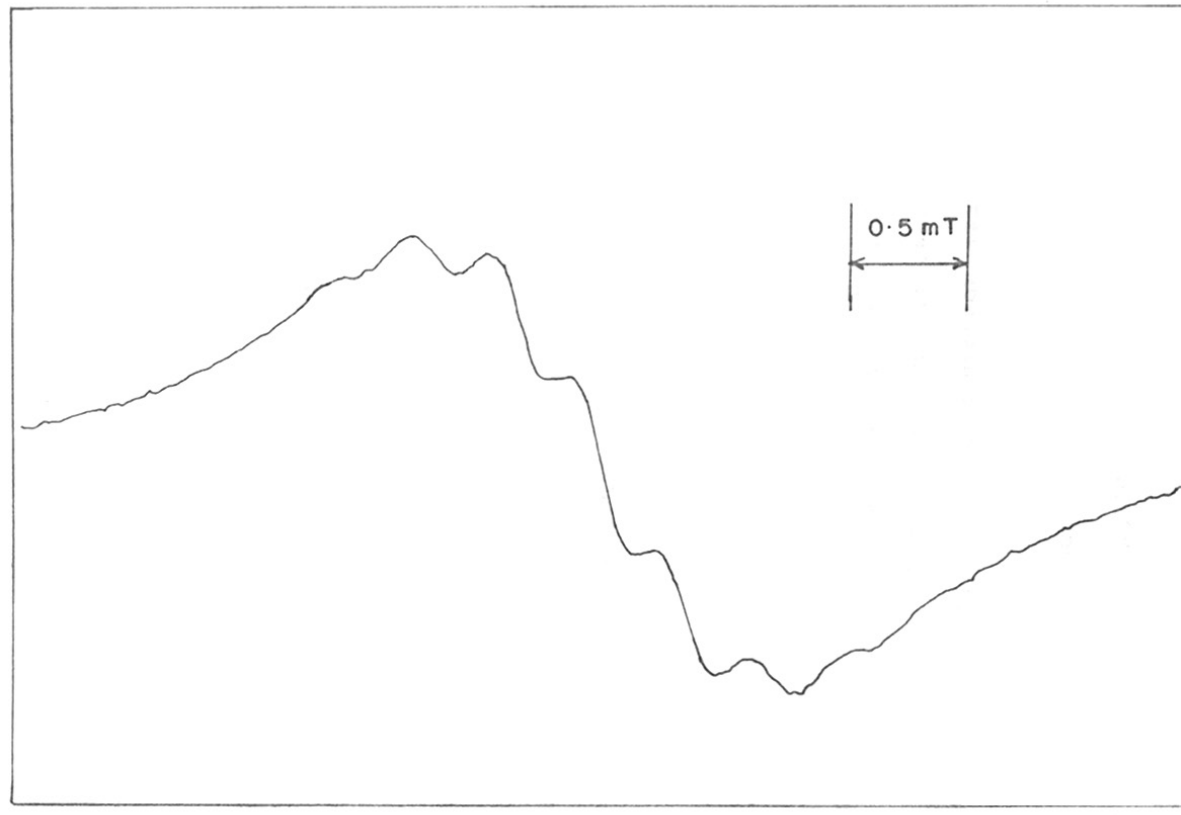

FIG. 3.8 : HIGH RESOLUTION EPR SPECTRUM OF Mn^{2+} IONS IN POLYCRYSTALLINE CdO (SAMPLE C) CORRESPONDING TO LOWER FIELD PEAK OF THE SIX LINES.

observed for CdS:Mn^{2+} system[128,129]. It was shown that unpaired electrons of Mn^{2+} interact with neighbouring ^{111}Cd and ^{113}Cd nuclei to give superhyperfine lines. The total natural abundance of these odd isotopes was taken as 25% because the magnetic moment values of ^{111}Cd ($I = \frac{1}{2}$, $\mu = 0.592\ \mu_n$) and ^{113}Cd ($I = \frac{1}{2}$, $\mu = 0.619\ \mu_n$) differ only by 4.5 percent[124,129]. The distribution of these two odd isotopes around Mn^{2+} ions was used to calculate the intensity ratio of the superhyperfine lines[128,129].

Our X-ray diffraction study of the samples has showed that the samples exhibit NaCl-type of structure. Mn^{2+} occupying normal substitution site in CdO will have six oxygen atoms at a distance of $\frac{a}{2}$ and twelve cadmium atoms at a distance of $\frac{a}{\sqrt{2}}$ as nearest neighbours[124]. The six oxygen atoms are directly bonded to the Mn^{2+} ion. Out of twelve neighbouring Cd ions, a group of four Cd ions is bonded through each of six oxygen ions to the Mn^{2+} ion. Now as 25% of naturally occuring Cd nuclei have nonzero spin, one out of four Cd nuclei will have nonzero spin. Thus, the Mn^{2+} ion is bonded to one Cd nuclei having nonzero spin through each of the six oxygen. Therefore, six equivalent Cd nuclei ($n = 6$), having nonzero spin ($I = \frac{1}{2}$), will give seven lines as observed by us. However, to calculate the intensity ratio of these lines, total

probable distribution of the odd isotopes of Cd amongst the twelve Cd neighbours is considered. As the total natural abundance of odd isotope of Cd is 25%, the twelve Cd nuclei will have three odd isotopes of Cd. This is the most probable distribution. Proceeding according to the procedure of Hitashi et al[129], the other probable distributions and their abundances were found. The abundance of three Cd nuclei, all having zero spin, one of them having nonzero spin, two of them having nonzero spin and all three having nonzero spin is 0.75^3, $3x0.75^2$ x 0.25/2, $3x0.75x0.25^2/4$ and $0.25^3/8$ respectively. This is equivalent to 128 : 64 : 10.67 : 0.59 respectively. Thus, theoretical intensity ratio is 1 : 11 : 64 : 128 : 11 : 1. The theoretical intensity ratio is in good agreement with the experimental intensity ratio.

The positions of superhyperfine lines were predicted by using the equation (8). The predicted positions are in good agreement with the observed positions as seen from the Table 3.7. The average splitting of these lines gave the magnitude of the superhyperfine splitting as A_{SHF} = 0.36 mT.

3.8 Aging effects

The EPR spectra of sample F aged for various time

Table 3.7

Calculated and observed positions of superhyperfine lines

Designation of hyperfine lines	Designation of superhyperfine lines	Position of superhyperfine lines (in mT)	
m	$\bar{m}_I$	Observed	Calculated
	+ 3	368.73	368.72
	+ 2	368.44	368.36
	+ 1	368.01	368.00
+ 5/2	0	367.66	367.63
	- 1	367.23	367.27
	- 2	366.79	366.90
	- 3	366.54	366.54
	+ 3	360.78	360.86
	+ 2	360.38	360.42
	+ 1	360.03	360.06
+ 3/2	0	359.61	359.70
	- 1	359.26	359.34
	- 2	358.94	358.98
	- 3	358.63	358.63
	+ 3	353.08	353.08
	+ 2	352.85	352.72
	+ 1	352.53	352.37
+ 1/2	0	352.15	352.01
	- 1	351.78	351.66
	- 2	351.43	351.31
	- 3	350.95	350.95
	+ 3	345.28	345.28
	+ 2	344.83	344.89
	+ 1	344.44	344.48
- 1/2	0	344.09	344.13
	- 1	343.75	343.72
	- 2	343.30	343.36
	- 3	342.98	342.98
	+ 3	337.65	337.65
	+ 2	337.31	337.28
	+ 1	336.95	336.91
- 3/2	0	336.58	336.54
	- 1	336.20	336.17
	- 2	335.73	335.80
	- 3	335.43	335.43
	+ 3	330.48	330.48
	+ 2	330.05	330.07
	+ 1	329.60	329.67
- 5/2	0	329.24	329.26
	- 1	328.86	328.86
	- 2	328.37	328.45
	- 3	328.05	328.05

period are shown in Figure 3.9 A to E. The freshly prepared sample was required to record at higher gain and modulation amplitude to observe the signals as shown in Figure 3.8 A and B. The aged samples (Figure 3.9 C to E) show an EPR signal at g = 2.778 in addition to the signals described in section 3.4. The linewidth of the signal is ΔH_{pp} = 1500 G. This type of broad signal have not yet been observed in systems containing Mn^{2+} ions. However, for isoelectronic Fe^{3+} in NH_4-y zeolite[130], it has been observed at g = 2.3 with ΔH_{pp} = 1300 G. In this system, the signal was assigned to hydroxy oxidic compounds of Fe^{3+}. In our X-ray diffraction studies of aged sample (section 3.2), impurity phases of $CdCO_3$, $Cd(OH)_2$, unidentified impurity were detected. Hence, Mn^{2+} in these impurity phases are likely to give such types of additional signal in the aged sample.

The EPR spectra of aged samples were recorded using the high resolution technique as shown in Figure 3.10 A to E. The freshly prepared sample shows a very weak hyperfine sextet even with relative higher gain of 10 x 10^5 (Figure 3.10A). On increasing the modulation amplitude, the sextet appears as shown in Figure 3.10 B. The aged samples show an additional hyperfine sextet growing with the period of aging (Figure 3.10 C to E). The new hyperfine sextet is prominent for the sample aged for 240 days as

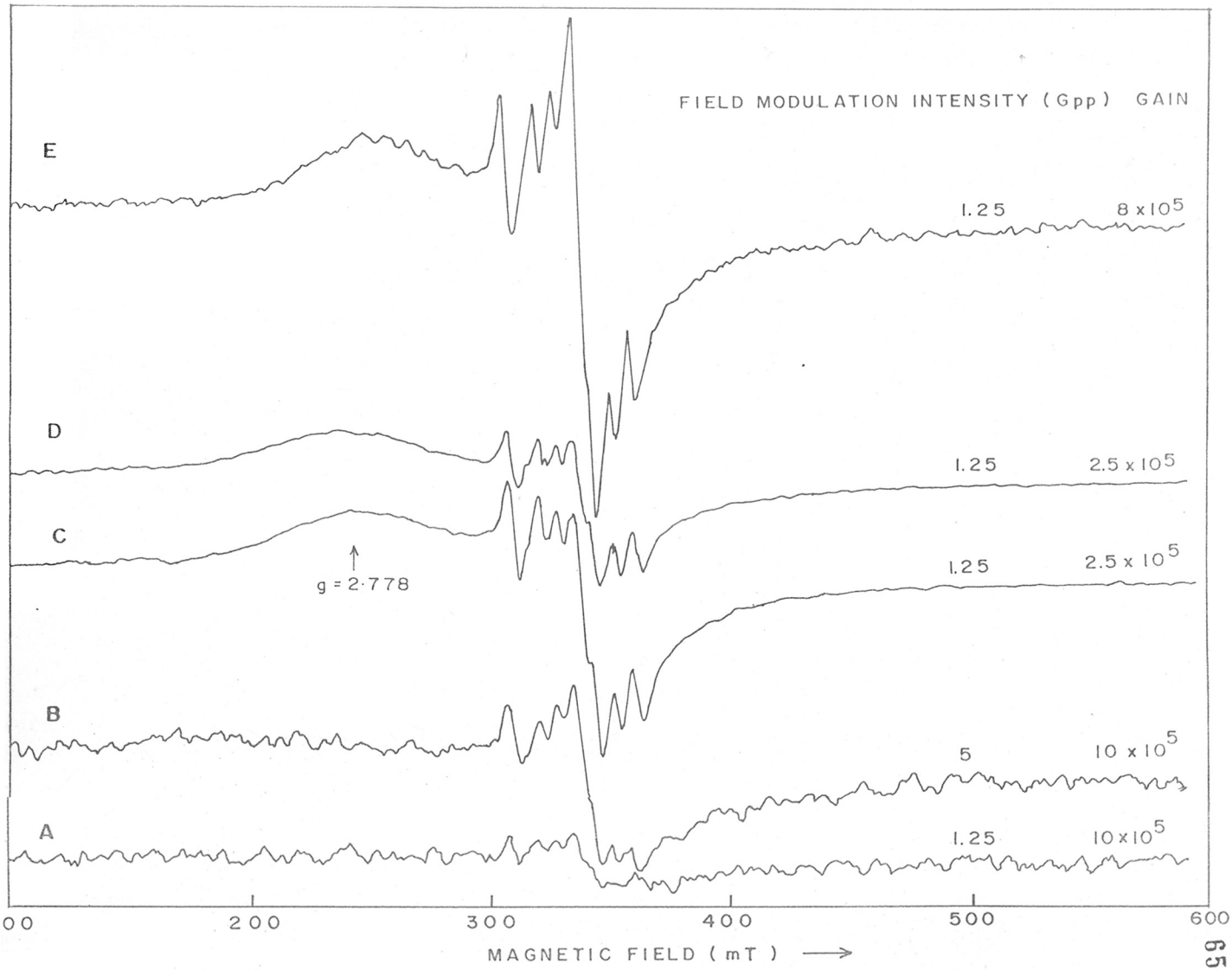

FIG. 3.9 EPR SPECTRA OF SAMPLE F. A AND B : FRESHLY PREPARED SAMPLE. C, D AND E : SAMPLE AGED FOR 169, 206 AND 230 DAYS.

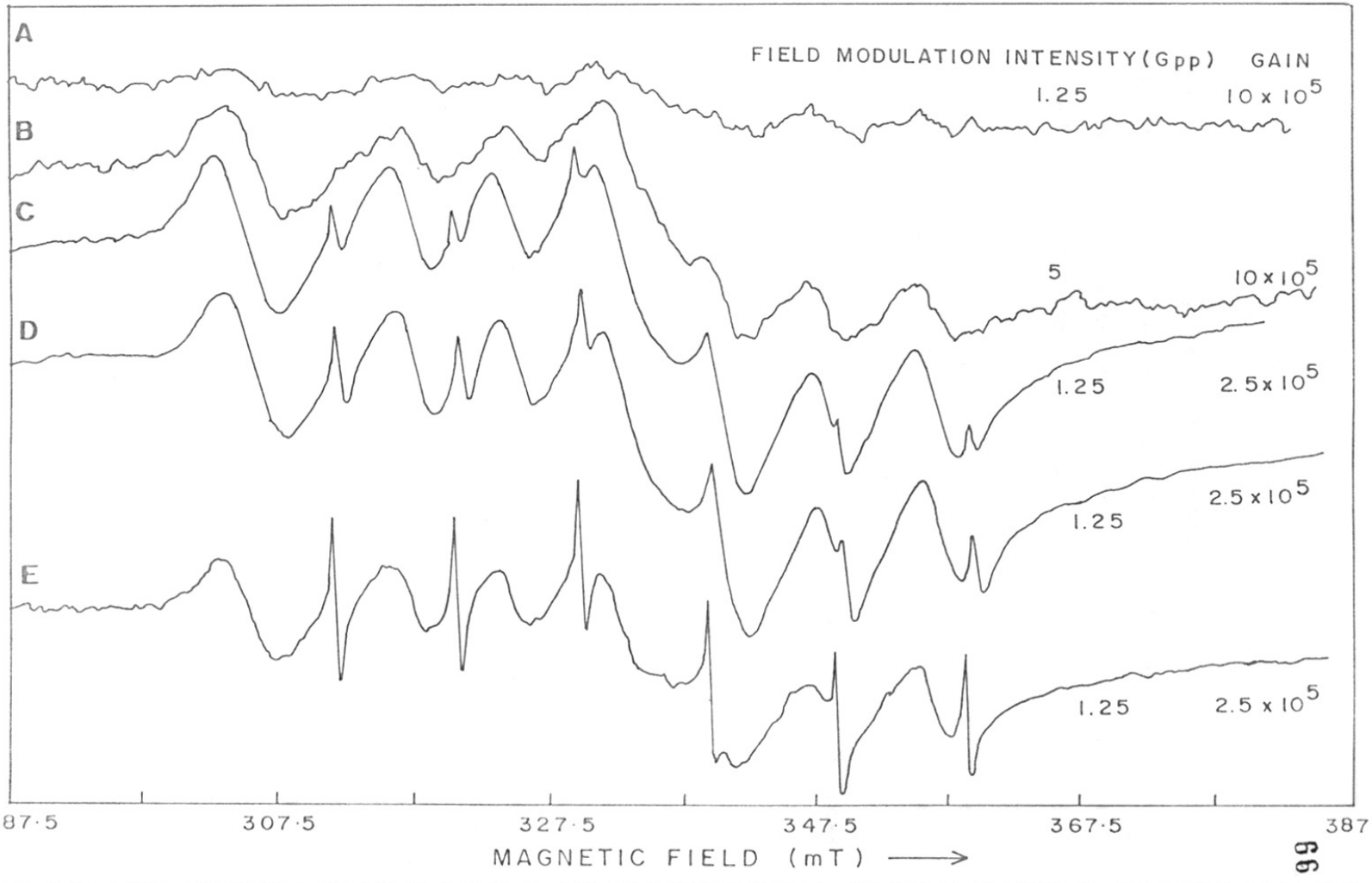

FIG. 3.10 EPR SPECTRA OF SAMPLE F. A AND B : FRESHLY PREPARED SAMPLE. C : AGED FOR 169 DAYS. D : AGED FOR 206 DAYS AND E : AGED FOR 240 DAYS.

shown in Figure 3.10 E. The spectrum of this sample is compared with the spectrum of $CdCO_3:Mn^{2+}$ sample in Figure 3.11. The new hyperfine sextet is comparable with the sextet of Mn^{2+} ions in $CdCO_3$ lattice. As the X-ray diffraction studies indicate $CdCO_3$ as majour impurity phase grown during the aging period, the new hyperfine sextet can be assigned to the presence of Mn^{2+} ions in the $CdCO_3$ impurity phase. The predicted and observed positions of the new hyperfine lines are compared with the position of the hyperfine lines of $CdCO_3:Mn^{2+}$ system in Table 3.8.

3.9 Conclusions

The synthesis of $Cd_{1-x}Mn_xO$ system was carried out by usual decomposition reaction, monitored through the simultaneous DTA/TG/DTG plots. The X-ray diffraction studies of the prepared compositions showed that the system exhibits cubic crystal structure. The lattice parameter values of the compositions are close to the reported values of CdO. The X-ray diffraction studies of the aged sample clearly revealed the presence of $CdCO_3$ and $Cd(OH)_2$. The phases grow during the aging period by the action of atmospheric CO_2 and H_2O on CdO.

The extensive EPR studies of the $Cd_{1-x}Mn_xO$ system are carried out for the first time. All the g values

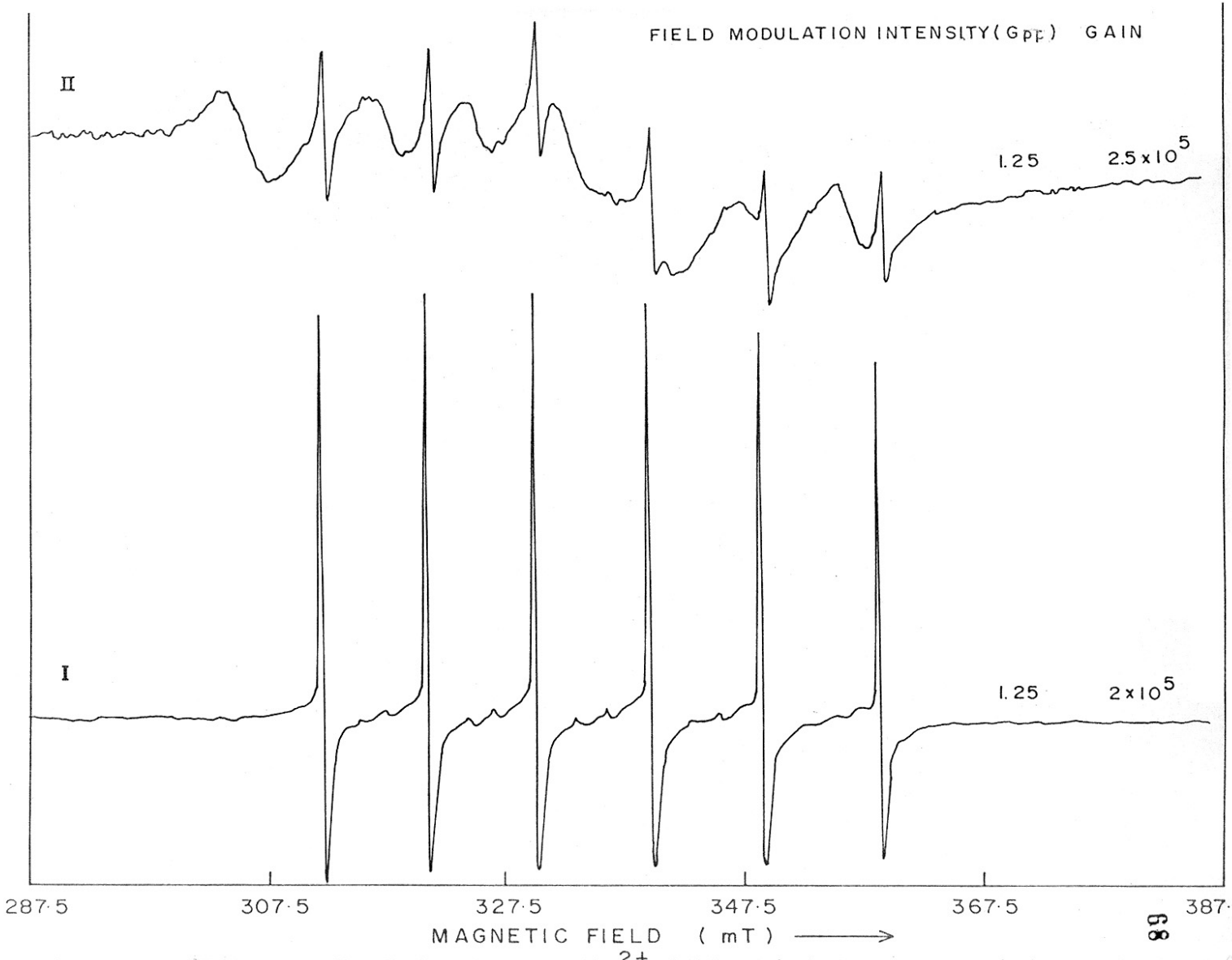

FIG. 3.11 : EPR DERIVATIVE SIGNAL OF Mn^{2+} IONS IN (I) $CdCO_3$ AND (II) SAMPLE-F AGED FOR 240 DAYS

Table 3.8

Calculated and observed positions of the new hyperfine lines and position of the hyperfine lines of $CdCO_3:Mn^{2+}$ system

Position of the new hyperfine lines in mT		Positions of the hyperfine lines of $CdCO_3:Mn^{2+}$ system (in mT)	
Obs.	Cal.	Obs.	Cal.
359.9	359.0	359.7	358.8
350.6	349.3	350.4	348.5
341.4	339.9	340.5	339.9
332.1	330.0	331.8	330.0
322.8	321.0	322.6	321.4
313.6	312.3	313.4	312.0

obtained for the EPR signal observed in the system are comparable with the reported g values for different paramagnetic centers present in a variety of non-stoichiometric specimens of CdO. This facilitated the assignment of the signals observed in our system.

The observation of hyperfine and superhyperfine lines for this system showed that Mn^{2+} ions occupy substitutional site in nearly cubic environment of oxygen octahedral in CdO. Further, the observation of superhyperfine lines suggested that Mn^{2+} electrons are delocalized and reaches into the crystal to give superhyperfine interaction with the Cd nuclei of nonzero spin. The spin Hamiltonian parameters are comparable with that reported for other cubic system.

The aged samples of the system showed an additional signal at g = 2.778 corresponding to the Mn^{2+} ions present in the impurity phases. The aged sample also showed an additional hyperfine sextet growing with the aging period. This sextet is likely to arise from Mn^{2+} ions in the $CdCO_3$ impurity phase.

In summary, it is clearly seen that Mn^{2+} ions can be used as a excellent EPR microprobe to monitor the local environment and stoichiometry in bulk CdO.

CHAPTER-4

Characterization of Thick Films of CdO

4.1 Introduction

This chapter describes the characterization of thick films of CdO, obtained by using different types of binders and their formulations. The characterization techniques like, X-ray diffraction, scanning electron microscopy and electrical resistivity measurements have been used to study the interesting properties of the CdO in thick film form. The analysis of experimental data is presented in the following pages.

4.2 X-ray diffraction studies

The X-ray diffraction pattern of the starting material, CdO, is shown in Fig. 4.1. From the XRD pattern, Bragg angle (2 θ), corresponding 'd_{hkl}' values and normalized intensity of the X-ray diffraction peaks were calculated. The 'd_{hkl}' values were compared with the standard ASTM pattern[83], as shown in Table 4.1.

The X-ray diffraction patterns of thick films of CdO, CdO-GL-1, CdO-GL-2 and CdO-GL-3 are shown in Figures 4.2, 4.3, 4.4 and 4.5 respectively. From these patterns, Bragg angle (2 θ), corresponding 'd_{hkl}' values and normalized intensity of the X-ray diffraction peaks were calculated. The 'd' values corresponding to CdO are summarized in Tables 4.2, 4.3, 4.4 and 4.5. The 'd' values

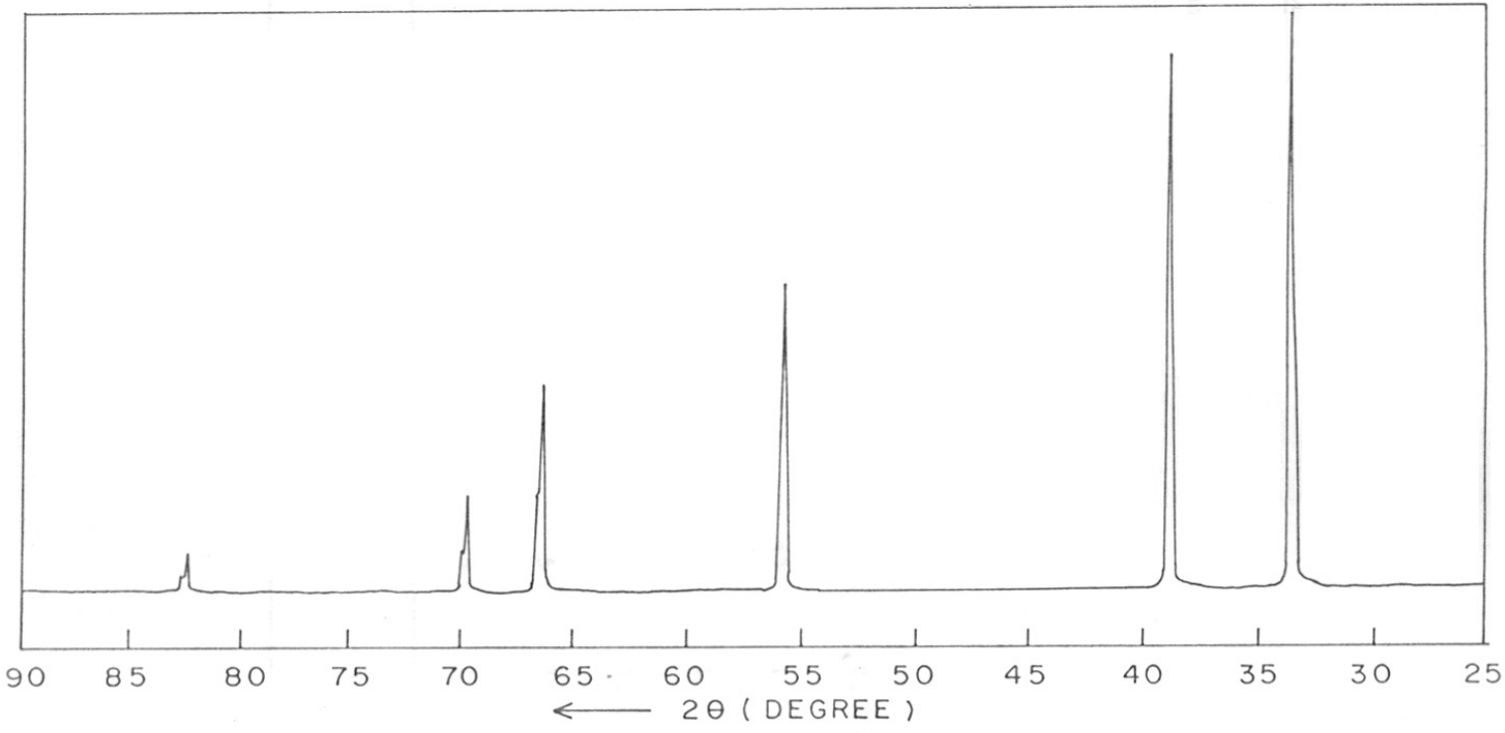

FIG. 4.1 : X-RAY DIFFRACTOGRAM OF THE STARTING MATERIAL, CdO

Table 4.1

Structural data for starting material, CdO

Sr. No.	Data for starting material, CdO			Reported data[83] for cubic CdO		
	Int.	2θ Degree	d values (Å)	Int.	d values (Å)	hkl
1	100	33.56	2.6620	100	2.712	111
2	93	38.80	2.3189	88	2.349	200
3	55	55.80	1.6461	43	1.661	220
4	37	66.48	1.4052	28	1.416	311
5	17	69.74	1.3473	13	1.355	222
6	7	82.52	1.1680	5	1.1742	400
7	12	91.72	1.0733	9	1.0772	331
	Lattice parameter		4.667		4.6953	

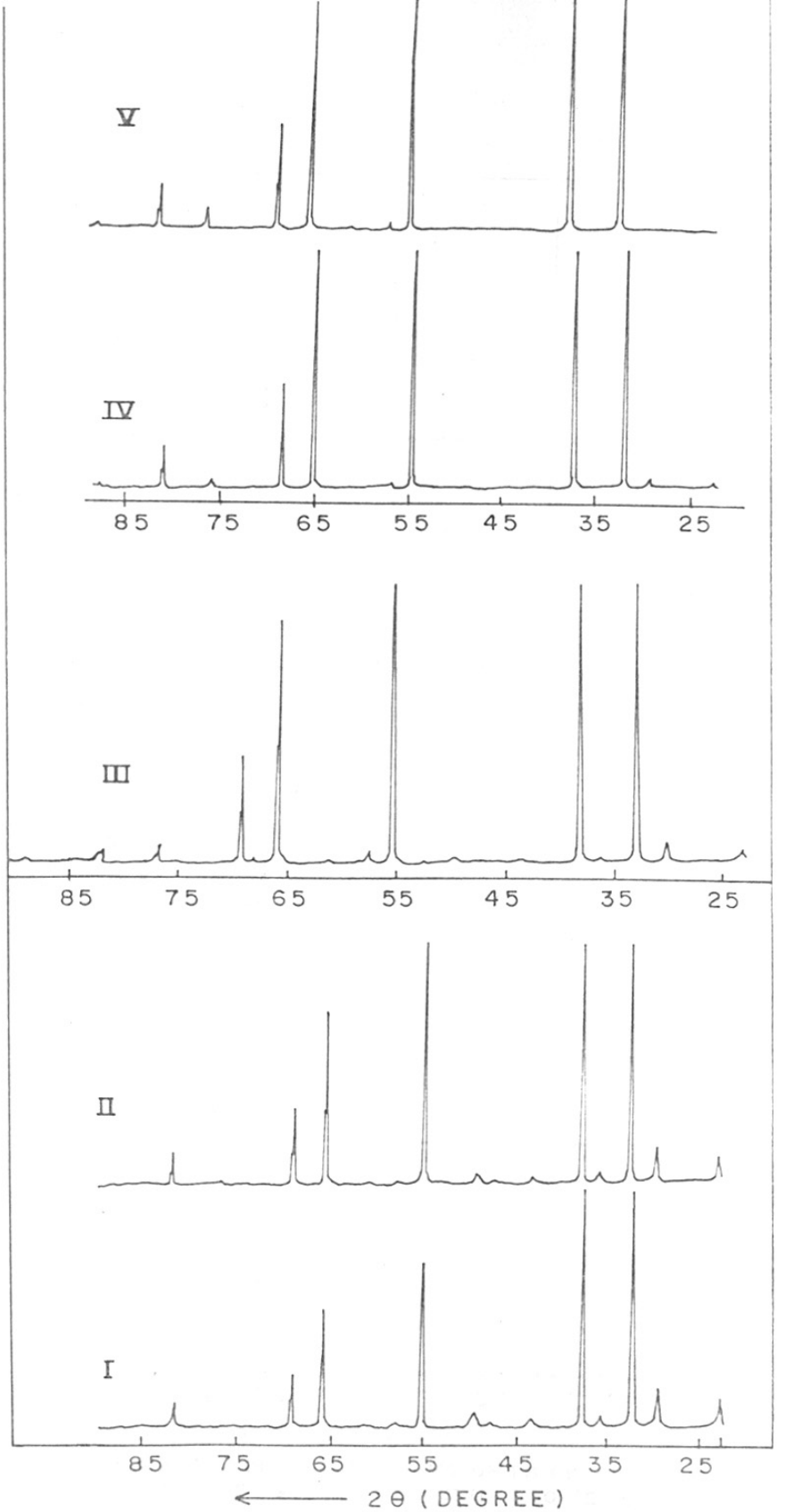

FIG. 4.2 : X-RAY DIFFRACTOGRAMS OF THICK FILMS OF CdO FIRED AT (I) 500, (II) 600, (III) 700, (IV) 800 AND (V) 900°C.

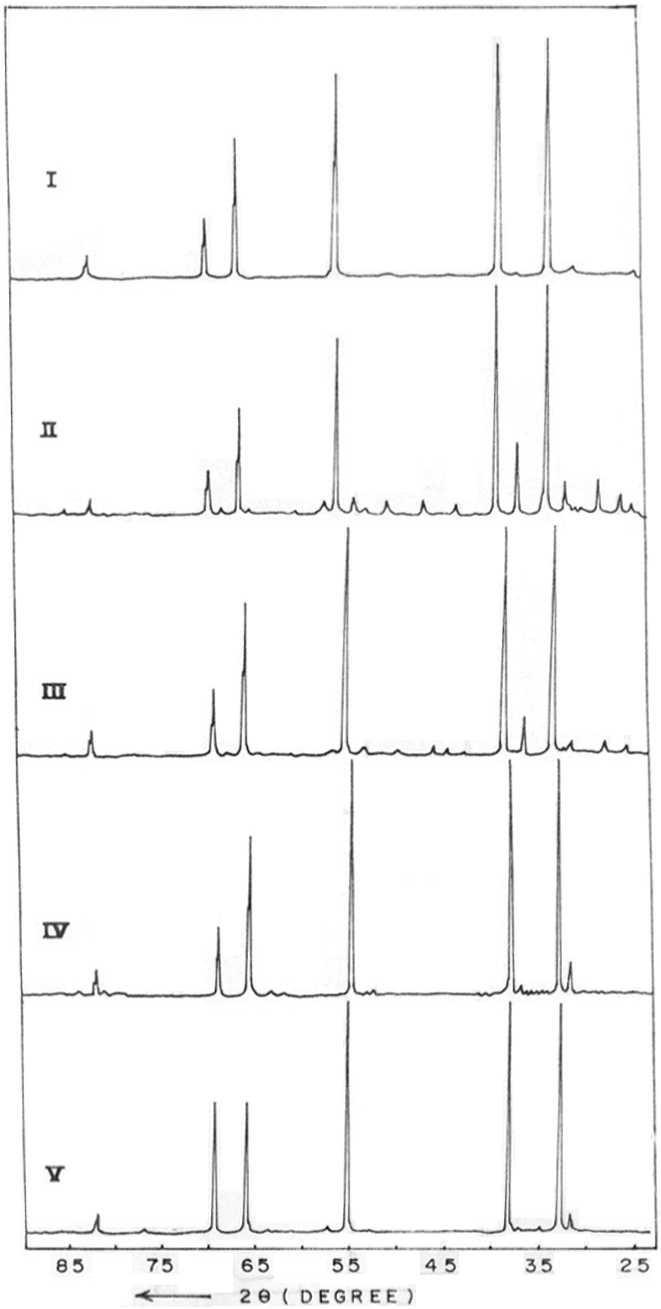

FIG. 4.3 X-RAY DIFFRACTOGRAMS OF THICK FILMS OF CdO - GL - I FIRED AT(I) 500,(II) 600, (III) 700, (IV) 800 AND (V) 900°C.

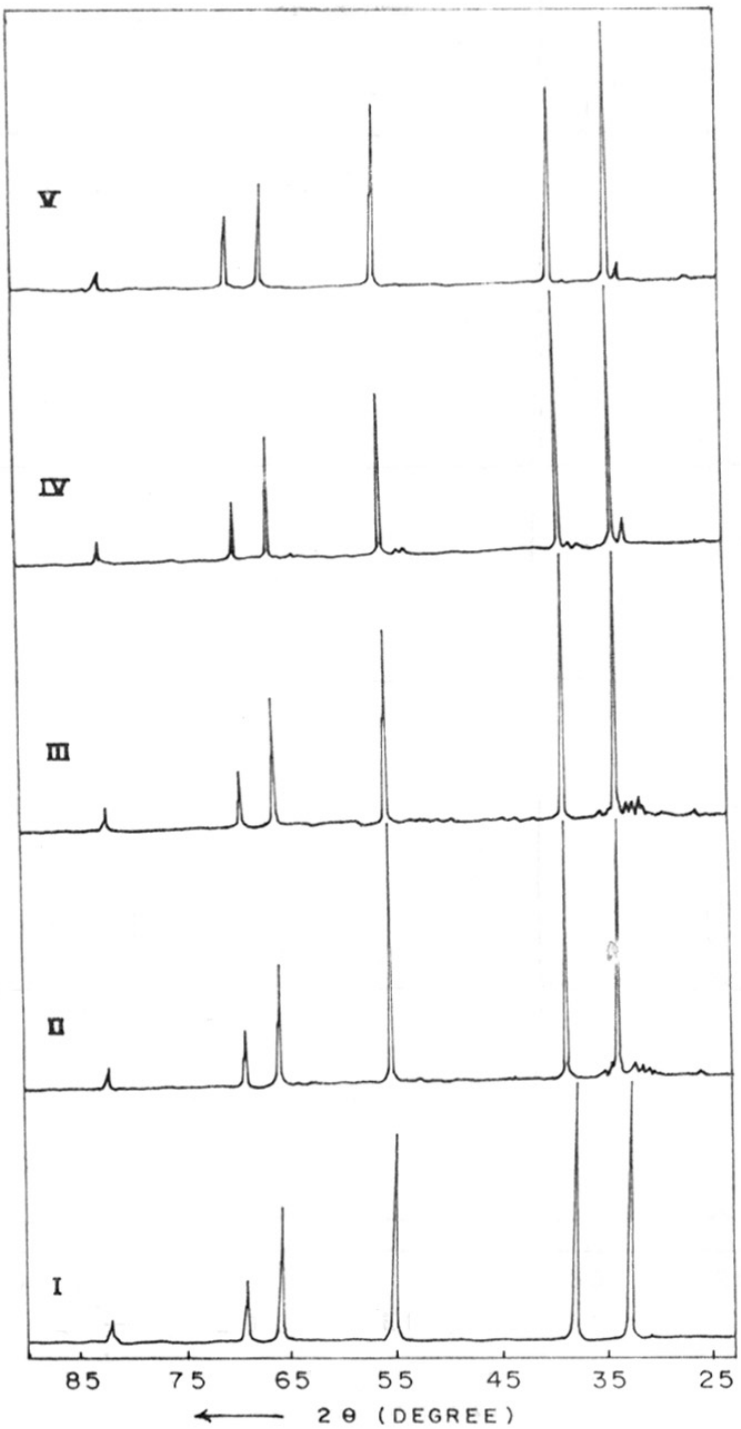

FIG. 4.4 X-RAY DIFFRACTOGRAMS OF THICK FILMS OF CdO - GL - 2 FIRED AT (I) 500, (II) 600, (III) 700, (IV) 800 AND (V) 900°C

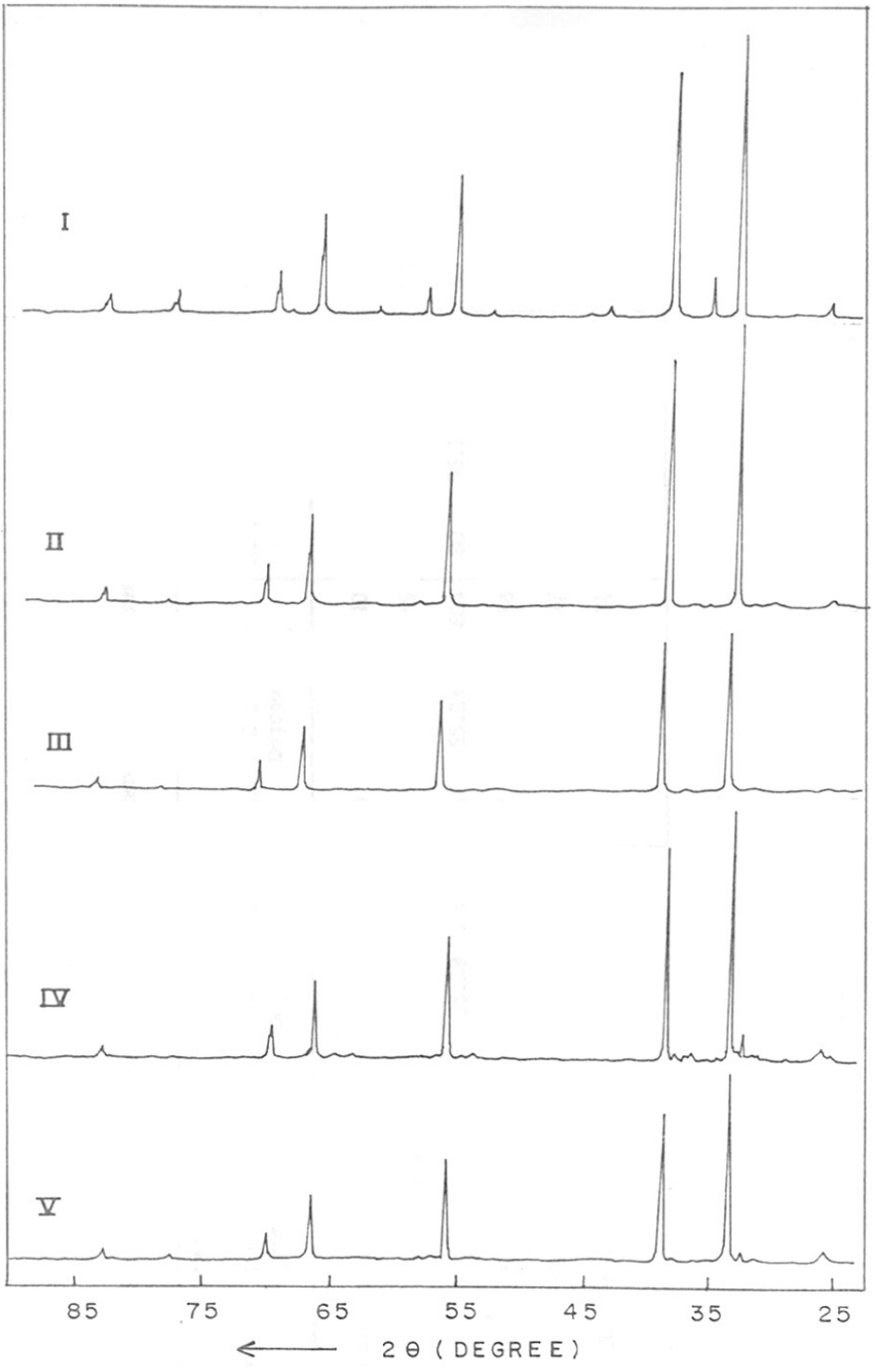

FIG. 4.5 : X-RAY DIFFRACTOGRAMS OF THICK FILMS OF CdO - GL-3 FIRED AT (I) 500, (II) 600, (III) 700, (IV) 800 AND (V) 900°C.

Table 4.2

Structural data for thick films of CdO fired at different temperatures

Sr. No.	500°C			600°C			700°C			800°C			900°C		
	Int.	2θ Degree	d Å	Int.	2θ Degree	d Å	Int.	2θ Degree	d Å	Int.	2θ Degree	d Å	Int.	2θ Degree	d Å
1	100	32.86	2.6451	100	33.04	2.7088	100	33.10	2.7040	100	33.00	2.7120	100	33.10	2.7040
2	84	38.08	2.3611	88	38.36	2.3445	89	38.36	2.3445	93	38.38	2.3433	93	38.44	2.3398
3	52	55.12	1.6648	75	55.28	1.6603	74	55.28	1.6603	80	55.34	1.6587	80	55.38	1.6576
4	35	65.80	1.4180	48	65.92	1.4158	57	65.90	1.4168	67	65.90	1.4161	67	65.94	1.4154
5	15	69.10	1.3582	22	69.32	1.3544	26	69.30	1.3547	28	69.30	1.3547	29	69.32	1.3544
6	5	81.90	1.1752	8	82.02	1.1738	11	82.08	1.1731	13	82.10	1.1729	12	82.12	1.1726

Table 4.3

Structural data for thick films of CdO-GL-1 fired at different temperatures

Sr. No.	500°C			600°C			700°C			800°C			900°C		
	Int.	2θ Degree	d Å	Int.	2θ Degree	d Å	Int.	2θ Degree	d Å	Int.	2θ Degree	d Å	Int.	2θ Degree	d Å
1	100	32.90	2.7200	100	33.00	2.7120	100	33.10	2.7040	100	33.00	2.7120	100	33.04	2.7088
2	87	38.32	2.3468	90	38.34	2.3457	88	38.36	2.3445	88	38.30	2.3480	64	38.44	2.3398
3	58	55.26	1.6609	49	55.30	1.6598	75	55.34	1.6587	65	55.28	1.6603	54	55.38	1.6576
4	39	65.90	1.4161	29	65.92	1.4158	40	66.00	1.4142	39	65.88	1.4165	31	66.04	1.4135
5	16	69.28	1.3551	13	68.30	1.3547	18	69.32	1.3544	17	69.22	1.3561	31	69.40	1.3530
6	7	82.00	1.1741	5	82.06	1.1733	7	82.10	1.1729	6	82.00	1.1741	4	82.16	1.1722

Table 4.4

Structural data for thick films of CdO-GL-2 fired at different temperatures

Sr. No.	500°C			600°C			700°C			800°C			900°C		
	Int.	2θ Degree	d Å	Int.	2θ Degree	d Å	Int.	2θ Degree	d Å	Int.	2θ Degree	d Å	Int.	2θ Degree	d Å
1	100	33.00	2.7120	100	32.90	2.7200	100	32.96	2.7152	100	32.92	2.7184	100	32.90	2.7200
2	93	38.26	2.3504	92	38.18	2.3551	88	38.18	2.3551	88	38.18	2.3551	50	38.18	2.3551
3	57	55.24	1.6614	71	55.16	1.6636	55	55.18	1.6631	67	55.16	1.6636	47	55.14	1.6642
4	33	65.94	1.4154	32	65.84	1.4173	36	65.86	1.4169	42	65.84	1.4173	27	65.62	1.4215
5	15	69.22	1.3561	13	69.18	1.3568	15	69.16	1.3571	19	69.14	1.3575	27	69.12	1.3578
6	5	82.02	1.1738	6	81.94	1.1748	7	81.92	1.1750	7	81.90	1.1752	5	81.86	1.1757

Table 4.5

Structural data for thick films of CdO-GL-3 fired at different temperatures

Sr. No.	500°C			600°C			700°C			800°C			900°C		
	Int.	2θ Degree	d Å	Int.	2θ Degree	d Å	Int.	2θ Degree	d Å	Int.	2θ Degree	d Å	Int.	2θ Degree	d Å
1	100	32.90	2.7200	100	33.00	2.7120	100	33.10	2.7040	100	33.06	2.7072	100	33.20	2.7775
2	87	38.16	2.3563	88	38.30	2.3480	96	38.38	2.3439	88	38.18	2.3551	78	38.58	2.3316
3	48	55.26	1.6609	48	55.36	1.6581	59	55.48	1.6548	47	55.48	1.6548	54	55.74	1.6477
4	32	65.94	1.4154	31	66.08	1.4127	40	66.12	1.4120	29	66.20	1.4104	31	66.30	1.4086
5	13	69.32	1.3544	13	69.46	1.3520	20	69.46	1.3520	12	69.58	1.3500	13	69.66	1.3486
6	5	82.18	1.1719	5	82.20	1.1717	7	82.30	1.1705	4	82.28	1.1708	6	82.50	1.1682

of additional peaks are listed in Tables 4.6, 4.7, 4.8 and 4.9. The tables showed the presence of $CdCO_3$, $Cd(OH)_2$ and traces of unidentified impurity. As discussed in section 3, these phases can arise due to aging effects. The lattice parameter values of the cubic phase, present in the films, are calculated and summarized in Table 4.10. The observed variation of the lattice parameter value as a function of firing temperature is explained as follows.

The lattice parameter value was found to decrease with increase in firing temperature for thick films of CdO without containing any binder. This decrease can be due to the decrease of Cd^+ ions (ionic radii 1.14 Å)[131], likely to be present as native imperfections in the place of Cd^{2+} ions (ionic radii 0.97 A)[131]. The similar decrease in the lattice parameter value for thick films of CdO-GL-2 is observed for the increase in firing temperature from 500 to 700°C. At 800°C, the lattice parameter value was same as that of the value observed for the film fired at 500°C. At 900°C the value was further decreased. The initial decrease is again likely to arise due to the decrease of Cd^+ ions. However, at 800°C, if the Pb^{2+} ions (ionic radii 1.2 Å)[131] from the glass phase gets incorporated into the lattice of CdO, then it is possible

Table 4.6

Additional X-ray diffraction peaks observed in thick films of CdO fired at different temperatures

Firing temp. °C	Additional peaks			Reported data for $CdCO_3$		$Cd(OH)_2$	
	Int.	2θ Degree	d Å	Int.	d Å	Int.	d Å
	8.0	23.36	3.8047	80	3.77		
	11	30.18	2.9587	100	2.94		
	4.0	36.20	2.4793	50	2.46		
	0.4	40.00	2.2521	3	2.23		
	2.0	43.60	2.0741	45	2.06		
	1.0	47.88	1.8982	33	1.88		
500	4.0	49.68	1.8335	80	1.83		
	2.0	58.00	1.5888	40	1.58		
	1.0	61.60	1.5043	17	1.50		
	0.4	62.80	1.4784	5	1.47		
	0.2	73.00	1.2949	5	1.30		
	0.8	74.98	1.2656	17	1.26		
	0.8	76.80	1.2400	5	1.23		
	6.0	23.52	3.7824	80	3.77		
	9.0	30.30	2.9472	100	2.94		
	2.0	36.46	2.4622	50	2.46		
	0.7	40.20	2.2413	3	2.23		
	2.0	43.84	2.0633	45	2.06		
	1.0	48.12	1.8893	33	1.88		
600	3.0	49.86	1.8273	80	1.83		
	0.3	57.50	1.6014			30	1.63
	1.0	58.24	1.5828	40	1.58		
	0.7	61.80	1.4999	17	1.50		
	0.3	63.20	1.3739	5	1.36		
	0.2	73.00	1.2949			15	1.27
	0.3	75.20	1.2624	17	1.20		
	1.0	76.82	1.2398	5	1.23		

Contd..

Table 4.6 (Continued)

Firing temp. °C	Additional peaks			Reported data for			
	Int.	2θ Degree	d Å	Int.	$CdCO_3$ d Å	Int.	$Cd(OH)_2$ d Å
	2.0	23.52	3.7824	80	3.77		
	3.0	30.30	2.9472	100	2.94		
	0.7	35.20	2.5472			100	2.56
	1.0	35.46	2.4622	50	2.46		
	0.3	40.20	2.2413	3	2.23		
	0.7	43.60	2.0741	45	2.06		
	0.3	48.12	1.8893	33	1.88		
700	1.0	49.86	1.8273	80	1.83		
	0.7	52.60	1.7384			30	1.74
	3.0	57.50	1.6014			30	1.63
	0.7	58.24	1.5282	40	1.58		
	1.0	61.32	1.5105			13	1.51
	0.7	68.20	1.3739	5	1.36		
	3.0	76.90	1.2387	5	1.23		
	0.7	89.00	1.0989			3	1.092
	1.0	23.56	3.7729	80	3.77		
	2.0	30.28	2.9491	100	2.94		
	0.3	36.40	2.4661	50	2.46		
	0.3	43.80	2.0651	45	2.06		
	0.7	49.80	1.8294	80	1.83		
800	0.2	55.56	1.6526				
	2.0	57.52	1.6009				
	0.2	61.30	1.5109			13	1.51
	0.3	68.20	1.3739	5	1.36		
	2.0	76.84	1.2395	5	1.23		
	2.0	89.00	1.0989			3	1.092

Contd..

Table 4.6 (Continued)

Firing temp. °C	Additional peaks Int.	2θ Degree	d Å	Reported data for $CdCO_3$ Int.	d Å	Int.	$Cd(OH)_2$ d Å
	0.3	35.28	2.5418			100	2.56
	0.3	43.46	2.0804	45	2.06		
	0.3	52.60	1.7384			30	1.74
	3.0	57.58	1.5993	40	1.58		
900	0.7	61.40	1.5087	17	1.50		
	0.7	68.24	1.3732			15	1.274
	5.0	76.92	1.2384	5	1.23		
	1.0	89.08	1.0981			3	1.098

Table 4.7

Additional X-ray diffraction peaks observed in thick films of CdO-GL-1 fired at different temperatures

Firing temp. °C	Additional peaks			Reported data for			
	Int.	2θ Degree	d Å	$CdCO_3$ Int.	$CdCO_3$ d Å	$Cd(OH)_2$ Int.	$Cd(OH)_2$ d Å
	1.3	23.40	3.7983	30	3.77		
	1.3	32.20	2.7775				
500	0.7	36.30	2.4727	50	2.46		
	0.7	43.68	2.0705	45	2.06		
	1.0	54.80	1.6737			30	1.63
	2.0	24.20	3.6745				
	5.3	25.38	3.5063				
	1.0	27.66	3.2222				
	1.3	29.58	3.0173			100	3.03
	1.3	30.18	2.9587	100	2.94		
	1.3	30.80	2.9005				
	8.0	31.10	2.8732				
	-	33.40	2.6804				
	1.9	36.08	2.4672	50	2.46		
	0.7	40.50	2.2254	3	2.23		
	2.7	42.60	2.1204	45	2.12		
	4.7	46.04	1.9697				
600	4.0	49.76	1.8308	80	1.83		
	2.0	51.88	1.7609			30	1.74
	0.7	52.40	1.7446				
	4.7	53.28	1.7178				
	3.3	56.60	1.6347			30	1.63
	0.3	57.00	1.6142				
	1.0	59.86	1.5438	40	1.58		
	1.3	64.90	1.4355	15	1.42		
	1.3	67.80	1.3810	5	1.36		
	0.5	77.60	1.2292	5	1.23		
	0.7	79.34	1.2066	8	1.19		
	1.3	84.98	1.1403	8	1.14		

Contd..

Table 4.7 (Continued)

Firing temp. °C	Additional peaks			Reported data for $CdCO_3$		Reported data for $Cd(OH)_2$	
	Int.	2θ Degree	d • Å	Int.	d • Å	Int.	d • Å
	1.9	25.40	3.5036				
	3.1	27.74	3.2131				
	1.0	30.88	2.8932				
	3.1	31.24	2.8607				
	0.3	34.10	2.6270				
	8.8	36.18	2.4806	50	2.46		
	1.3	42.70	2.1157				
	0.3	44.78	2.0221	45	2.06		
	1.3	46.16	1.9648				
700	1.3	49.80	1.8294	80	1.83		
	0.6	52.02	1.7564			30	1.74
	2.5	53.30	1.7172				
	1.3	56.70	1.6221			30	1.63
	0.3	57.10	1.6116				
	0.6	59.88	1.5433	40	1.58		
	0.6	65.00	1.4336			20	1.44
	0.6	68.00	1.3774	5	1.37		
	0.3	77.70	1.2279	5	1.23		
	0.3	79.40	1.2058	8	1.19		
	0.6	85.00	1.1401	8	1.14		
	7.6	31.78	2.8133				
	0.3	36.40	2.4661	50	2.46		
	2.4	37.16	2.4174				
	0.3	41.00	2.1994				
	0.3	41.68	2.1651				
800	1.2	53.00	1.7262			30	1.74
	0.9	53.58	1.7089				
	0.3	62.80	1.4784	5	1.47		
	1.2	63.68	1.4600				
	0.3	86.80	1.1210	8	1.12		

Contd..

Table 4.7 (Continued)

Firing temp. °C	Additional peaks			Reported data for $CdCO_3$		Reported data for $Cd(OH)_2$	
	Int.	2θ Degree	d Å	Int.	d Å	Int.	d Å
	3.3	31.88	2.8047				
	1.1	35.20	2.5474			100	2.56
	1.1	37.36	2.4049	50	2.46		
	0.3	41.80	2.1592				
	0.3	43.50	2.0786	45	2.06		
	0.3	45.58	1.9885				
900	0.3	52.60	1.7384			30	1.74
	0.6	53.20	1.7202				
	1.3	57.64	1.5978	40	1.58		
	0.3	61.40	1.5087	17	1.50		
	0.3	62.80	1.4784	5	1.47		
	0.6	63.86	1.4564			20	1.44
	1.7	76.88	1.2389	5	1.23		

Table 4.8

Additional X-ray diffraction peaks observed in thick films of CdO-GL-2 fired at different temperatures

Firing temp. °C	Additional peaks			Reported data for $CdCO_3$		$Cd(OH)_2$	
	Int.	2θ Degree	d Å	Int.	d Å	Int.	d Å
500	0.2	30.48	2.9302	100	2.94		
	1.1	25.10	3.5448				
	0.2	28.26	3.1552				
	1.1	29.38	3.0374				
	1.4	30.00	2.9760	100	2.94		
	2.1	30.64	2.9153				
	2.9	31.38	2.8482				
	2.1	33.60	2.6649				
	1.4	34.50	2.5974			100	2.56
	0.2	39.40	2.2850	3	2.23		
600	0.2	41.10	2.1943				
	0.2	42.78	2.1119				
	0.2	43.80	2.0651	45	2.06		
	0.2	49.86	1.8273	80	1.83		
	0.7	50.20	1.8158				
	0.2	51.40	1.7762				
	0.7	52.60	1.7384			30	1.74
	0.2	57.80	1.5938	40	1.58		
	0.2	59.70	1.5475				
	0.7	62.68	1.4809	5	1.47		
	0.2	63.78	1.4580	15	1.42		

Contd..

Table 4.8 Continued)

Firing temp. °C	Additional peaks Int.	2θ Degree	d Å	Reported data for $CdCO_3$ Int.	d Å	$Cd(OH)_2$ Int.	d Å
	1.5	25.20	3.5309				
	0.8	28.30	3.1508				
	0.8	29.60	3.0153				
	3.1	30.20	2.9568	100	2.94		
	6.2	30.70	2.9097				
	5.4	31.40	2.8464				
	4.6	31.90	2.8030				
	1.2	33.70	2.6572				
	2.3	34.54	2.5945			100	2.56
	0.8	38.84	2.3166				
700	0.4	39.40	2.2850	3	2.23		
	0.4	41.38	2.1801				
	0.8	42.98	2.1026				
	0.8	44.20	2.0473	45	2.06		
	0.4	46.80	1.9395				
	1.2	49.00	1.8574	33	1.88		
	1.2	50.40	1.8090	80	1.83		
	0.8	51.40	1.7762				
	0.4	52.38	1.7452				
	1.2	52.98	1.7269				
	0.8	57.90	1.5913	40	1.58		
	0.4	62.80	1.4784	5	1.47		

Contd..

Table 4.8 (Continued)

Firing temp. °C	Additional peaks Int.	2θ Degree	d Å	Reported data for $CdCO_3$ Int.	d Å	$Cd(OH)_2$ Int.	d Å
	8.2	31.80	2.8115				
	0.9	36.38	2.4674	50	2.46		
	1.8	37.18	2.4161				
	0.5	41.60	2.1691				
800	1.8	52.92	1.7287			30	1,74
	0.9	53.58	1.7089				
	0.9	62.60	1.4826	5	1.47		
	1.4	63.60	1.4617				
	0.5	76.90	1.2387	5	1.23		
	0.4	77.12	1.2360				
	4.7	31.78	2.8133				
	0.7	37.18	2.4161				
900	0.3	52.86	1.7305				
	1.7	63.60	1.4617	5	5.147		
	0.5	76.80	1.2400	5	1.23		

Table 4.9

Additional X-ray diffraction peaks observed[23-96] in thick films of CdO-GL-3 fired at different temperatures

Firing temp. °C	Additional peaks Int.	2θ Degree	d Å	Reported data for $CdCO_3$ Int.	d Å	$Cd(OH)_2$ Int.	d Å
	4.8	25.50	3.4901				
	0.6	31.40	2.8464				
	1.3	35.04	2.5586			100	2.56
	0.6	37.60	2.3901				
	0.6	41.58	2.1701				
	4.2	43.24	2.0905	45	2.06		
500	1.2	44.80	2.0213				
	2.4	52.50	1.7415			30	1.74
	8.3	57.48	1.6019				
	2.4	61.30	1.5109	17	1.50		
	1.2	68.20	1.3739	5	1.36		
	7.1	76.98	1.2376	5	1.23		
	1.2	89.10	1.0980	8	1.02		
	2.3	25.58	3.4793				
	1.8	30.10	2.9664	100	1.94		
	0.6	31.00	2.8823				
	0.6	31.78	2.8133				
	0.6	34.10	2.6270				
600	0.6	34.48	2.5989				
	1.2	35.18	2.5488			100	2.56
	0.6	36.28	2.4740	50	2.46		
	0.6	36.66	2.4492				
	0.6	43.40	2.0998	45	2.06		
	1.2	57.54	1.6004			30	1.63
	1.2	77.04	1.2368	5	1.23		

Contd..

Table 4.9 (Continued)

Firing temp. °C	Additional peaks Int.	2θ Degree	d Å	Reported data for $CdCO_3$ Int.	d Å	$Cd(OH)_2$ Int.	d Å
	1.1	24.80	3.5870				
	1.1	25.60	3.4767				
	1.1	28.50	3.1291				
	1.1	31.00	2.8823				
	1.1	31.40	2.8464				
700	1.1	31.80	2.8115				
	1.1	35.20	2.5474			100	2.56
	2.2	36.30	2.4727	50	2.46		
	2.2	36.68	2.4479				
	1.1	50.80	1.7957			30	1.74
	1.1	77.12	1.2357	5	1.23		
	2.7	24.76	3.5927				
	4.0	25.58	3.4793				
	1.3	28.58	3.1206				
	0.7	30.30	2.9472	100	2.94		
	2.7	30.98	2.8841				
	2.7	31.40	2.8464				
	0.7	31.80	2.8115				
	9.3	32.10	2.7859				
	2.7	32.60	2.7444				
	0.7	34.40	2.6048				
800	1.4	36.28	2.4740	50	2.46		
	0.7	36.70	2.4466				
	1.4	37.68	2.3852				
	0.7	45.68	1.9844				

Contd..

Table 4.9 (Continued)

Firing temp. °C	Additional peaks Int.	2θ Degree	d Å	Reported data for $CdCO_3$ Int.	d Å	$Cd(OH)_2$ Int.	d Å
800	0.7	50.80	1.7957				
	0.7	51.40	1.7762			30	1.74
	1.3	53.40	1.7143				
	0.6	54.40	1.6851				
	0.6	57.60	1.5988	40	1.58		
	1.3	62.98	1.4746	5	1.47		
	1.3	64.60	1.4415			20	1.443
	0.6	77.00	1.2373	5	1.23		
	3.7	25.60	3.4767				
	0.9	31.20	2.8642				
	3.7	32.20	2.7775				
	0.9	35.40	2.5334			100	2.56
	0.9	37.78	2.3791				
	0.9	43.70	2.0676	45	2.06		
900	0.9	44.70	2.0256				
	0.9	53.60	1.7083			30	1.74
	0.9	56.98	1.6148				
	0.9	57.80	1.5938	40	1.58		
	0.9	61.60	1.5043	17	1.50		
	0.9	63.00	1.4742	5	1.47		
	0.9	64.60	1.4415			20	1.443
	2.8	77.20	1.2346	5	1.23		

Table 4.10

Lattice parameter values for the films of CdO, CdO-GL-1, CdO-GL-2 and CdO-GL-3 as a function of their firing temperature

Sr. No.	Firing Temp. (°C)	Lattice parameter 'a' (Å) for thick films of			
		CdO	CdO-10% GL-1	CdO-10% GL-2	CdO-10% GL-3
1	500	4.704	4.696	4.697	4.693
2	600	4.695	4.694	4.700	4.686
3	700	4.694	4.691	4.701	4.683
4	800	4.693	4.697	4.702	4.679
5	900	4.688	4.688	4.707	4.669

to have higher lattice parameter value. Further decrease of the value at 900°C can arise due to the further loss of Cd^{+} ion or due to the oxidation of Pb^{2+} ions to Pb^{4+} ions (ionic radii 0.87 Å)[131].

The films of CdO-GL-3 also showed decrease in the lattice parameter value with the increasing firing temperature as observed for the films of CdO. The decrease is more pronounced for the films of CdO-GL-3. In the glass GL-3, the main ingredient is ZnO. The ionic radii[131] of Zn^{2+} ions is 0.74 Å. Thus, any incorporation of Zn^{2+} ions in CdO during firing will result in lowering of the lattice parameter. The decrease will be significant for the decrease of Cd^{+} ions as it has higher ionic radii. The combined effect of both the phenomenon is likely to show pronounced decrease of the lattice parameter value as observed by us.

The films of CdO-GL-2 showed the increase in lattice parameter value with the increase of firing temperature. The main ingredient of GL-3 glass is Bi_2O_3. The ionic radii[131] of Bi^{3+} is 0.74 Å. Thus, the incorporation of Bi^{3+} ions in CdO during the firing will result in lowering of the lattice parameter. However, we have observed increase in the lattice parameter. This can be explained

as follows.

The binary oxide system, that is an oxide containing foreign atom, can be classified into two categories[132]. The simplest case is that in which foreign atom has the same valence as the atom it replaces and forms compounds of same formula and same crystal structure as the compound in which it is dissolved. The solid solutions thus obtained are termed as "normal" mixed crystal. The examples[133-139] of such types of mixed crystals are (CaMn)O, (CdSr)O, (CdZn)O, $(Al,Cr)O_3$ etc. In such compounds, the physical properties like lattice parameter, vary linearly with the amount/concentration of the foreign atom present in the host crystal lattice. In thick films of CdO-GL-1 and CdO-GL-3, such types of normal mixed crystal, (Cd,Pb)O and (Cd,Zn)O are likely to form during the firing of the films. The PbO and ZnO are respectively present in glasses GL-1 and GL-3 as main ingredients. The second type of binary oxide system is the one in which the dopant atoms or foreign atoms have a valence different from that of the atom which they replace. Such oxide system may belong to one of the following three categories[132]:

(1) The incorporation of foreign atom may form atomic imperfections with well defined concentrations. For

example the incorporation of $CaCl_2$ in NaCl forms vacancies of Na or interstitial chlorine. In either case, the concentration of atomic imperfections formed is well defined viz., one per Ca_{Na} atom. It is termed as 'controlled atomic imperfections'[140] . Koch and Wagner first studied the properties related to this type[141] .

(2) Atoms of the host crystal may change their valency as a consequence of the incorporation of foreign atom. For example, when Li is incorporated in NiO, equivalent amount of Ni atoms changes its valence from 2 to 3 without the formation of atomic imperfections. Verwey and coworkers first reported this and named as 'control valence'.

(3) It may occur that foreign atom (pure), when dissolved in host oxide, it may adapt itself and form a compound similar to the host compound. Thus, with manganese in Al_2O_3 and TiO_2, solid solutions Al_2O_3-Mn_2O_3 and TiO_2-MnO_2 are formed[143] . Selwood introduced the term 'induced valence' for such type.

The properties of CdO-Bi_2O_3 solid solutions can be explained by means of controlled valence process. If Bi^{3+} from the glass phase is incorporated into the lattice of CdO, the quasichemical reaction on the basis of ZnO:Ga^{3+}

system [144] can be written as

$$Bi_2O_3 \rightleftharpoons 2Bi^{+}(Cd) + 2\ominus + 2CdO(s) + \tfrac{1}{2}\,O_2(g)$$

Here, the sequence of events can be explained as: (i) The two oxides Bi_2O_3 and ZnO react. (ii) The Bi ions displae Cd^{2+} ions from their normal position to give rise to excess positive charge at those locations. (iii) Two of the three O^{2-} ions derived from Bi_2O_3 and the two displaced Cd^{2+} ions form additional $Cd^{2+}O^{2-}$ units CdO(s). (iv) The third O^{2-} ion originally associated with Bi_2O_3 is ejected into the gas phase as $\tfrac{1}{2}\,O_2(g)$. Two electrons left behind convert two Cd^{2+} ions in lattice to give pair of Cd^{2+} ions. The mixed oxide is designated as $Bi_x^{3+}\,Cd_{1-x}^{2+}\,Cd_x^{+}O_{1+x}^{2-}$ which indicate that Cd is encountered in two valence state Cd^{2+} and Cd^{+}. The Cd^{+} ions increase with the Bi^{3+} ions that get incorporated into CdO. With increase in firing temperature, more of Bi^{3+} ions can get incorporated into the lattice CdO, thereby increasing the concentration of Cd^{+} ion and consequently increasing the lattice parameter.

4.3 Scanning electron microscopic studies

Scanning electron micrographs of thick films of CdO without containing any binder were obtained using a

From: R.F. Shinde
Scientist B
Physical Chemistry Div.
N.C.L., Pune-8.

Dec. 18,1989

To,
The Documentation Officer
NCL Library
NCL, Pune-8.

Sir,

I am submitting a copy of my Ph.D. thesis entitled "Structural investigations in oxide ceramics" to be submitted to the University of Poona for the award of Ph.D. degree, for retention in the NCL Library.

Thanking you,

Yours faithfully,

RFShinde

(R.F. Shinde)

SKDate

(S.K. DATE)
Research Guide

Received a copy of the above mentioned Ph.D. thesis.

Dec. 18,1989

आर. एस. सिंह/R. S. Singh
प्रलेखन अधिकारी (ग्रे-II)
Documentation Officer (G-II)
राष्ट्रीय रासायनिक प्रयोगशाला
National Chemical Laboratory,
पुणे/PUNE-411 008.

Mr. Powell

Cambridge Steroscan 150 Scanning Electron Microscope. The micrographs, obtained after each firing, are shown in Fig. 4.6 A to E. The micrographs of the films show increasing grain growth with the peak firing temperature. However, the grains were agglomerated and it was difficult to measure the grain size.

4.4 Determination of crystallite size

In the physicochemical characterization of the oxide ceramics, a knowledge of particle and crystallite size has become increasingly important because of the fact that the kinetic reactions in powders are strongly influenced by the crystallite size of the ceramics[145]. The X-ray line broadening effects are frequently used to follow sintering process and crystallite-growth kinetics. The first such application was to study the growth of MgO crystallite prepared by decomposition of carbonate[146] at temperature above 400°C. The crystallite growth of BeO from sulfate, hydroxide and oxalate sources has also been reported[147]. The crystallite size measurements were therefore carried out from the X-ray diffractograms of thick films of CdO. The relationship between the crystallite size and X-ray diffraction peak broadening was first given by Scherrer as[145,148]

$$D = \frac{K\lambda}{\beta \cos\theta}$$

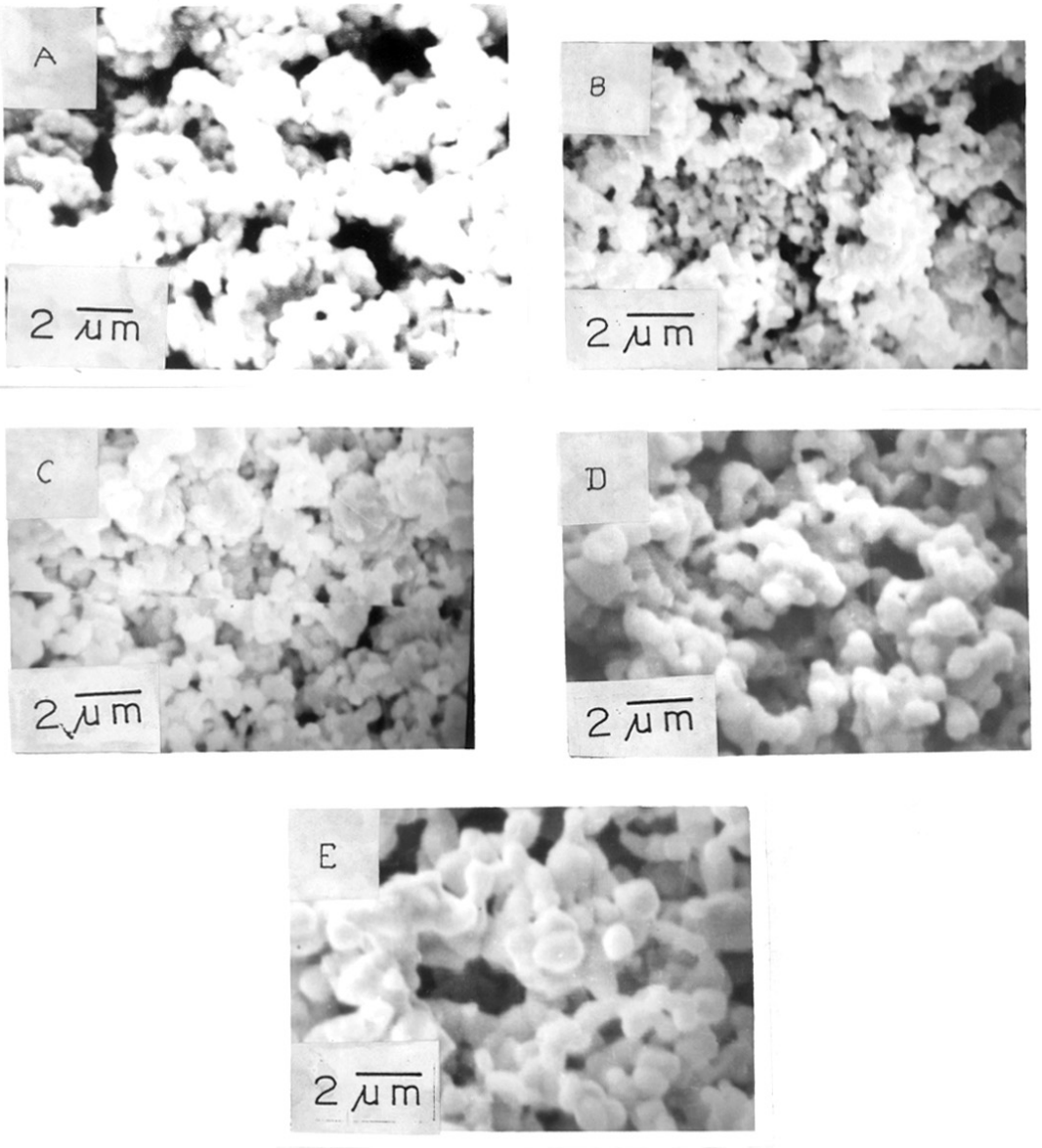

Fig. 4.6 : SCANNING ELECTRON MICROGRAPHS OF THICK FILMS OF CdO FIRED AT (A) 500, (B) 600, (C) 700, (D) 800 AND (E) 900°C

where D is crystallite size, λ is wavelength, θ is Bragg angle, β is pure diffraction broadening and K is the constant. Using this relation, crystallite size for cubic crystals of different polyhedral shape has been calculated [145,149,150]. The detailed procedure has been given by Bratram [145]. He had described three different methods, viz, half breadth, Warren equation and integral breadth. We have used the half breadth method to calculate crystallite size of CdO in thick films of CdO. The initial crystallite size of the starting polycrystalline CdO was also calculated ($D_o = 0.1015\,\mu_m$). The crystallite size D for the different peak firing temperatures are listed in Table 4.11.

4.5 Grain growth studies in thick films of CdO

Scanning electron micrographs of the films showed the increasing grain growth with firing temperature. However, the grains were agglomerated and it was difficult to measure the grain size. The relative grain size of the air fired films at successive firing temperature was obtained from the X-ray diffractograms using the half width method as listed in Table 4.11. The observations can be explained as follows.

The rapid grain growth in porous CdO sintered in

Table 4.11

Variation of crystallite size with peak firing temperature in thick films of CdO

Sr. No.	Peak firing temp.(K)	Crystallite size D (μm)	D^3 $(\mu m)^3$	$\log[\frac{(D^3-D_o^3)}{t}]$ $(\mu m)^3/min$
1	873	0.3116	0.0302	-2.5345
2	973	0.5639	0.1793	-1.7489
3	1073	0.9868	0.9609	-1.0178
4	1173	1.3158	2.27808	-0.6426

hydrogen was attributed to vapour transport, but the activation energy was reported to be much higher than that expected from vapour transport[151,152]. Grain growth controlled by volume diffusion resulting from impurity drag in dense polycrystalline CdO was found to follow one-third time-dependent relation[153]

$$D^3 - D_o^3 = Ae^{-Q/RT} t, \qquad \ldots (1)$$

where D is the grain diameter at time t, D_o is the initial grain diameter, A is a constant and Q is the activation energy for grain growth. Fig. 4.7 shows linear variation of log $[(D^3 - D_o^3)/t]$ with the reciprocal of the absolute temperature T. The activation energy, Q = 125 ± 11 KJ/mole found from the slope is close to the activation energy of 134 ± 16.8 KJ/mole observed for grain growth of dense polycrystalline oxide in temperature range 1173-1373 K. The present experimental data fit well in equation(1) indicating that the grain growth in thick films of CdO in temperature range 873-1173 K is controlled by volume diffusion due to impurity drag. The comparison between the activation energy values for different specimens of CdO is shown in Table 4.12.

4.6 Resistivity of thick films of CdO

The sheet resistivity values of thick films of CdO

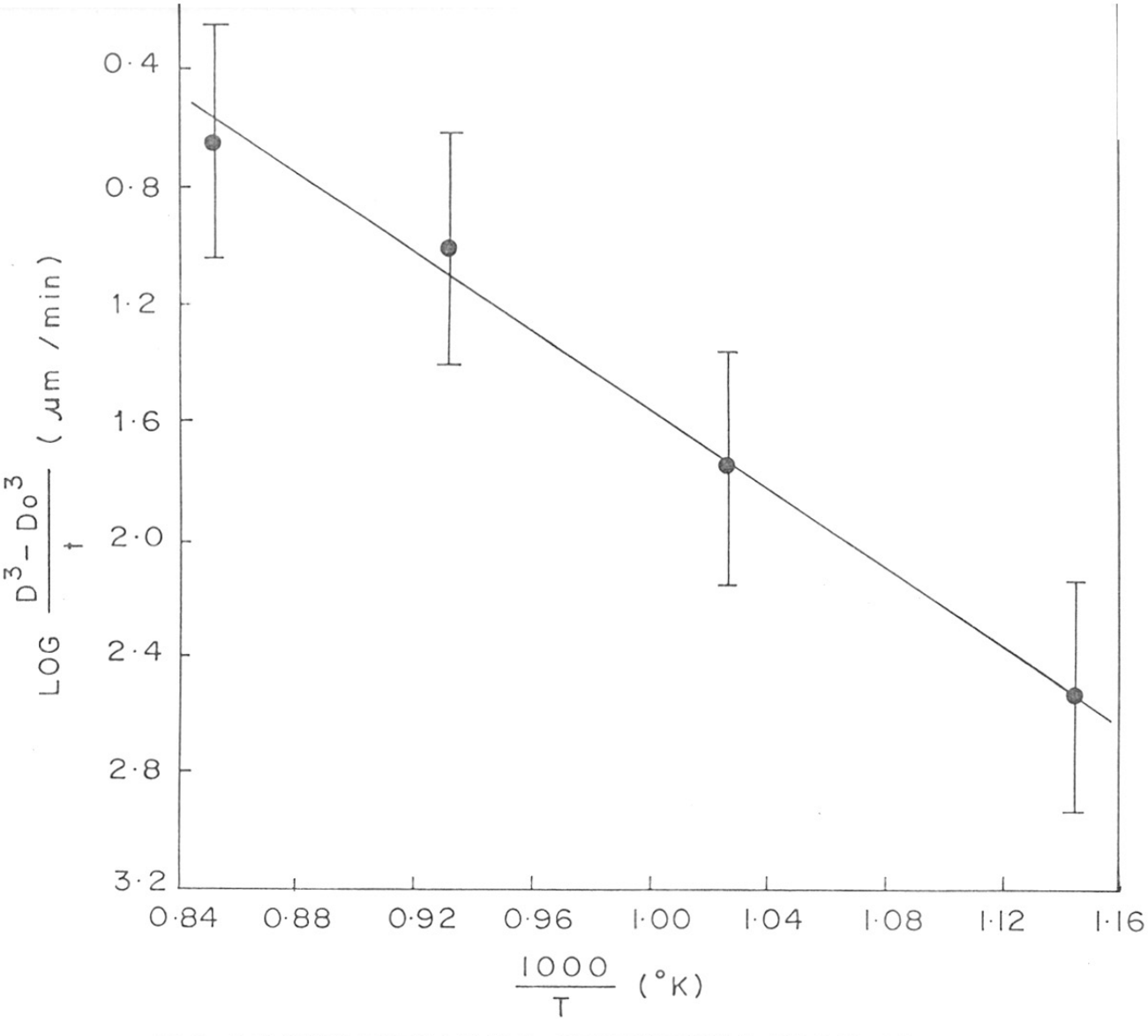

FIG. 4.7 : TEMPERATURE DEPENDENCE OF RELATIVE GRAIN SIZE IN THICK FILMS OF CADMIUM OXIDE FIRED IN AIR

Table 4.12

Comparison of activation energy for different specimens of cadmium oxide

Sr. No.	Nature of specimen	Atmosphere	Temp. range (K)	Activation energy (KJ/mole)	Ref.
1	Porous CdO	Hydrogen	1173-1373	108 ± 19	151
2	Polycrystalline CdO	Air	1173-1373	134 ± 17	153
3	Thick films of CdO	Air	873-1173	125 ± 11	This work

without containing any binder were measured after each firing of the films and are summarized in Table 4.13. The variation of sheet resistivity as a function of the firing temperature is shown in Fig. 4.8. The figure shows almost linear decrease of the resistivity values as the temperature increases from 600 to 900°C. However, the value observed for the films fired at 500°C is lower. The variation can arise because of the following facts.

As discussed in section 4, the Cd^+ content in the film decreases with the increase in firing temperature. The concentration of Cd^+ ions will, therefore, be highest in the film fired at 500°C to decrease the resistivity to its observed lowest value. At 600°C, the considerable decrease in the lattice parameter value suggests the decrease of Cd^+ ions to increase the resistivity considerably. The slight decrease in the lattice parameter value above 600°C indicates further loss of Cd^+ ions and increase of the resistivity value. However, above 600°C the figure shows continuous decrease of the resistivity value with increase of firing temperature. This can be explained with the help of microstructure attained after each firing.

The scanning electron micrographs of thick films

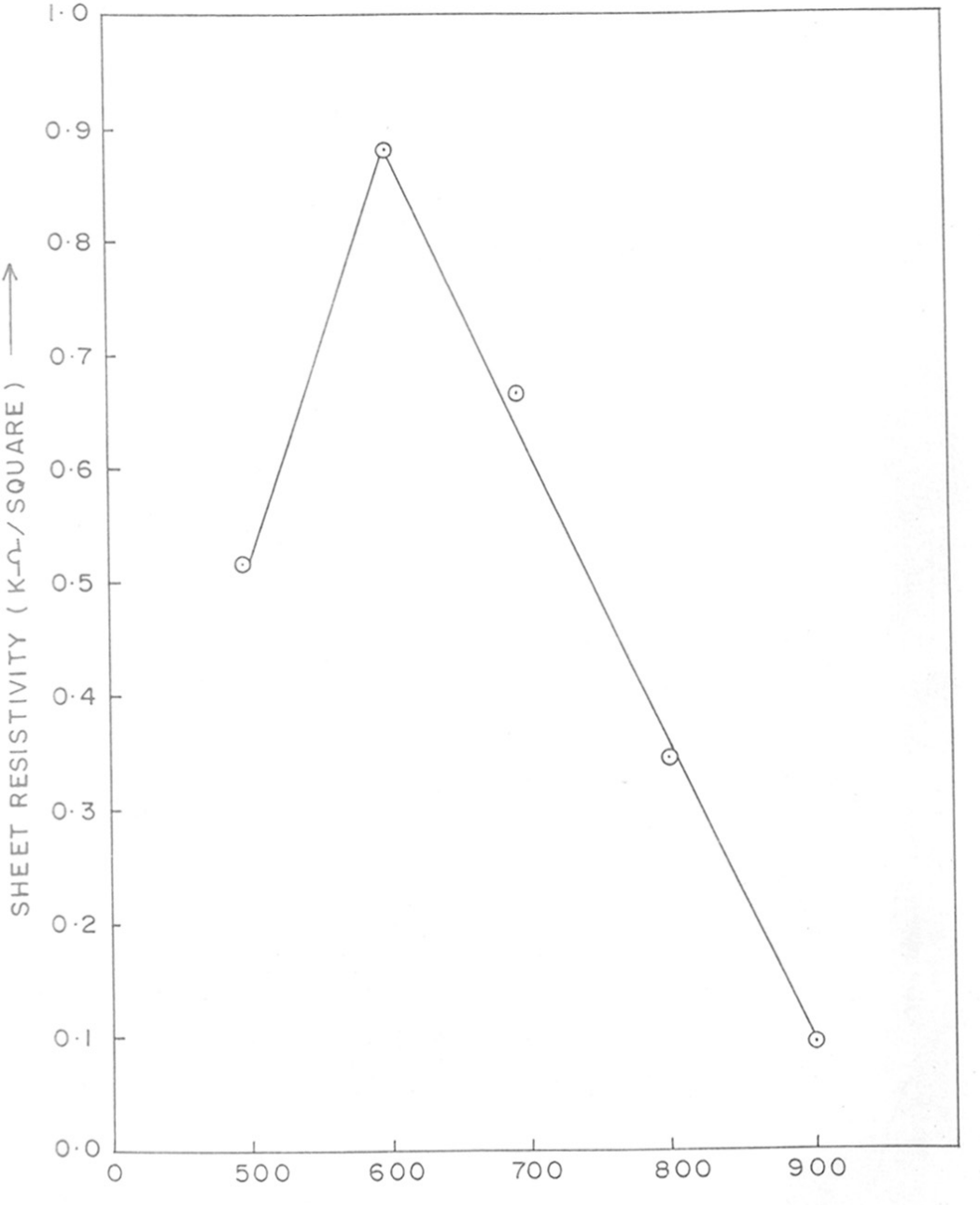

FIG. 4.8 : VARIATION OF SHEET RESISTIVITY AS A FUNCTION OF FIRING TEMPERATURE FOR THICK FILMS OF CdO.

Table 4.13

Variation of resistivity with firing temperature and with % of glass frit binders of different types

Sr. No.	Firing temp. (°C)	Sheet resistivity in KΩ/square						
		CdO	CdO-5% GL-1	CdO-10% GL-1	CdO-5% GL-2	CdO-10% GL-2	CdO-5% GL-3	CdO-10% GL-3
1	500	0.4403	2.3788	0.2629	8.7086	0.1849	0.7797	0.1007
2	600	0.7574	1.6034	0.6028	2.9457	225.77	0.3809	0.08009
3	700	0.5691	0.3568	0.2683	2.5777	35.34	0.1110	0.0444
4	800	0.2946	0.0812	0.0243	8.8843	98.37	0.0289	0.0170
5	900	0.0803	0.0341	0.0109	31.6	225.49	0.0588	0.0074

of CdO fired in temperature range 600 to 900°C show progressive grain growth which can lower the contact resistance. It has been observed that the major portion of the total resistivity comes from electron scattering at the grain boundaries [154,155]. The quantitative relation was given as

$$\frac{\rho_o}{\rho_g} = 1 - \frac{3}{2}\gamma - 3\gamma^2 - 3\gamma^3 \ln(1+\gamma) \qquad \ldots (1)$$

with $= \frac{\lambda_o}{d_{av}} \quad \frac{R}{1-R}$

where ρ_o and ρ_g are bulk and grain boundary resistivity, λ_o is background mean free path, R is the reflection coefficient and d_{av} is the average grain diameter. The equation(1) has been simplified as [154]

$$\frac{\rho_o}{\rho_g} \approx 1 + \frac{3}{2}\gamma \qquad \gamma << 1 \qquad \ldots (2)$$

$$\frac{\rho_o}{\rho_g} \approx \frac{4}{3}\gamma \qquad \gamma >> 1 \qquad \ldots (3)$$

These equations (2) and (3) were used to relate the observed resistivity values to the d_{av} as shown in Fig. 4.9.

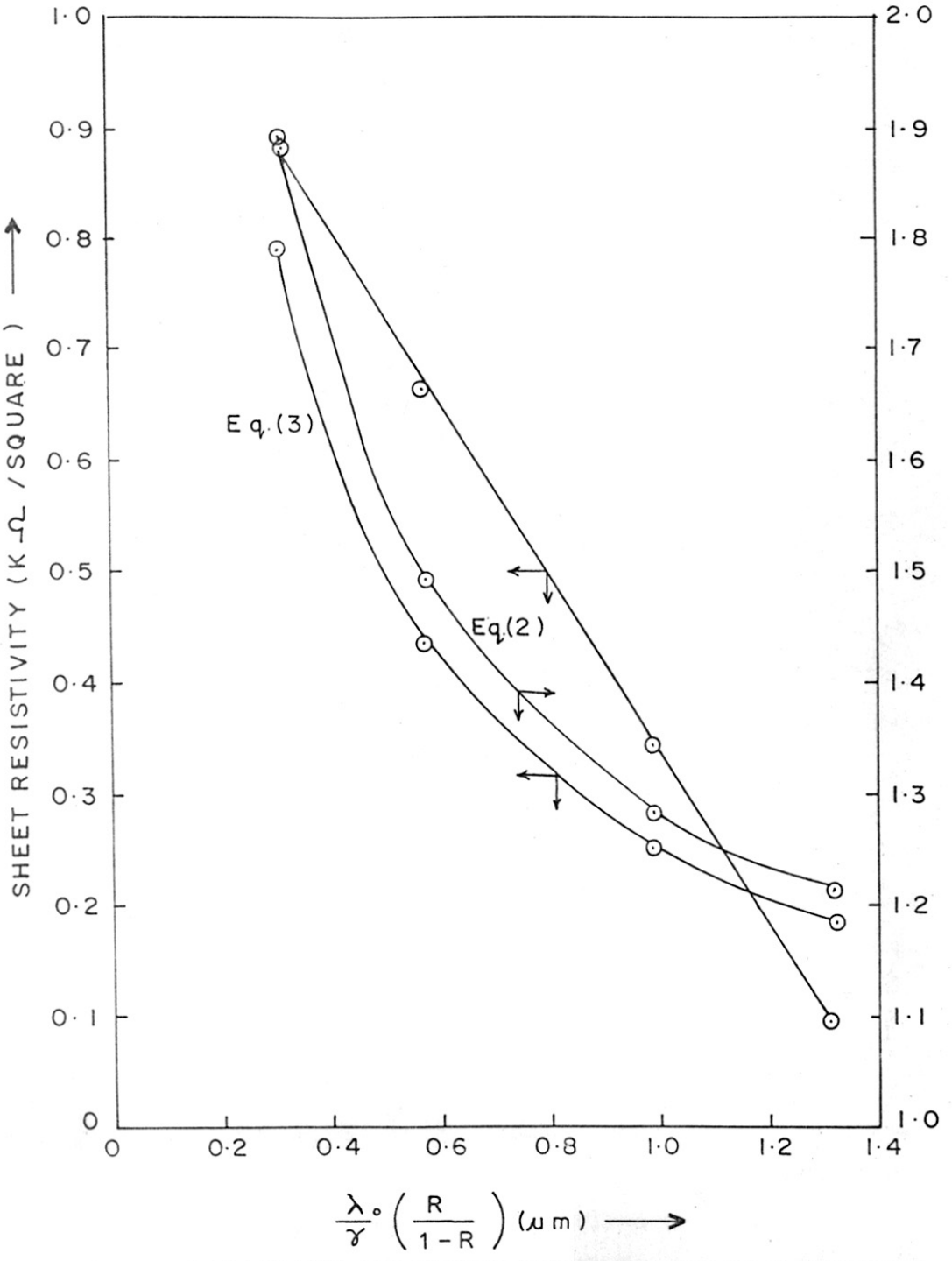

FIG. 4.9: VARIATION OF SHEET RESISTIVITY AS A FUNCTION OF GRAIN DIAMETER.

4.7 Influence of the binder on the sheet resistivity

The sheet resistivity values of thick films of CdO containing different types of binders were measured after each firing of the films and are listed in Table 4.13.

The variation of sheet with the content of GL-1 type of binder (PbO-based glass) is shown in Fig. 4.10. The figure shows maxima in the sheet resistivity value for 5 wt % of the binder and for firing temperature of 500 and 600°C. The variation is almost linear for firing temperature of 700°C. The similar variation is observed for GL-3 type of binder (ZnO-based glass) as shown in Fig. 4.12. However, for this type of binder the linear variation is observed for the firing temperature of 600°C. The variation of sheet resistivity with the content of GL-2 type of binder is shown in Fig. 4.11. In this case, maximum values of sheet resistivity were observed for the films containing 10 weight percent of the binder and fired in temperature range of 600 to 900°C. No linear variation is observed for any of the firing temperature.

The variation of sheet resistivity with firing temperature were plotted for all three of binders as shown in Figs. 4.13 and 4.14. The films containing GL-1 type of binder (5 wt %) show the behaviour resembling to the

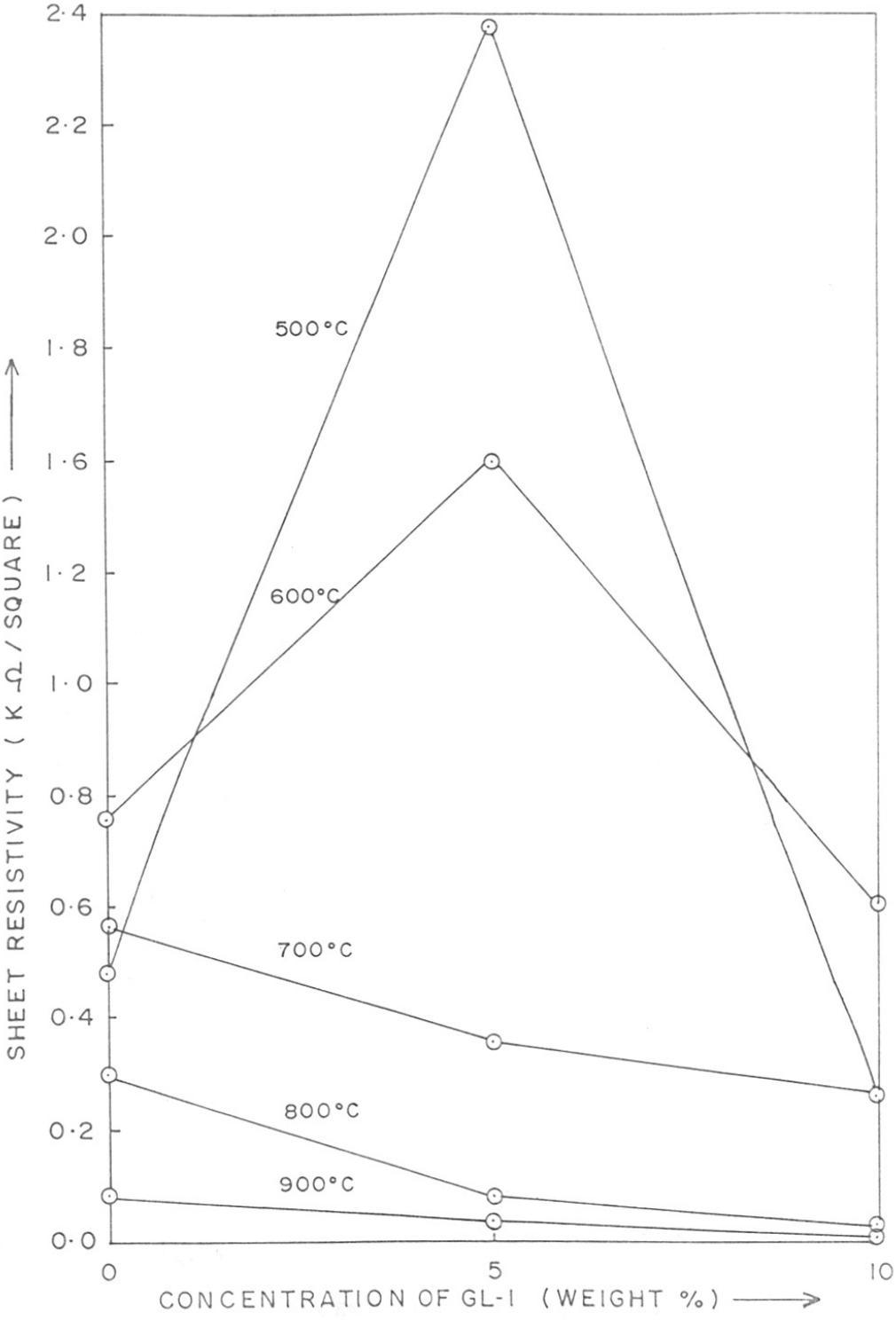

FIG. 4.10 : VARIATION OF SHEET RESISTIVITY WITH THE CONTENT OF GL-I TYPE OF BINDER.

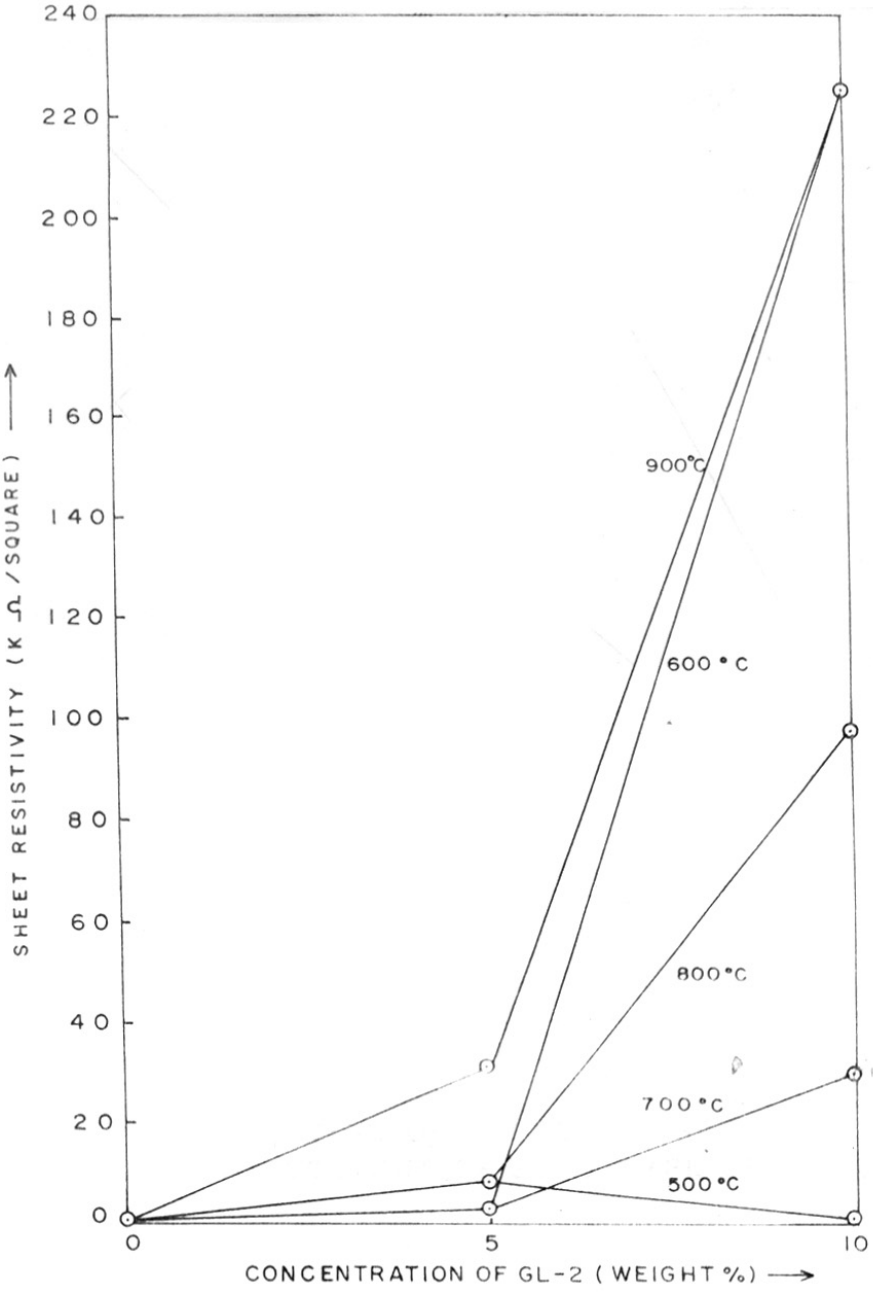

FIG. 4·11 VARIATION OF SHEET RESISTIVITY WITH THE CONTENT OF GL-2 TYPE OF BINDER.

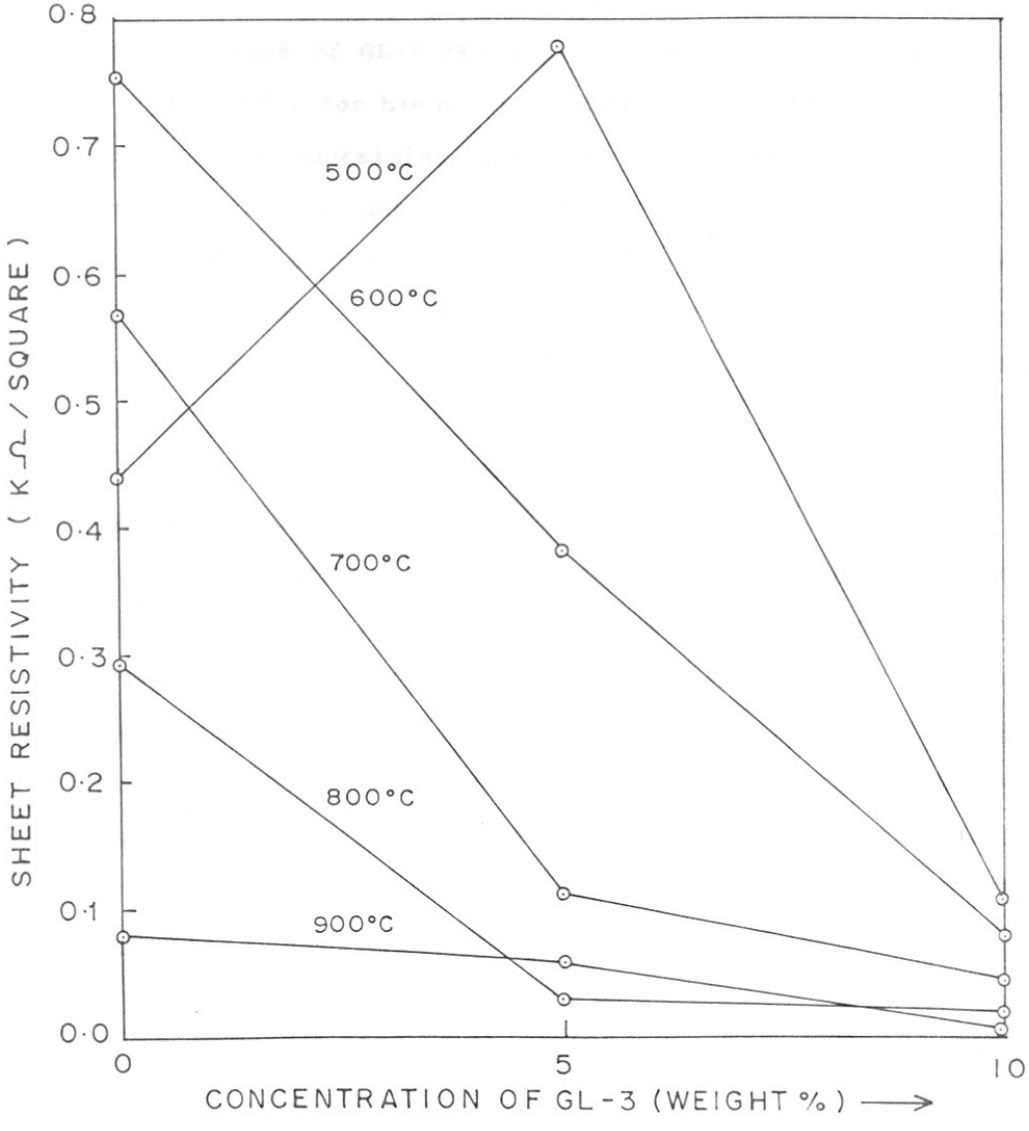

FIG. 4.12 : VARIATION OF SHEET RESISTIVITY WITH THE CONTENT OF GL-3 TYPE OF BINDER.

films without containing any binder (Fig. 4.8). For the binder GL-3, the behaviour is almost linear. However, in the case of GL-2 binder, no definite trend is observed (Fig. 4.13). For higher concentration of binder (10 wt %), the films containing GL-1 and GL-3 show decrease in resistivity values with increase in firing temperature as shown in Fig. 4.14. The films containing GL-2 first show decrease in the resistivity values in firing temperature range 500 to 700°C and the increase in the range 700 to 900°C.

4.8 Conclusions

Thick films of cadmium oxide were obtained by screen printing and firing in temperature range 500-900°C. Three different glass frit binders were prepared and used to prepare thick films of CdO. These four different series of the films, viz, CdO, CdO-GL-1, CdO-GL-2 and CdO-GL-3 are studied by X-ray diffraction techniques. These studies indicated the presence of cubic CdO and additional impurity phases of $CdCO_3$ and $Cd(OH)_2$.

The variation of the lattice parameter for the films of CdO indicates change of Cd^+ ions to Cd^{2+} ions with increase in firing temperature. The films of CdO-GL-1 also show similar changes and indicate the incorporation

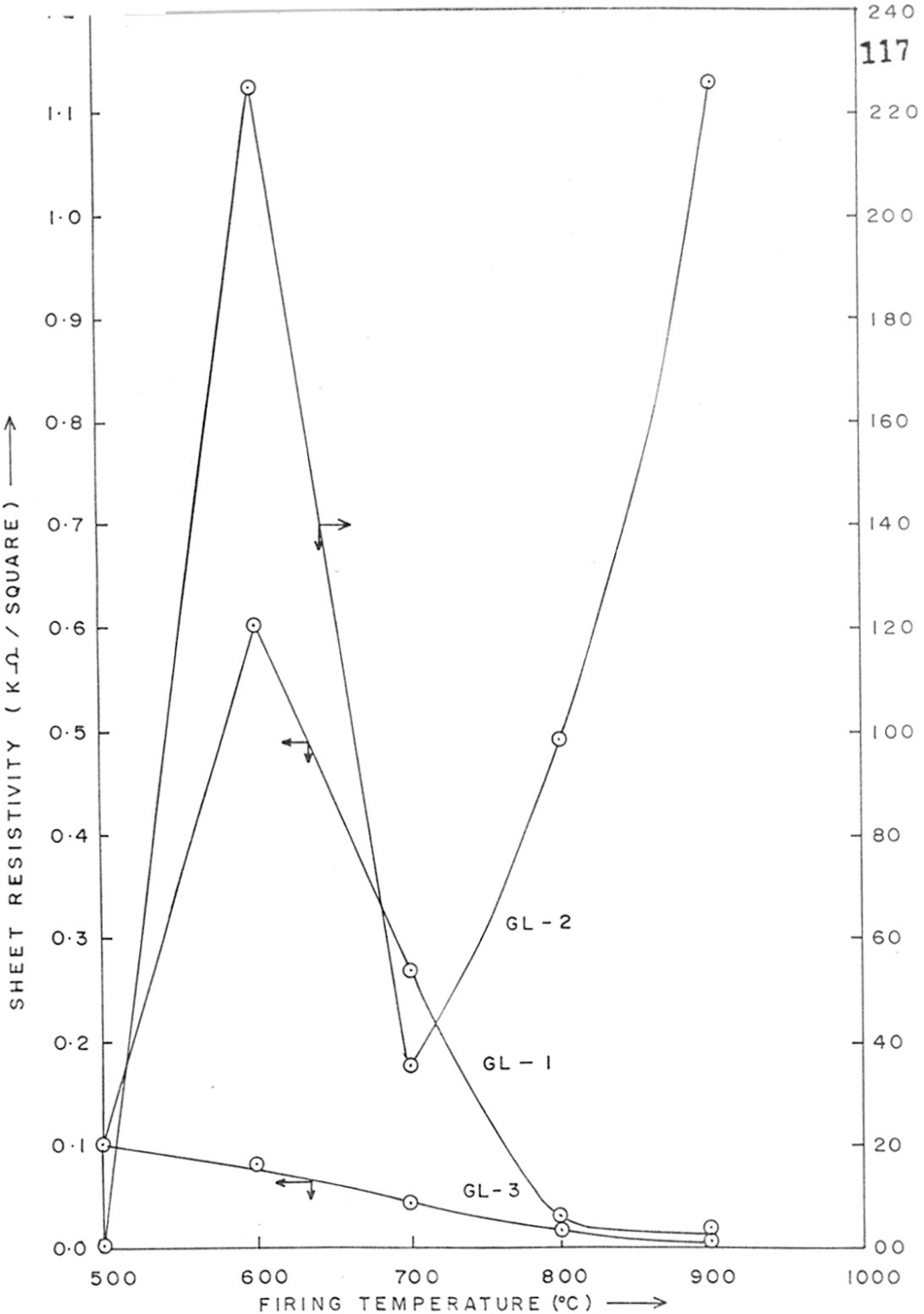

FIG. 4·13 : VARIATION OF SHEET RESISTIVITY AS A FUNCTION OF FIRING TEMPERATURE FOR THICK FILMS OF CdO - GL-1, CdO - GL-2, AND CdO - GL-3, CONTAINING 5 WEIGHT % OF GL.

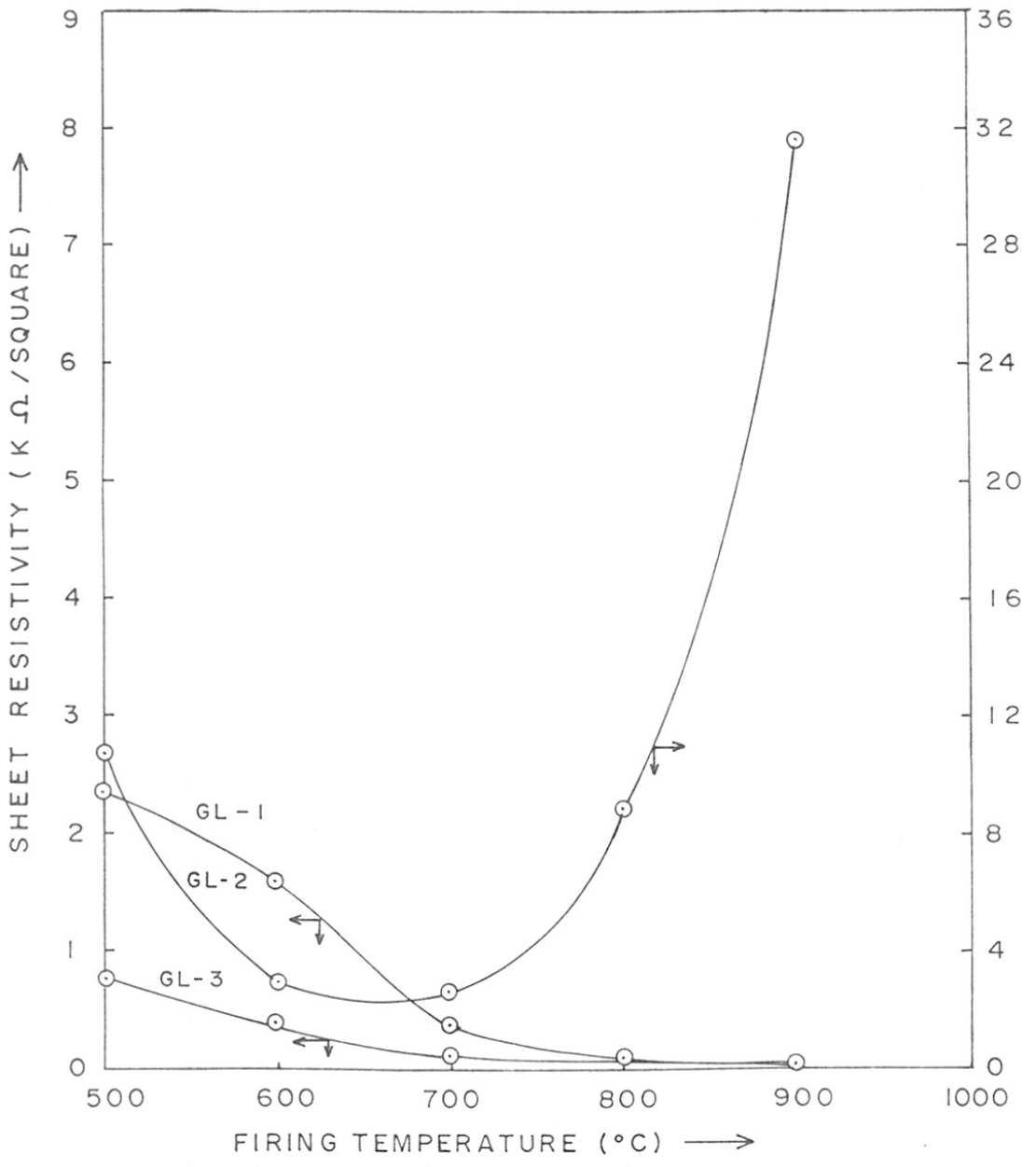

FIG. 4.14 : VARIATION OF SHEET RESISTIVITY AS A FUNCTION OF FIRING TEMPERATURE FOR THICK FILMS OF CdO - GL-1, CdO - GL-2 AND CdO - GL-3 CONTAINING 10 WEIGHT % OF GL.

of Pb^{2+} ions into the lattice of CdO at firing temperature of 800°C. The films of CdO-GL-3 showed continuous decrease in the lattice parameter values and decrease in the concentration of Cd^{+}. In the case of CdO-GL-2 films, increase in the lattice parameter value is observed. This is explained on the basis of controlled valence process, similar to that observed in $ZnO:Ga^{3+}$ system.

Scanning electron micrographs of thick films of CdO showed the increasing grain growth with increase in firing temperature. The relative grain size was estimated using the X-ray diffractograms of the films. The variation of relative grain size with temperature gave an activation energy of 125 ± 11 KJ/mole. In conclusion, grain growth in thick films of cadmium oxide fired in air at 600-900°C is observed for the first time. The comparison of these studies with the reported data of related system suggests that the grain growth is most likely due to the volume diffusion resulting from impurity drag.

The resistivity of thick films of CdO was studied as a function of firing temperature. The studies indicate that two processes occur in thick films of CdO. (i) The Cd^{+} ions change considerably to Cd^{2+} ions when the firing temperature is increased from 500 to 600°C, to increase

the resistivity value. (ii) The decrease in intercrystalline resistance is the major part of the firing process and may reduce the resistivity due to lowering of the electron scattering at grain boundaries.

The influence of the binder on the resistivity of thick films of CdO was studied for the amount of content and type of binder. These studies indicate that with PbO-based (GL-1) and ZnO-based (GL-3) binders, the resistivity can be controlled with the concentration of binder and for firing temperature of 700 and 600°C respectively.

In summary, CdO is prospective candidate for its wide usage as a conducting material in thick film resistors.

References

1. C. Konak, P. Hoschl, J. Dillinger and V. Prosser, J. Phys. Chem. Solids Suppl. No.1, (1967) 341 [C.A. 68: 73125h].
2. S.A. Abd. El.-Hody, I.F. Hewaidy, K.A. Khadre and M.S. Farag, U.A.R. J. Phys., 1 (1970) 185 [C.A. 74: 80725f].
3. M.E. Straumanis, P.M. Vora and A.A. Khan, Z. Anorg. Allg. Chem., 383 (1971) 211 [C.A. 75: 81222x].
4. M.E. Straumanis, P.M. Vora and A.A. Khan, Trans. Mo. Acad. Sc., 6 (1972) 92 [C.A. 81: 112264t].
5. H.P. Singh and D. Dayal, Solid State Commun., 7 (1969) 725.
6. G. Greenwood, Ind. J. Phys., 8 (1933) 269.
7. J.C. Felip and R. Revta, Cience. Exact. Fis. Nat. Madr., 34 (1940) 180.
8. K. Kodera, I. Kasunoki and S. Shionizu, Bull. Chem. Soc. Japan, 41 (1968) 1039.
9. I.G.F. Gilbert and J.A. Kitchner, J. Chem. Soc., (1956) 3919.
10. A.F. Varobiv and A.F. Broier, Zh. Fiz. Khim., 45 (1971) 2390.
11. A.D. Mah, J. Am. Chem. Soc., 76 (1954) 3363.
12. L. Schuffenecker, D. Balesent and J. Houriez, J. Chem. Thermodynamics, 13 (1981) 849.

13. A.C. Egerton and F.V. Raleigh, J. Chem. Soc., 123 (1923) 3024.

14. J.A. Bastin and R.W. Wright, Proc. Phys. Soc., 72 (1958) 65.

15. C.A. Howarth, Proc. Phys. Soc., B64 (1951) 691.

16. J.A. Bastin and R.W. Wright, Proc. Phys. Soc., A68 (1955) 312.

17. R.W. Wright, Proc. Phys. Soc., 64 (1951) 949.

18. R.W. Wright, Proc. Phys. Soc., A64 (1951) 350.

19. E.F. Lamb and F.C. Tompkins, Trans. Fara. Soc., 58 (1962) 1424.

20. R.W. Wright and J.A. Bastin, Proc. Phys. Soc., 71 (1958) 109.

21. Z.M.Jarzebski, Bull. Acad. Pol. Sc., 17 (1969) 221.

22. F.P. Koffyberg, Phys. Lett., A30 (1969) 37.

23. F.P. Koffyberg, J. Solid State Chem., 2 (1970) 176.

24. F.P. Koffyberg, Can. J. Phys., 49 (1971) 435.

25. H.J. Angell, Z. Elektrochem., 60 (1956) 905.

26. H. Finkenrath and M. Von. Ortenberg, Z. Angew. Phys., 22 (1967) 279.

27. R. Haul and D. Just, J. Appl. Phys., 33 (1962) 487.

28. T. Mookherjee, J. Electrochem. Soc., 117 (1970) 1201.

29. K.A. Muller and J. Schneider, Phys. Letters, 4 (1963) 288.

30. B. Elschner and M. Schlaak, Phys. Letters, 24A (1967) 10.

31. R.H. Meinhold, J. Phys. Chem. Solids, 48 (1987) 927.

32. K. Maschke and U. Rossler, Phys. Stat. Solidi, 28 (1968) 577.

33. S. Tewari, Solid State Commun., 12 (1973) 437.

34. A. Breez and P.G. Perkins, Solid State Commun., 13 (1973) 1031.

35. J.C. Boettger and A.B. Kunz, Phys. Rev., B27 (1983) 1359.

36. C.A. Harper (editor), Handbook of Thick Film Hybride Microelectronics (McGraw-Hill, New York, 1974).

37. K.H. Behrndt, in Thin Films (American Society for Metals, Metal Park Ohio, 1964) p. 1-43.

38. C.A. Harper (editor), Handbook of Materials and Processes for Electronics (McGraw-Hill, New York, 1970).

39. D. Dimitrov, S. Metev, I. Gugov and V. Kozhukhorov, J. Mater. Sc. Lett., 1 (1982) 334.

40. M. Altwin, H. Finkenrath, C. Konak, J. Stuke and G. Zimmerer, Phys. Stat. Solidi, 29 (1968) 203.

41. K. Tanaka, A. Kunioka and Y. Sakai, Japanese J. Appl. Phys., 8 (1969) 681.

42. T.S. Wu, T. Shiramatsu and T.S. Young, Thin Solid Films, 62 (1979) 265.

43. Shen-Li Fu and Gi-Chang Lin, in Proceedings of 31st Electronic Component Conference (IEEE, New York, 1981) p. 46.

44. W. Mitsuo and I. Yoshio, U.S. 3,551,195 (1971), C.A. 74: 56910s.

45. M. Masaki, H. Tadashi, A. Masaki and W. Mitsuo, Japan 7401,929 (1974), C.A. 81: 95615p.

46. M. Masaki, H. Tadashi, A. Masaki and W. Mitsuo, Japan 7401,930 (1974), C.A. 81: 95616q.

47. M. Masaki, H. Tadashi, A. Masaki and W. Mitsuo, Japan 7401,931 (1974), C.A. 81: 95617r.

48. M. Masaki, H. Tadashi, A. Masaki and W. Mitsuo, Japan 7401,928 (1974), C.A. 81: 95614n.

49. O. Mitsuhiro and W. Mitsuo, Japan Kokai 75 79 791 (1975), C.A. 84: 37894e.

50. O. Mitsuhiro and W. Mitsuo, Japan Kokai 75 79 788 (1975), C.A. 84: 37885c.

51. O. Mitsuhiro, W. Mitsuo and T. Shinichi, Japan Kokai 75 79 787 (1975), C.A. 84: 37886d.

52. O. Mitsuhiro and W. Mitsuo, Japan Kokai 75 79 786 (1975), C.A. 84: 37887e.

53. O. Mitsuhiro, W. Mitsuo and T. Shinichi, Japan Kokai 75 79 785 (1975), C.A. 84: 37888f.

54. O. Mitsuhiro and W. Mitsuo, Japan Kakai 75 79 784 (1975), C.A. 84: 37889g.

55. O. Mitsuhiro and W. Mitsuo, Japan Kokai 75 79 789 (1975), C.A. 84: 37892c.

56. O. Mitsuhiro and W. Mitsuo, Japan Kokai 75 79 790 (1975), C.A. 84: 37893d.

57. O. Mitsuhiro, W. Mitsuo and T. Shinichi, Japan Kokai 75 79 792 (1975), C.A. 84: 37895f.

58. O. Mitsuhiro and W. Mitsuo, Japan Kokai 75 79 795 (1975), C.A. 84: 37898j.

59. O. Mitsuhiro and W. Mitsuo, Japan Kokai 75 79 796 (1975), C.A. 84: 37899k.

60. O. Mitsuhiro and W. Mitsuo, Japan Kokai 75 79 798 (1975), C.A. 84: 37900d.

61. O. Mitsuhiro and W. Mitsuo, Japan Kokai 75 79 799 (1975), C.A. 84: 37904h.

62. A. Masaki, N. Ikuo, W. Mitsuo and N. Hiroshi, Japan 7505389 (1975), C.A. 81: 89773p.

63. A. Masaki, N. Ikuo, W. Mitsuo and N. Hiroshi, Japan 7505386 (1975), C.A. 83: 89776s.

64. A. Masaki, N. Ikuo, W. Mitsuo and N. Hiroshi, Japan 7505385 (1975), C.A. 83: 89777t.

65. A. Masaki, N. Ikuo, W. Mitsuo and N. Hiroshi, Japan 7505391 (1975), C.A. 83: 89778u.

66. A. Masaki, N. Ikuo, W. Mitsuo and N. Hiroshi, Japan 7505393 (1975), C.A. 83: 89781q.

67. F.F. Lange, H. Shubert, N. Claussen and M. Ruhle, J. Mater. Sc., 21 (1986) 768.

68. P. Miranzo, P. Pena, J.S. Moya and S. Deaza, J. Mater. Sc., 20 (1985) 2702.

69. M.K. Dongare and A.P.B. Sinha, J. Mater. Sc., 19 (1984) 49.

70. Q. Ming Yuan, J. Qi Tan, J. Yao Shen, X. Hui Zhu and Z. Fang Yang, J. Am. Ceram. Soc., 69 (1986) 268.

71. S. Doeuff, M. Henry, C. Sanchez and J. Livage, J. Non-Crystalline Solids, 89 (1987) 84.

72. S. Komaarnehi, R. Roy, E. Breval, M. Ollinen and Y.K. Suwa, Adv. Ceram. Mater., 1 (1986) 87.

73. R. Vivekanandan, S. Philip and T.R.N. Kutty, Mater. Res. Bull., 22 (1987) 99.

74. M. Avudaithai and T.R.N. Kutty, Mater. Res. Bull., 22 (1987) 641.

75. T.R.N. Kutty and R. Vivekanandan, Mater. Res. Bull., 22 (1987) 1457.

76. T. Ono, M. Kagawa and Y. Syono, J. Mater. Sc., 20 (1985) 2483.

77. T. Sakuma, Y. Ichi Yoshizawa and H. Me Suto, J. Mater. Sc., 20 (1985) 2399.

78. P. Singh and S.K. Date, J. Mater. Sc., 6 (1987) 621.

79. M.S. Setty and R.F. Shinde, Active and Passive Electronic Components, 12 (1986) 111.

80. F.H. Norton, Elements of Ceramics (Addison - Wesley Publishing Co., Inc. Philippines, 1974).

81. H.J. Sanders, Special Report C. and E.N. Washington, July 9,1984.

82. R.R. Hirwani, Chemical Business, (1987) 45-48.

83. ASTM Card for X-ray diffraction data, No.5-0640.

84. ASTM Card for X-ray diffraction data, No.1-0907.

85. ASTM Card for X-ray diffraction data, No.1-0305.

86. A. Bencini and D. Gatteschi, in: Transition Metal Chemistry, Vol.8, Edited by G.A. Melson and B.N. Figgis (Marcel Dekker, Inc. New York 1982) p. 1-178.

87. A. Abragam and B. Bleaney, Electron Paramagnetic Resonance of Transition Metal Ions (Clarendon Press, Oxford, 1970).

88. J.E. Wertz and J.R. Bolton, Electron Spin Resonance, Elementary Theory and Practical Applications (Mc Graw-Hill, New York, 1972).

89. C.P. Poole, Jr., and H.A. Farach, Theory of Magnetic Resonance (Wiley-Interscience, New York, 1987).

90. N.M. Atherton, Electron Spin Resonance: Theory and Applications (Ellis Horwood Ltd., John Wiley and Sons. Inc., 1973).

91. B. Bleaney, Phil. Mag., 42 (1951) 441.

92. G.H. Azarbayejani, Phys. Lett., A25 (1967) 767.

93. R.E.D. McClung, Can. J. Phys., 46 (1968) 2271.

94. R.M. Golding, Applied Wave Mechanics (van Nostrand, London, 1969).

95. U. Sakaguchi, Y. Arota and S. Fujiwara, J. Magn. Res., 9 (1973) 118.

96. W.C. Lin, Mol. Phys., 25 (1973) 247.

97. R. Kirmse, S. Wartewig, W. Windsch and E. Hoyer, J. Chem. Phys., 56 (1972) 9273.

98. J.R. Pilbrow and M.E. Winfield, Mol. Phys., 25 (1973) 1073.

99. R.M. Golding and W.C. Tennant, Mol. Phys., 25 (1973) 1163.

100. A. Rockenbauer and P. Simon, J. Magn. Res., 11 (1973) 217.

101. A. Rockenbauer and P. Simon, Mol. Phys., 28 (1974) 1113.

102. J.A. Weil, J. Magn. Res., 18 (1975) 113.

103. R. Skinner and J.A. Weil, J. Magn. Res., 21 (1976) 271.

104. R. Skinner and J.A. Weil, J. Magn. Res. 29 (1978) 223.

105. R.M. Golding and W.C. Tennant, Mol. Phys., 28 (1974) 167.

106. J.S. Shaffer, H.A. Farach and C.P. Pool, Jr., Phys. Rev., B13 (1976) 1869.

107. R.C. Barklei and K. O'Donnell, J. Phys. C: Solid State Phys., 10 (1977) 4127.

108. D.H. Lyons and R.W. Kedzie, Phys. Rev., 145 (1966) 148.

109. R.S. DeBiasi and A.A.R. Fernandes, J. Amer. Ceram. Soc., 67 (1984) C-173.

110. J.E. Drumheller and R.S. Rubins, Phys. Rev., 133 (1964) A1099.

111. V.J. Folen, Phys. Rev., 125 (1962) 1581.

112. A. Hausmann and H. Huppertz, J. Phys. Chem. Solids, 29 (1968) 1369.

113. L. Abbello, S.J. Schurdlfeger and C.F. Schwerdtfeger, Solid State Commun., 44 (1982) 497.

114. W. Low, Phys. Rev., 105 (1975) 793.

115. W. Low, Phys. Rev., 105 (1957) 792.

116. W. Low, Proc. Phys. Soc., B69 (1956) 1169.

117. W. Low, Bull. Am. Phys. Soc., 1 (1956) 283.

118. T.P.P. Hall, W. Hayes and F.I.B. Williams, Proc. Phys. Soc., 78 (1961) 883.

119. A.F.M.Y. Haider, Indian J. Phys., 62A (1988) 148.

120. L.V. Holroyd and J.L. Kolopus, Phys. Stat. Solidi, 3 (1963) K456.

121. L.S. Sochava, Y.N. Tolparov and N.N. Kovalev, Sov. Phys. Solid. State, 16 (1974) 205.

122. J. Rubio, Y. Chen and M.M. Abraham, J. Chem. Phys., 64 (1977) 4804.

123. J. Rubio, Y. Chen and M.M. Abraham, J. Phys. Chem. Solids, 38 (1976) 215.

124. W. Low and J.T. Suss, Phys. Rev., 119 (1960) 132.

125. F. Fesmundo and P.F. Rossi, J. Solid State Chem., 8 (1973) 297.

126. C.Z. van Doorn and Y. Haven, Philips Research Reports, 11 (1956) 479.

127. P. Singh, S.R. Sainkar, M.V. Kuber, V.G. Gunjikar, R.F. Shinde and S.K. Date, Materials Letters, under communication.

128. P.B. Dorain, Phys. Rev., 112 (1958) 1058.

129. H. Ueda, M. Yoncmura and T. Sokini, Phys. Rev., B35 (1987) 4602.

130. B. Wichterlova, J. Novakova, L. Kubelkova and P. Mikusik, Zeolite, 5 (1985) 21.

131. R.C. Weast and M.J. Astle, (editors), Handbook of Chemistry and Physics (CRC Press, Inc. 1980).

132. F.A. Kroger, "The Chemistry of Imperfect Crystals" 2nd edn. (North Holland, 1974).

133. B. Bezny, W.R. Ryall and A. Muan, Mater. Res. Bull., 5 (1970) 481.

134. M. Volkmann and W. Wadelich, Phys. Lett., 24A (1967) 404.

135. W. Lehman, J. Electrochem. Soc., 115 (1968) 538.

136. W. Gunsser, W. Hiller and A. Knappwost, Z. Phys. Chem., 65 (1969) 326.

137. C.E. Deshpande, L.M. Pant and M.N.S. Murthy, Ind. J. Chem., 16 (1978) 251.

138. S.F. Koltashkina and G.P. Popov, C.A. 72: 48132h (1970).

139. C.E. Deshpande, P.P. Bakare, M.N.S. Murthy, N.Y. Vasanthacharya and P. Ganguly, Proc. Indian Acad. Sc., 91 (1982) 261.

140. F.A. Kroger and H.J. Vink, Solid State Phys., Eds. F. Seitz and D. Turnbull, 3 (1956) 307.

141. W. Koch and C. Wagner, Z. Phys. Chem., B38 (1957) 295.

142. E.J.W. Vermey, P.W. Haaijman, F.C. Rameijn and G.W. van Oosterhout, Philips Res. Rep., 5 (1950) 173.

143. P.W. Selwood, T.E. Moore, M. Ellis and W. Wethington, J. Am. Chem. Soc., 71 (1949) 693.

144. J.M. Honig, J. Chem. Education, 43 (1966) 76.

145. E.F. Kaelble, editor, Handbook of X-rays, (McGraw-Hill Book Company, New York 1967) pp. 17-9.

146. L.W. Briks and H. Friedman, J. Appl. Phys., 17 (1948) 687.

147. S.F. Bartram, Advances in X-ray Analysis, Vol. 4, (Plenum Press, Inc. New York 1961) pp. 40-63.

148. P. Scherrer and P. Gottinger, Nachr., 2 (1918) 98.

149. A.R. Stokes and A.J.C. Wilson, Proc. Cambridge Phil. Soc., 38 (1942) 313.

150. A.R. Stokes and A.J.C. Wilson, Proc. Cambridge Phil. Soc., 40 (1944) 197.

151. T. Quadir and D.W. Readey, in Material Science Research, Vol. 16, eds. G.C. Kuczynski, A.E. Miller and G.A. Sargent (Plenum Press, New York, 1984) p. 159.

152. J. Lee and B.W. Readey, in: Material Science Research, Vol. 16, eds. G.C. Kuczynski, A.E. Miller and G.A. Sargent (Plenum Press, New York, 1984) p. 145.

153. T. Quadir and D.W. Readey, J. Am. Ceram. Soc., 69 (1986) C-152.

154. A.F. Mayadas and M. Shatzkes, Phys. Rev., B1 (1970) 1382.

155. L. Kusin-Elbaum, Thin Solid Films, 169 (1989) 17.

Summary

Summary

In the last decade, a large number of high value added high-tech materials are available which exhibit or deliver superior mechanical, electrical, magnetic and optical properties. These are now commercially produced from readily available materials such as oxides, nitrides, carbides of iron, zirconium, titanium, aluminium, silicon, etc. through the optimization of many process parameters. The experimental research efforts on high-tech ceramics are focussed on what happens to these products at atomic, molecular or crystal level during their synthesis, processing, characterization and extensive usage. Physicochemical characterization of cadmium oxide ceramics dealing with synthesis, electronic processes and thick film form are therefore carried out in our laboratory.

The synthesis of $Cd_{1-x}Mn_xO$ system was carried out by ususl decomposition reaction, monitored through simultaneous DTA/TG/DTG plots. The X-ray diffraction studies of the prepared composition showed that the system exhibits cubic crystal structure. The lattice parameter values of the compositions are close to the reported value of CdO. The X-ray diffraction studies of the aged samples clearly revealed the presence of

$CdCO_3$ and $Cd(OH)_2$. These phases grow during the aging period by the action of CO_2 and H_2O on CdO.

The extensive EPR studies of the $Cd_{1-x}Mn_xO$ system are carried out for the first time. All the g values obtained for the EPR signal observed in the system are comparable with the reported g values of different paramagnetic centers present in a variety of non-stoichiometric specimens of CdO.

The observations of hyperfine and superhyperfine lines for this system showed that Mn^{2+} ions occupy substitutional site in nearly cubic environment of oxygen octahedra in CdO. Further, the observation of superhyperfine lines suggested that Mn^{2+} electrons are delocalized to give superhyperfine interactions with the nearest neighbouring Cd nuclei of nonzero spin. The spin Hamiltonian parameters are comparable with that reported for other cubic system.

The aged sample of the system showed an additional signal at g = 2.778 corresponding to the Mn^{2+} ions present in the impurity phases. The aged sample also showed an additional hyperfine sextet growing with the aging period. This sextet is likely to arise from Mn^{2+}

ions in the impurity phase of $CdCO_3$.

Thick films of CdO were prepared by using different types of binder. The concentration of the binder varied from 0 to 10 wt %. The X-ray diffraction studies of the films showed the presence of impurity phases of $CdCO_3$ and $Cd(OH)_2$. The variation of lattice parameter for the films of CdO indicated the oxidation of Cd^+ ions to Cd^{2+} ions during the firing process. The films of CdO-GL-1 also showed similar changes and indicated the incorporation of Pb^{2+} ions into the lattice of CdO at firing temperature of 600°C. The films of CdO-GL-3 showed continuous decrease in the lattice parameter values and decrease in the concentration of Cd^+. In the case of CdO-GL-2 films, increase in the lattice parameter value is observed. This is explained on the basis of controlled valency process similar to that observed in $ZnO:Ga^{3+}$ system.

The grain growth in thick films of CdO fired in the temperature range of 600-900°C is observed for the first time. The comparison of these studies with the reported data of related system suggests that the grain growth is most likely due to the volume diffusion resulting from impurity drag.

The variation of sheet resistivity of thick films of CdO is explained on the basis of oxidation of Cd^{+} ions to Cd^{++} ions and electron scattering at grain boundaries. The influence of the binder on sheet resistivity values of the films is discussed.

In conslusion, Mn^{2+} ions are found to be an excellent EPR microprobe to monitor the local environment and stoichiometry in bulk CdO and CdO is prospective candidate for its wide usage as a conducting material in thick film resistors.

List of Publications

1. Effect of V_2O_5 Dopant on the Electrical Conductivity of RuO_2 Thick Film Resistors, M.S. Setty and R.F. Shinde, Active and Passive Electronic Components, 12 (1986) 111.
2. CdO, A Low-Cost Substitute for RuO_2 Thick Film Resistors, R.F. Shinde and M.S. Setty, Proceedings of International Society of Hybride Microelectronics, India Chapter, (May 1986) p.19.
3. Grain Growth Studies in Thick Films of Cadmium Oxide, R.F. Shinde, A. Mitra, M.S. Setty and S.K. Date, Mater. Letts., 7 (1988) 299.
4. X-band EPR Studies of Hyperfine and Superhyperfine Structures of Mn^{2+} Ions in Polycrystalline CdO, R.F. Shinde and S.K. Date, Materials Chemistry and Physics, 24 (1989) 71.
5. La-Stabilized Zirconia: Synthesis and Characterization, P. Singh, S.R. Sainkar, M.V. Kuber, V.G. Gunjikar, R.F. Shinde and S.D. Date, Mater. Letts., In Press.
6. Ageing Effects in CdO:Mn^{2+} Systems: An EPR Study, R.F. Shinde and S.K. Date, To be published.
7. Effect of Grain Growth on Sheet Resistivity of Thick Films of CdO, R.F. Shinde and S.K. Date, To be published.

ACKNOWLEDGEMENT

I am indebted to Dr. S.K. Date for his invaluable and inspiring guidance during the course of this work. Dr. S.K. Date is more than a research guide to me. It is only because of his unfliching support, sympathetic view and enthusiasm, I could overcome many difficulties related to science and other personal matters. I honestly wish to state that without his mentorship this work would not have become materialised.

I am very grateful to Dr. P. Ratnasamy, F.N.A., Head of Physical Chemistry and Inorganic Chemistry Divisions for his kind support for this work.

I am very thankful to Mr. P.M. Suryawanshi for his ungrudging cooperation and help rendered to me during the experimental work, especially on EPR spectroscopy.

I am thankful to Dr. M.S. Setty for his guidance in the early phase of this work and particularly in carrying out the experimental measurements on thick films. I am very much thankful to Dr. S. Pal and Dr. P. Thankachan for introducing me to the important concepts in quantum chemistry. I am thankful to

Mr. M.V. Kuber, Dr.(Mrs.) A. Mitra and Dr. V.G. Gunjikar for their kind support in the field of X-ray diffraction, scanning electron microscopy and thermal analysis.

Very special thanks are also due to my colleagues from Inorganic and Materials Chemistry Unit (IMC U-2) for their cooperation. In particular, I am thankful to Dr. C.E. Deshpande, Dr. P.P. Bakare, Mrs. J.J. Shrotri, Mrs. S.D. Kulkarni, Dr. S. Badrinarayanan, Dr. S.R. Sainkar, Dr. A.B. Mandale and Dr. Prabhat Singh.

I am indebted to my parents, wife and children for their continuous encouragement and support throughout my post-graduate educational career.

Finally, I am grateful to the Director, National Chemical Laboratory, Pune, for his permission to submit this work in the form of thesis.